AN INVESTIGATION OF OPTIMAL PRESSURIZATION FOR BUILDINGS IN HOT AND HUMID CLIMATES

A Dissertation

by

WEI-JEN CHEN

Submitted to the Office of Graduate and Professional Studies of
Texas A&M University
in partial fulfillment of the requirements for the degree of

DOCTOR OF PHILOSOPHY

Chair of Committee,	David E. Claridge
Committee Members,	Charles H. Culp
	Michael B. Pate
	Juan Carlos Baltazar
Head of Department,	Andreas A. Polycarpou

May 2017

Major Subject: Mechanical Engineering

ABSTRACT

Buildings in a hot and humid climate usually are kept at a positive pressurization level to avoid infiltration induced issues such as mold growth within building envelopes. This dissertation combines existing models of infiltration and mold growth to predict the influence of pressurization level on the risk of mold growth. The simulation results indicate that a 3 meter high unpressurized building in College Station, TX with 22°C indoor temperature set-pint will experience an annual increase in mold index, and 1.5 Pa positive pressurization should theoretically eliminate the long-term risk of an increasing mold index on all walls. The model also indicates that only 1 Pa pressurization is required if the same building is moved to Fort Worth, TX and no pressurization is required if it is moved to Atlanta, GA.

Furthermore, a field experiment indicates that the conventional pressurization system fails to pressurize each floor of the eight-floor Harrington Tower building equally due to stack effect; extra make-up air is required to compensate the leaked air through the over-pressurized floors which results in extra energy consumption. An Internal Fan Balancing Pressurization System is proposed to solve this problem. The building energy simulation results suggest that the annual energy cost savings from using the proposed system can range from 3.7% to 6.7% of the total utility bill depending on different assumptions. To verify the feasibility of the proposed system, a scaled three-floor model is developed; on the scale model the Internal Fan Balancing

System is able to reduce 28% to 32% of required make-up air flow by keeping better pressurization levels.

I dedicate this dissertation to my lovely family

ACKNOWLEDGEMENTS

I would like to thank my advisor as well as committee chair Dr. David Claridge. He always provides insightful comments on my research and helps me solving problems. Furthermore, during these years he always invites my family for Thanksgiving dinner, it makes me feel really warm and this certainly means a lot for an international student.

I would like to thank my committee members, Dr. Michael Pate, Dr. Charles Culp, and Dr. Juan Carlos Baltazar for their tireless assistance. Dr. Pate was literally my first teacher in Texas A&M University, his alternative energy course is inspirational which makes me keep thinking ways to make buildings more energy efficient. In Dr. Culp's course I learned to operate building simulation programs, this skill is applied to complete this dissertation. Dr. Claridge and Dr. Baltazar were my two teachers in the energy management course, those fundamental knowledge makes me being able to analyze cases in terms of energy consumption. This dissertation won't happen without all of my respectful teachers.

I would like to thank Dr. Morad Atif for his helpful comments on my dissertation, I would like to thank Dr. Andrew Persily for his helpful suggestions on improving modified mold growth index model. I would like to thank Mr. Homer Bruner and Mr. Ali Syed from Texas A&M University Utilities and Energy Management Service Office for their support on experiments performed on Harrington Tower Building. I would like to thank Mr. Chae Rohrs for his assistance on completing field experiments. I would like to thank Mr. Jiajun Liao for his support on completing the solar absorption calculation

module applied in modified mold growth index model. I would like to thank Elsevier for granting permission to me to reprint certain materials published in the paper "Modeling to predict positive pressurization required to control mold growth from infiltration in buildings in a hot and humid climate" in this dissertation.

(DOI: http://dx.doi.org/10.1016/j.buildenv.2016.05.001)

TABLE OF CONTENTS

Page

LIST OF FIGURES

Page

LIST OF TABLES

Page

1. INTRODUCTION

1.1 Background

In hot and humid climates, infiltration through the building envelope impacts several aspects of building operation. When too much warm and moist outside air enters a conditioned zone, both sensible and latent cooling loads are rapidly increased, the indoor relative humidity (RH) could be out of control, and the indoor air quality (IAQ) might be degraded due to infiltrated outdoor particles. Furthermore, per psychrometric principles, the RH of air goes up when the air temperature goes down if the moisture content of the air is constant. This occurs with infiltrating air when the outside air temperature is higher than the indoor air temperature. Since RH is generally believed to be the key parameter of mold growth, unfiltered infiltration could cause a mold growth issue within the building envelope, most likely on the layer that is in contact with the inner space or close to the inner wall surface, where moist infiltrated air reaches its highest RH.

To avoid infiltration induced issues, building pressure is typically maintained at a slightly positive level compared to outdoor pressure in warm seasons. In practice, most building HVAC systems pull in more outside air and exhaust less to achieve positive pressurization. While both extra OA intake and infiltration raise energy consumption except for times when an airside economizer cycle is desirable, an appropriate pressure set-point is essential to maximize energy efficiency.

For existing buildings, a common pressurization method is to place the indoor-outdoor differential pressure sensor at either the top floor or the ground floor; exhaust

fan / relief fan speed is then adjusted accordingly to maintain the desired pressure level. However, a single sensor may fail to represent the indoor-outdoor pressure difference of all building levels. This is especially true for high-rise buildings. For example, on a hot day, a ground-level sensor may indicate that the building is under highly positive pressurization, but in fact the top floor of the same building is probably under negative pressurization, which results in unwanted infiltration through the building envelope. One possible solution is to calculate the required pressure level for the top floor and raise the pressure set-point accordingly; however, under this solution, bottom floors are over pressurized and may induce security problems due to compromised door operation.

1.2 Objectives of the Study

This study focuses on two main issues regarding building pressurization, the ultimate goal is to improve the building pressurization system's efficiency.

The first objective is to develop a method to quantify the required minimum pressure level needed to reduce mold growth risk to an acceptable level. Most buildings in hot and humid climates in the United States have a pressure set-point ranging from 0.01 in. w.g. (2.5 Pa) to 0.03 in. w.g. (7.5 Pa). However, the level of positive pressurization used appears to have a very limited engineering basis. If two similar buildings are located in the same climate zone, there should be an engineering-based explanation that one building requires only 2.5 Pa, but the other one requires 7.5 Pa of pressurization, which is three times higher. Since one of the major benefits of building pressurization is to limit the danger of mold growth in building envelopes, a method to

quantify the required minimum pressure level needed to reduce mold growth risk to an acceptable level is developed and proposed.

The second objective is to develop a pressurization system that is capable of maintaining each floor of a multi-floor building just above the minimum required pressurization level. As noted in the previous section, a conventional pressurization system working in a high-rise building can only leave top floors at negative pressurization or largely over-pressurize the bottom floors to maintain the top floor pressure barely positive. To address this issue, an internal fan balancing pressurization system is developed. The system utilizes a series of variable speed internal balancing fans, which are installed between floors, to adjust each floor's pressurization level individually. Indoor-outdoor differential pressure sensors are installed on each floor to provide feedback signals for the fan controller; thus the desired pressurization level can be maintained on each floor.

A comparison can be made to further describe the advantages of the internal fan balancing system. Assuming there is a 4-floor building with uniform leakage area distribution. When the outdoor air temperature is higher than the indoor air temperature and the wind effect is negligible, the indoor and outdoor pressure curve for the unpressurized building can be shown as in Figure 1-1. The direction of arrows on the left side of the building indicates whether a specific section of the building is experiencing infiltration or exfiltration. The length of each arrow indicates the infiltration/exfiltration intensity, which is related to the indoor-outdoor pressure difference. The indoor and outdoor pressure curves are shown on the right side of the figure. Note that the slopes of

the two curves are different due to indoor-outdoor temperature difference, which is generally described as the stack effect.

A conventional pressurization system is shown in Figure 1-2. To positively pressurize the whole building, certain sections of the building are inevitably over pressurized, which results in unwanted extra loss of conditioned air. The shaded area between the indoor-outdoor pressure curves indicates the total exfiltration flow rate. The proposed system is shown in Figure 1-3. Multiple fans are installed between floors to adjust each floor's pressurization level individually to the appropriate level. As a result, the shaded area is significantly reduced, which means reduced make-up air requirement as well as improved system efficiency.

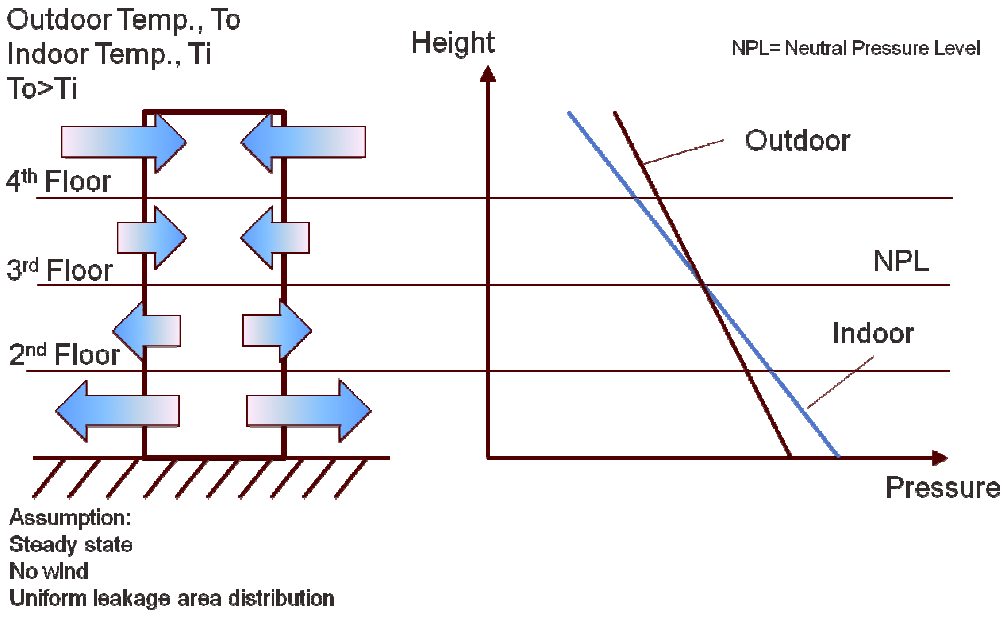

Figure 1-1 Building flows and indoor-outdoor pressure curve, unpressurized

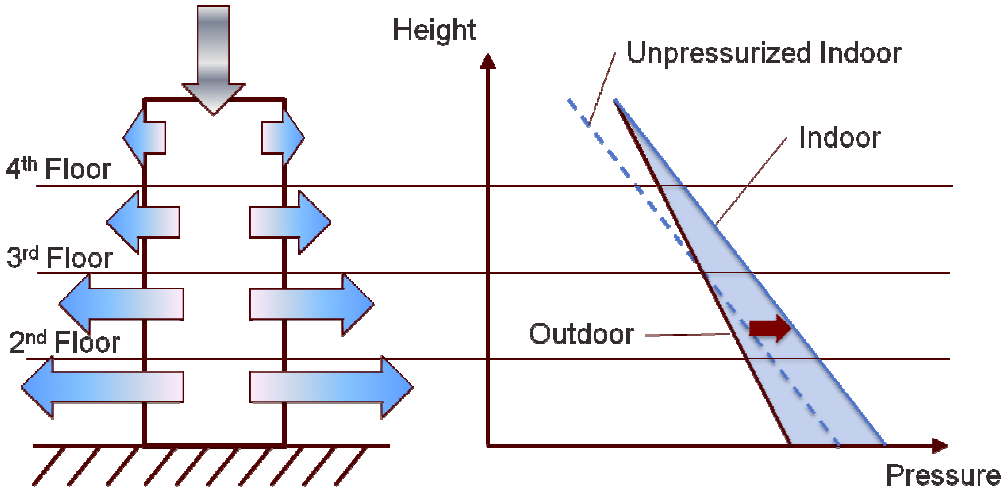

Figure 1-2 Building flows and indoor-outdoor pressure curve, conventional system

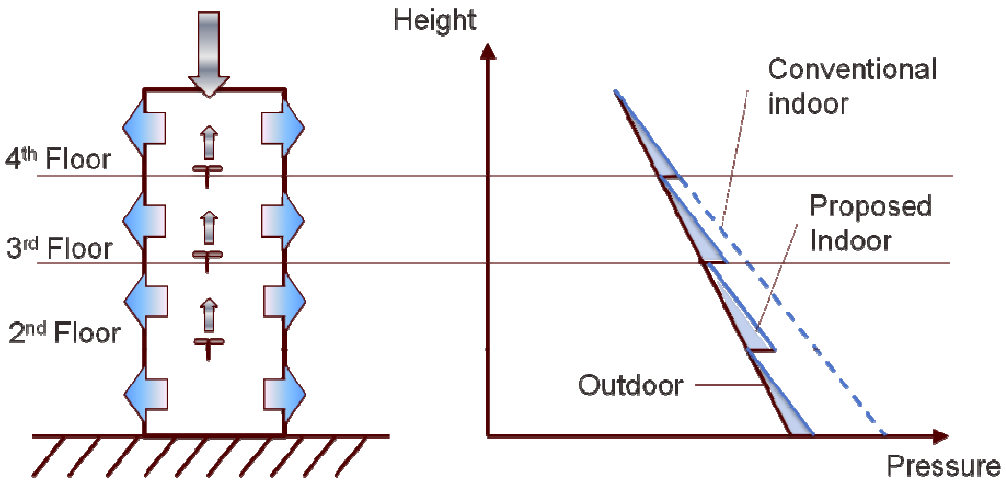

Figure 1-3 Building flows and indoor-outdoor pressure curve, proposed system

1.3 Organization of the Dissertation

This dissertation is organized into six sections.

Section one introduces the background and the objectives of the study

Section two reviews literature related to this research including the driving forces of building infiltration/exfiltration, infiltration measurement techniques, leakage flow rate modeling, mold growth models, and building pressurization methods.

Section three describes a modified mold growth index model that may quantify the minimum pressurization level required to control mold growth.

Section four describes a prototype Internal Fan Balancing System running on a scale-model building.

Section five describes the predicted energy savings that may be achieved by using the internal fan balancing system on an eight-floor building located on the Texas A&M University main campus in College Station, TX.

Section six summarizes this study and discuss the recommendations for future research.

2. LITERATURE REVIEW

2.1 Building Infiltration and its Driving Forces

Infiltration is defined in ASHRAE Standard 90.1[1] as *" the uncontrolled inward air leakage through cracks and crevices in any building element and around windows and doors of a building caused by pressure differences across these elements due to factors such as wind, inside and outside temperature differences (stack effect), and imbalance between supply and exhaust air systems".* As described above, infiltration occurs when a leakage path and a pressure difference across the building envelope are both present.

Infiltration in commercial buildings can have many negative consequences, including reduced thermal comfort, interference with the proper operation of mechanical ventilation systems, degraded indoor air quality, moisture damage of building envelope components, and increased energy consumption. [2]

Differential pressures on a structure are caused by the stack effect and the wind effect. [3]

The size of the stack effect is given by following equation:

$$P_s = \rho g H \frac{\Delta T}{T} \qquad (2.1)$$

Where:

P_s is the stack pressure (Pa)

ρ is the density of air (kg/m^3)

g is the acceleration of gravity ($9.81\ \mathrm{m}/sec^2$)

H is the height of the structure (m)

ΔT is the inside-outside temperature difference (K)

T is inside temperature (K).

The effect of moisture on density is generally negligible except in hot and humid climates; for example, saturated air at 105°F has a density about 5% less than that of dry air [4].

The size of the wind effect is given by the following equation:

$$\Delta P_j^w = C_j * \frac{1}{2}\rho V^2 \qquad (2.2)$$

Where:

ΔP_j^w is the exterior pressure rise due to the wind for the jth face

ρ is the density of air (kg/m^3)

V is the actual wind speed (m/s)

C_j is the shielding coefficient for the jth face.

To determine the actual wind speed, the following equation is used:

$$V = V_o \alpha \left[\frac{H}{10}\right]^{\gamma} \qquad (2.3)$$

Where:

V is the actual wind speed (m/s)

V_o is the wind speed measured at the nearest 10 meter-high weather station, and

α and γ are constants that depend on terrain class.

Experiments were performed by Sherman [3] to obtain such constants; he found α and γ values for several types of terrain. For Class IV terrain (urban, industrial or forest areas), α will be 0.67 and γ will be 0.25, approximately.

Due to its complex relationships with wind speed and direction, building direction and shape, and local terrain, the shielding coefficient is generally calculated from data obtained through CFD modeling[5-7], wind tunnel measurements[8-10], or full-scale tests[11-13], on various building shapes and heights [14]. For simple-shaped buildings (i.e. rectangular shape), different charts / equations are also available for estimating the shielding coefficient[4].

2.2 Infiltration Measurement

2.2.1 Air Changes per Hour (ACH)

Pressure difference is the driving force which causes infiltration, but the available leakage path area is another important factor in the amount of infiltration. When describing the infiltration flow rate of a building, the building size should also be considered. For example, if a small single-family house and a large office building both have the same infiltration flow rate, the small single-family house is surely more leaky. Air changes per hour (ACH) compares airflow to volume and is [15]:

$$ACH = \frac{Q}{V} \qquad (2.4)$$

Where:

Q is the flow rate into the building ($ft^3/hour$)

V is the interior volume of the building (ft^3).

ACH is sometimes given at a specified pressure difference, for example, ACH_{50} means air changes per hour under 50 Pa pressure difference through the building envelope.

2.2.2 Blower Door Test and Effective Leakage Area (ELA)

To quantify the area of cracks and crevices in the building envelope, Sherman [3] utilized a fan pressurization test to extrapolate the leakage curve down into the pressure range of natural weather effects.

The fan pressurization test, or blower door test, was first used in Sweden around 1977 as a window-mounted fan. [16] It is one of the most common methods to measure airtightness of the building. A fan can be installed to pressurize or depressurize the building at a certain level to eliminate the natural weather effects. In pressurized operation, with all known ducts, windows, and funnels sealed, all air flow through the fan is assumed to leak out through unknown cracks or crevices.

Air leakage typically follows the power law:

$$Q = C(\Delta P)^n \qquad (2.5)$$

Where:

Q is the air flow (m^3/sec)

C is the flow coefficient

n is the pressure exponent, and

ΔP is the pressure difference (Pa)

The air flow Q can be measured at several pressure difference levels, ΔP, to determine C and n. The pressure exponent is normally found to be in the vicinity of 0.65 but has the limiting values of 0.5 and 1 from simple physical considerations. [16]

After C and n are found, the relation between Q and ΔP is determined. Sherman then introduced the Effective Leakage Area, (ELA), by the following equation:

$$Q = A\sqrt{\frac{2}{\rho}\Delta P} \qquad (2.6)$$

Where:

Q is the air flow ($m^3/\sec$)

A is the effective leakage area (m^2),

ρ is the density of air (kg/m^3)

ΔP is the applied pressure (Pa).

Sherman [3] picked 4 Pa as the applied pressure, and the ELA is defined as the area that would leak the same amount of air as the building does at a pressure of 4 Pascals.

Numerous research projects have tested building airtightness, and most of them present air leakage in either ACH or flow rate per unit area at a specific pressurization level, where the area is the above-ground surface area of the building.

ÄSK [17] measured the infiltration rate of an elementary school in Florida using a fan pressurization test before and after certain remediation, and found a 55% reduction in infiltration after remediation. The author also pointed out that after remediation, the pressure exponent "n" was also changed.

Persily [18] analyzed 139 commercial and institutional buildings located in the United States, Canada, the United Kingdom, and Sweden in which infiltration rates were measured by a fan pressurization test at 75 Pa No correlation was found between airtightness and the building age. Wall construction and building type do not appear to have a significant impact on envelope airtightness except that frame walls and retail buildings were found to be somewhat leakier than other types of wall and building types, respectively.

2.2.3 Tracer Gas Techniques

The tracer gas technique is another common method used to determine building infiltration. Several tracer gas measurement procedures exist, all involving an inert or nonreactive gas used to label the indoor air. [4]

These techniques are usually classified by the manner of the injection, such as constant injection, pulse injection, concentration decay, and constant concentration. [19]

Despite the different measurement procedures, all tracer gas measurement techniques are based on a mass balance of the tracer gas in the building. Assuming the indoor air is well mixed, the total balance takes the following form: [4]

$$V\left(\frac{dC}{d\theta}\right) = F(\theta) - Q(\theta) * [C(\theta) - C_0(\theta)] \qquad (2.7)$$

Where:

V is the volume of the building being tested (ft^3),

$C(\theta)$ is tracer gas concentration at time θ

$\frac{dC}{d\theta}$ is time rate of change of concentration (min^{-1})

$F(\theta)$ is tracer gas injection rate at time θ (CFM)

$Q(\theta)$ is airflow rate out of building at time θ (CFM)

$C_0(\theta)$ is outdoor tracer gas concentration at time θ

θ is time (min).

Lagus and Persily [20] compared different types of tracer-gas, including helium (He), carbon dioxide ($\mathrm{CO_2}$), nitrous oxide ($\mathrm{N_2O}$), sulfur hexafluoride ($\mathrm{SF_6}$), bromotrifluoromethane ($\mathrm{CBrF_3}$), and perfluorodimethylcyclohexane (PDCH). Both relative gas cost and detection techniques are compared. They found sulfur hexafluoride, bromotrifluoromethane, and perfluorodimethylcyclohexane to be relatively economical choices for measuring large building.

Grot and Clark [21] measured infiltration rates of 266 dwellings of low-income families in 14 cities in the United States by the tracer gas (concentration decay) technique. It was found that 19% of the data sample had rates of less than 0.5 ACH, 40% had moderate rates between 0.5 and 1.0 ACH, 20% had high rates between 1.0 and 1.5ACH, and 20% had very high rates greater than 2.0 ACH.

Niemelä, Toppila [22] utilized dichlorodifluoro-methane, ($\mathrm{CCl_2F_2}$) and nitrous oxide ($\mathrm{N_2O}$) in a multiple tracer gas technique. They showed this technique to be applicable in investigations of airflow patterns in industrial premises.

Nederhoff and Van de Vooren [23] discussed using carbon dioxide ($\mathrm{CO_2}$) in a practical tracer gas (concentration decay) technique to determine ventilation in greenhouses. Concentration of carbon dioxide was raised to 2,000 v.p.m (volume per

million volume), then allowed to decay. The effect of plants on concentration of carbon dioxide was estimated by appropriate equations. They found this method can be used with or without a crop, but it is necessary to correct for the effect of the crop on the CO_2 concentration.

Montoya and Pastor [24] measured the infiltration rate of 16 single-family dwellings across Catalonia by the tracer gas (concentration decay) technique. The ACH varied from 0.056 to 0.579, which is substantially lower than values reported for buildings in United States.

Cheong [19] compared the tracer-gas (constant injection) technique and the pitot-static traverse method in measuring airflow rates in air distribution systems. Results from these tests indicated that measurements obtained using the constant injection technique were in close agreement with the measurements obtained using the pitot-static traverse method.

Labat and Woloszyn [25] measured the infiltration rate of a single-room building 12 times by the tracer gas (concentration decay) technique under different weather conditions. The result indicated that it is important to make tracer gas measurements under representative weather. Another set of experiments would need to be carried out if different average weather conditions were to be considered.

Persily and Grot [26] measured the air flow rate of seven pressurized federal buildings by using the tracer gas (constant injection) technique. It was found that when tested buildings were under 25 Pa pressurization level, the ACH varied between 0.45 to 1.45.

Emmerich and Persily [27] summarized airtightness experiment results on U.S. commercial and institutional buildings reported from 5 different institutions. Sources of data included 9 buildings tested by the National Institute of Standards and Technology (NIST) [26, 28, 29], 90 buildings tested by the Florida Solar Energy Center [30, 31], 2 buildings tested by Pennsylvania State University [32], 23 buildings tested by Camroden Associates [33] (and previously unpublished data), and 79 buildings tested by the U.S. Army Corps of Engineers (previously unpublished data including some partial school buildings). The data indicates that the average air leakage at 75Pa for the 201 buildings is 28.4 $m^3/h * m^2$. The average of the U.S. Commercial buildings is 21 $m^3/h * m^2$ for offices, 32 $m^3/h * m^2$ for factories and warehouses, and 26.5 $m^3/h * m^2$ for superstores built in the United Kingdom prior to new building regulations.

2.2.4 Alternative Form of Leakage Air Equation

Instead of using the power law, research [34] suggests that the infiltration flow rate can be presented as:

$$\Delta P = \frac{12\mu z}{Ld^3} * Q + \frac{\rho C}{2d^2L^2} * Q^2 \qquad (2.8)$$

Where:

ΔP is the pressure difference

μ is the dynamic viscosity

z is the dimension in the direction of flow

d is the gap thickness

L is the breadth of the plates

C is a dimensionless constant

ρ is the density

This dimensionally homogenous quadratic equation is derived from the basic flow equation for infinite parallel plates proposed by previous research [35]. Baker and Sharples [34] performed a series of experiment on cracks with known dimension which showed that the equation described above fit the data better than using a power law.

Etheridge [36] suggested another equation:

$$\frac{1}{{C_d}^2} = k\frac{z}{Re_h D_h} + C \qquad (2.9)$$

Where:

C_d is the discharge coefficient of the crack

D_h is the hydraulic diameter

Re_h is the Reynolds number based on the hydraulic diameter

C is an empirical constant

k is an apparent coefficient which varies with Reynolds number and aspect ratio.

Similarly, experiments were performed on cracks with known characteristics and results were found to better support the proposed equation.

The latter equation can be organized to a similar form as the former equation as shown in Table 2-1:

Author(s) Name	Organized form	Notes
Baker, Sharples [34]	$\Delta P = \frac{12\mu z}{Ld^3} * Q + \frac{\rho C}{2d^2 L^2} * Q^2$	
Etheridge [36]	$\Delta P = \frac{k\mu z}{8Ad^2} * Q + \frac{\rho C}{2A^2} * Q^2$	A=L*d*

Table 2-1 Comparison of two alternative leakage air equations

By comparing the two equations, both equations treat laminar flow and turbulent flow separately. The only difference seems to be the coefficient of the laminar flow portion. While the equation of [34] assumes a constant value 12, the equation of [36] assumes an empirical value k divided by eight. In Etheridge's original paper k was found to be close to 96 for straight-through and L-shaped cracks. Thus the equation of [34] can be considered a special case of the equation of [36].

2.3 Mold Growth Models

Various mold growth prediction models have been developed, and most of these models treat relative humidity and temperature as the two main factors related to mold growth. Existing research generally indicates that there is a critical value of RH above which mold growth becomes probable; this critical value is typically a function of temperature but is treated as a function of temperature and target substrate in some research. Thus the results are usually presented as isopleth curves to determine conditions favorable or unfavorable for mold growth.

Sedlbauer [37] proposed a series of lowest isopleth curves called Lowest Isopleth for Mold (LIM). Due to the difficulty of testing a massive number of mold species, Sedlbauer categorized mold species into three groups, ranging from A: highly pathogenic that should not be allowed to occur in occupied dwellings, B: pathogenic when people are exposed to it over a long period of time and may cause allergic reactions, and C: not dangerous to health but may cause economic damage. The isopleth curves represent minimum RH required at specific temperature for mold growth related activities, such as spore germination and mycelial growth. As an example, Figure 2-1 shows isopleth curves for spore germination from different species.

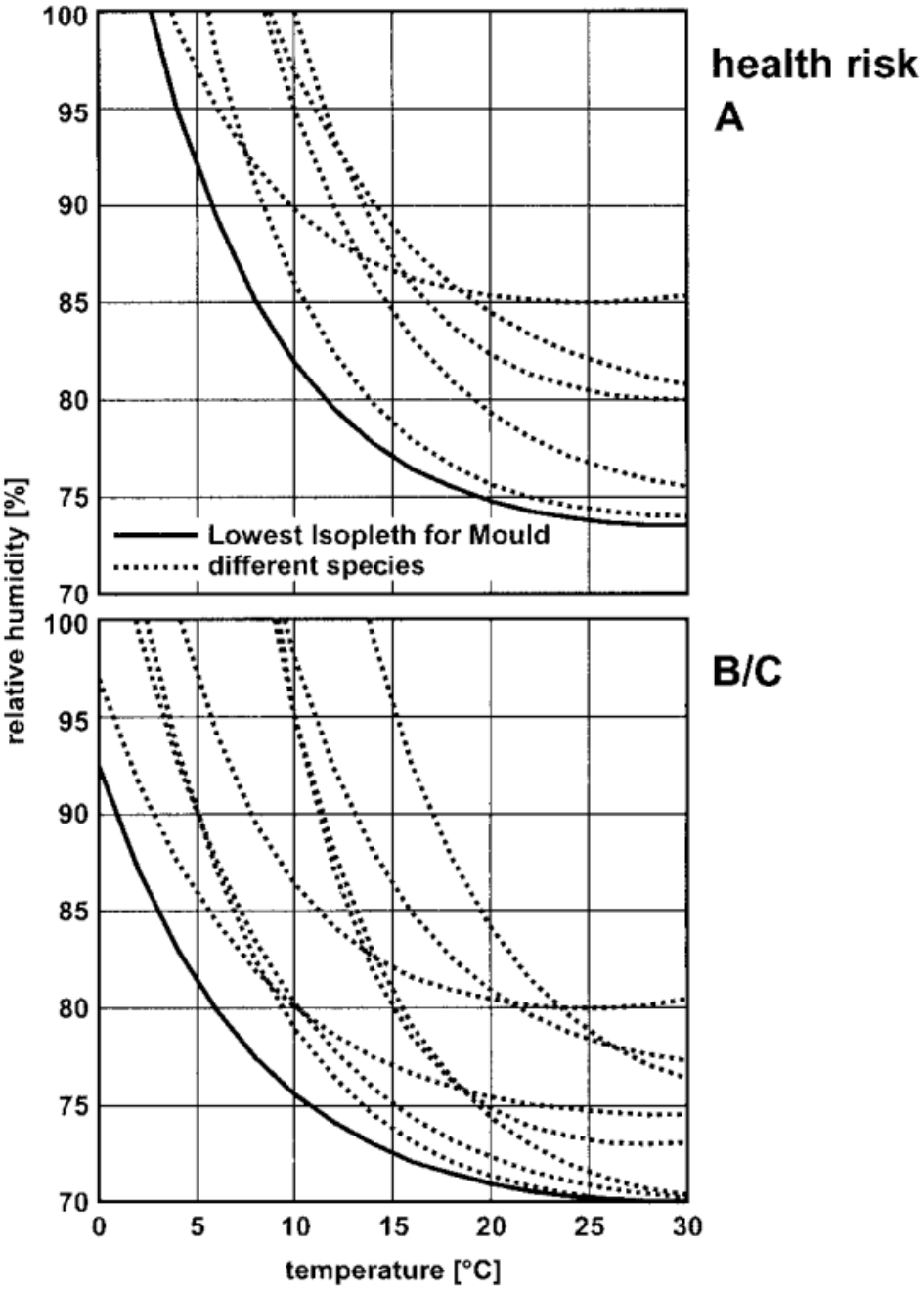

Figure 2-1 Development of the lowest isopleth for spore germination from isopleths of different species [37]. top: health risk class a; bottom: health risk class b/c.

Hens [38] proposed a lowest isopleth curve for *Aspergillus versicolor*, where the critical RH reaches its lowest value of 79% at 22.7°C and increases to 96% at 0°C. Hens also indicated that the isopleth curve reflects the situation for wheat extract agar, which is a substrate with a richer nutrient content than most building materials. The same experiment done on wall finishes rarely gave visible mold below 83% RH.

Clarke, Johnstone [39] tested six mold species (*Cladosporium sphaerospermum*, *Penicillium spp*, *Alternaria alternata*, *Aureobasidium pullulans, Aspergillus versicolor, Eurotium herbariorum,* and Yeasts separately. Based on results from a 120 day incubation period at 25°C, mold species were divided into six categories ranging from A: highly xerophilic to F: highly hydrophilic species. No mold growth was observed at and below 74.5% RH after 120 days for any of the species. At a 25°C steady state condition, it was discovered that the critical RH can be as high as 94.5% for category F species like Yeasts and as low as 78.5% for category A species like *Eurotium herbariorum*.

Hukka and Viitanen [40] proposed a mathematical model to predict mold growth on wooden material, using critical RH as the key factor. Conditions with RH exceeding critical RH are considered favorable for mold growth; otherwise they are unfavorable for mold growth. Critical RH varies with different materials and temperature ranges.

Viitanen and Ojanen [41], [42, 43] tested more building materials to improve their previous model. Small samples were exposed to various constant humidity and temperature conditions. Based on these results, the declining model for unfavorable conditions is multiplied by a relative coefficient for materials different from the pine

wood tested originally. This model is utilized to predict mold growth and the results are presented in terms of the mold index.

Johansson and Wadsö [44] performed an experiment lasting over 20 months on walls facing either south or north with different color and construction configurations. Temperature and RH were monitored hourly and utilized as inputs of mold growth indexes. Three mold growth indexes were proposed and discussed. The first index considers only the fraction of time RH is above a constant value, which was set at 80%. The second index considers the potential of mold growth per the isopleth method that was developed by previous research [45-53]. The third index is the same as Index 2 but includes a recovery time delay parameter. The results indicate that for all indexes, the wall color is the most important factor for the surface humidity levels on a south-facing facade in the northern hemisphere, while on a north-facing facade the thermal inertia is most important.

Vereecken and Roels [54] reviewed several mold prediction models and indicated that cardinal influencing factors in the mold growth process are temperature, moisture, substrate and exposure time, while Johansson and Bok [55] pointed out that the duration of both favorable and unfavorable conditions are also decisive for mold growth.

2.4 Building Pressurization Methods

Building pressure can be kept at a certain positive level to minimize infiltration, and this requires an automated control system. Typical building pressure control methods

include fan tracking, direct building pressure control, and volumetric tracking. [56] There is also a combined method to achieve better results.

As mentioned in the previous section, while the wind effect and stack effect can be determined by separate equations, a number of studies focus on the combination of both effects. The simplest method is to combine wind effect induced and stack effect induced flow rates linearly, but this method produces large errors [57].

Walker and Wilson [57] evaluated four different models for superposition of wind and stack effect in air infiltration, including linear addition, pressure addition, quadrature, and the Alberta Infiltration Model (AIM-2) [58]. The results suggested that pressure addition is physically realistic, simple, and seems to be the best choice for combining independent wind effect and stack effect flows to estimate their combined effect.

Persily [59] compared total ventilation rate and infiltration rate of an office building under three different operation modes (main, minimum, and sub-minimum). Volumetric tracking and direct building pressure control were applied in different modes, with the result that infiltration divided by total ventilation rate ranged from 31% to 58%.

Liu [56] developed the VSD volumetric tracking (VSDVT) method to minimize thermal and fan energy while meeting the requirements of outside air intake and the positive building pressure under all load conditions. The annual fan energy savings from the VSDVT method are up to 50% for the return fan and 30% for the supply fan compared with the fan tracking method.

Pang, Liu [60] compared two building pressure control methods, with either return fan or relief fan. The results suggested that the relief fan method paired with volumetric tracking does improve the building pressure control.

Emmerich and Persily [2] simulated the infiltration rate of 25 buildings under negative, neutral, and positive pressure. The volumetric tracking method was applied, and the buildings were pressurized by having 10% more supply airflow than return flow and de-pressurized by having 10% lower supply airflow than return flow. The buildings with negative pressure had ACH values from 0.18 to 0.74, the buildings with positive pressure had ACH from 0.025 to 0.55, and buildings with neutral pressure had ACH values between those of positive and negatively pressurized buildings.

2.5 Summary of Literature Review

In most building air leakage studies, the leakage intensity is presented in a form of either ACH or CFM/ft^3(m^3/s for SI units) and is usually determined by blower door testing or the tracer gas method. Studies suggest that several equations are more accurate for determining leakage air flow than the widely used power law equation. However, due to the difficulty of determining the leakage path shape and its distribution profile, the power law is still the major method used in most studies.

The two major effects causing indoor-outdoor pressure differences are the wind effect and the stack effect. The stack effect is a function of building height and indoor-outdoor air temperature difference, so it becomes more severe in high-rise buildings and also in extreme hot/cold weather conditions.

To estimate the wind effect, several equations are readily available and they usually involve the shielding coefficient. Due to its complex relationships with wind speed and direction, building direction and shape, and local terrain, the shielding coefficient is generally calculated from data obtained through CFD modeling, wind tunnel measurements, or full-scale tests.

To predict mold growth, several models are readily available including the VTT Model (the one applied to calculate mold growth intensity in certain conditions in this dissertation), WUFI®-Bio, Sedlbauer Isopleth System, Hens Isopleth Curve, ESP-r Isopleth Model, Temperature Ratio Method, Time of Wetness Method, and Moon's Mold Germination Graph Method. Essentially all prediction models utilize temperature and RH as key parameters, while some of them also take substrate materials into consideration. It is worth mentioning that most of models mentioned above predict no mold growth when temperature is below 0 °C.

Typical building pressure control methods, including fan tracking, direct building pressure control, and volumetric tracking, are commonly applied to buildings to maintain a positive pressurization level; this is especially true for buildings in hot and humid climates. When both stack effect and wind effect present, research suggests that the pressure addition method is realistic, simple, and seems the best choice compared to linear addition, quadrature, or AIM-2 models.

3. MODIFIED MOLD GROWTH INDEX BASED ON PRESSURIZATION LEVELS*

3.1 Introduction

One of the major benefits of building pressurization is to limit the danger of mold growth in building envelopes. This method is used in almost all large buildings in humid regions in the United States. Since excessive pressurization results in extra energy consumption, a method to quantify the required minimum pressure level needed to reduce mold risk to an acceptable level is developed.

The modified mold growth index based on pressurization levels developed combines existing models of infiltration and mold growth to predict the influence of pressurization level on the risk of mold growth. Walls are treated differently depending on their height and the direction they face. Local weather data are utilized to generate the outside pressure field. Temperature measurements performed on an actual building are applied to a multi-layer envelope temperature prediction model, used to simulate the performance of different envelope constructions.

When the outside air temperature is higher than the indoor air temperature, the RH of cooled infiltration air will increase and the process is as shown on the psychrometric chart in Figure 3-1. Hence, in hot and humid climates, mold growth and condensation will most likely occur on a building envelope layer that is in contact with the inner space or close to the inner wall surface (where moist infiltrated air reaches its highest RH).

*Part of this chapter is reprinted with permission from "Modeling to predict positive pressurization required to control mold growth from infiltration in buildings in a hot and humid climate" by Wei-Jen Chen, David E. Claridge, Chae Rohrs, Jiajun Liao. Building and Environment. 2016;104:102-113.

Due to this reason, such a layer is considered as the target layer and is the focus of the model developed.

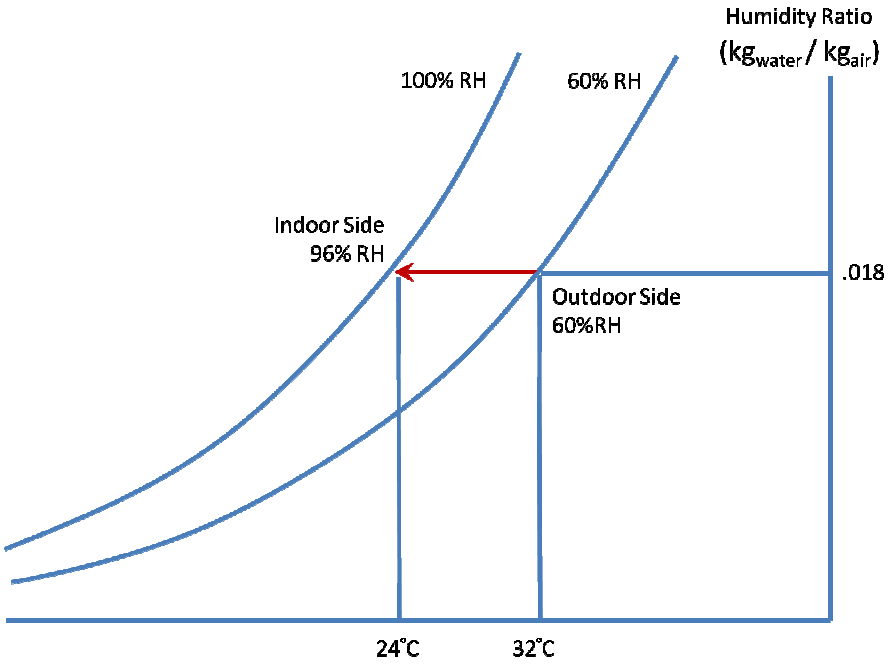

Figure 3-1 A psychrometric chart example showing that the RH of infiltration air increases to 96% from 60% when the temperature decreases from 32°c to 24°c.

3.2 Methodology

Hukka and Viitanen [40] proposed a mathematical model to predict mold growth on wooden material, using critical RH as the key factor. Conditions with RH exceeding critical RH are considered favorable for mold growth; otherwise they are unfavorable for mold growth. Critical RH varies for different materials and temperature ranges. For gypsum board at 22°C, the critical RH is estimated to be 89% to 95% [61, 62]. Here 89% is selected to represent the worst case scenario.

Under this model, mold growth intensity is categorized in seven levels called the "mold index M" where, M=0 – 6. A detailed definition of each mold index level is given in Table 3-1. Under conditions favorable for mold growth, the following equation applies:

$$\frac{dM}{dt} = \frac{1}{7 * exp\,(-0.68\,ln\,T - 13.9\,ln\,RH + 0.14W - 0.33SQ + 66.02)} * k_1 k_2$$

(Per Day) (3.1)

Where:

T is temperature (°C)

RH is relative humidity

k_1 is intensity of growth

k_2 is calculated based on M and M_{max}

W is a wood species factor

SQ is a surface quality factor

For unfavorable mold growth conditions, the following equation is applied:

$$\frac{dM}{dt} = \begin{cases} -0.00133, when\ t - t_1 \leq 6h \\ 0, \quad when\ 6h < t - t_1 \leq 24h \\ -0.000667, when\ t - t_1 > 24h \end{cases} \qquad \textit{(Per Hour) (3.2)}$$

Where:

t is the time (h) from the moment t_1 when the conditions changed from favorable to unfavorable conditions.

Index	Description of the growth rate
0	No growth
1	Small amounts of mould on surface (microscope), initial stages of local growth
2	Several local mould growth colonies on surface (microscope)
3	Visual findings of mould on surface, < 10 % coverage, or, **< 50 % coverage of mould (microscope)**
4	Visual findings of mould on surface, 10 - 50 % coverage, or, **>50 % coverage of mould (microscope)**
5	Plenty of growth on surface, > 50 % coverage (visual)
6	Heavy and tight growth, coverage about 100 %

Table 3-1 Mold index for experiments and modeling [41]

This model is then expanded to cover other building materials [42] [41, 43]. By referencing the original pine wood experimental result, the k_1, intensity of growth for a specific building material, is determined by following equation:

$$k_1 = \frac{t_{M=1,pine}}{t_{M=1}} \; when \; M < 1 \qquad (3.3)$$

$$k_1 = 2 * \frac{(t_{M=3,pine} - t_{M=1,pine})}{(t_{M=3} - t_{M=1})} \; when \; M \geq 1 \qquad (3.4)$$

Where:

$t_{M=1}$ is the time required for the material to start growing mold (mold index reaches level M = 1), and $t_{M=3}$ is the time needed for the material to reach the level M =3. The subscript pine refers to the value with the reference pine material.

The declining model for unfavorable conditions is multiplied by a relative coefficient C_{mat} for materials different from the pine wood tested originally. This model

is utilized to predict mold growth under specified pressurization conditions, and the results will be presented in terms of the mold index.

Parameters applied in the mold index model are summarized in Table 3-2 with the basis for each choice. The primary uncertainty in the required pressurization depends on the value of the relative coefficient C_{mat} for the declining mold index model. In the original paper the authors defined four “decline” classes and mentioned that "*This classification is based on few measurements with relatively large scattering and it should be considered as the first approximation of these classes.*" [43]

Per the experimental results from [43], gypsum board is in between the "Relatively low decline class" and the "Significant Relative decline class". It is assumed that gypsum board is in "Relatively low decline class" as a worst-case scenario as what was done when determining the critical RH for gypsum board. Making these conservative assumptions should produce an upper limit to the required pressurization level.

Parameter	Value	Basis for Value
T	Hourly target layer temperature	From ANSYS® Simulation
RH	Hourly target layer RH	Eqs. (3.12-3.14)
$\mathbf{k_1}$	0.333	Eqs. (3.3-3.4) and reference [43]
$\mathbf{k_2}$	Calculated by hourly target layer M level	Reference [43]
W	0	Reference [43]
SQ	0	Reference [43]
$\mathbf{C_{mat}}$	0.25	References [41, 43]

Table 3-2 Parameters in mold index model (gypsum board)

Typically, indoor RH is controlled within a range that is unfavorable for mold growth, which means that for the building envelope, exfiltration has a low risk for mold growth and is generally ignored. To find out when exfiltration will occur, both the outside and indoor pressure fields must be generated.

The outside pressure field is mainly affected by two factors: stack effect and wind effect. Assigning outside ground level as the reference point, the stack effect is calculated by the following equation:

$$P(h) = 0 - \rho g h \qquad (3.5)$$

Where:

$P(h)$ is outside pressure (Pa) at height h (meters)

ρ is the density of air (kg/m^3)

g is the gravity constant ($9.81 m/s^2$)

The wind effect is calculated by the following equation: [3, 63]

$$\Delta P_j^w = C_j * \frac{1}{2}\rho V^2 \qquad (3.6)$$

Where:

ΔP_j^w is the exterior pressure rise due to the wind for the jth face

ρ is the density of air (kg/m^3)

V is the actual wind speed (m/s)

C_j is the shielding coefficient for the jth face.

For V, the following equation is applied:

$$V = V_o \alpha \left[\frac{H}{10}\right]^{\gamma} \qquad (3.7)$$

where:

V is the actual wind speed

V_o is the wind speed measured at the nearest 10 meter high weather station

α and γ are constants that depend on terrain class.

Assuming Class III terrain (rural area with low buildings, trees, etc.), which is appropriate for the building simulated, $\alpha = 0.85$ and $\gamma = 0.2$ are applied.

For the shielding coefficient (or pressure coefficient), the following equation is applied with typical values $C_p(1) = 0.6, C_p(2) = -0.3, C_p(3) = C_p(4) = -0.65$ [4]:

$$C_p(\Phi) = \frac{1}{2} * \left\{ \begin{array}{c} \left[C_p(1) + C_p(2)\right](cos^2\Phi)^{\frac{1}{4}} \\ +\left[C_p(1) - C_p(2)\right](cos\,\Phi)^{\frac{3}{4}} \\ +\left[C_p(3) - C_p(4)\right](sin^2\Phi)^2 \\ +\left[C_p(3) - C_p(4)\right] sin\,\Phi \end{array} \right\} \qquad (3.8)$$

where:

$C_p(1)$ is the pressure coefficient when wind is at 0°

$C_p(2)$ is the pressure coefficient when wind is at 180°

$C_p(3)$ is the pressure coefficient when wind is at 90°

$C_p(4)$ is the pressure coefficient when wind is at 270°

Φ is the wind angle measured clockwise from the normal to wall

The indoor pressure field is also affected by the stack effect; however, when the building achieves steady state, the infiltration/exfiltration flow should be equal when mechanical ventilation is not present. The flow through a leakage path is calculated by the following equation [3, 57]:

$$Q = C(\Delta P)^n \qquad (3.9)$$

where:

Q is the air flow (m^3/sec)

C is the flow coefficient

n is the pressure exponent

ΔP is the pressure difference (Pa)

While C and n should be determined by experiment, here the leakage area is assumed evenly distributed on walls, C and n are assumed constant and n = 0.65 is assumed. The following equation is then utilized to determine the indoor pressure field:

$$\Sigma Q_j = \Sigma \ sgn\left(P_{i,j} - P_{o,j}\right) * C_j |P_{i,j} - P_{o,j}|^{0.65} = 0 \qquad (3.10)$$

where:

Q_j is the air flow for the jth leakage area ($m^3/\sec$)

C_j is the flow coefficient for the jth leakage area, which can be canceled assuming leakage area is evenly distributed

$P_{i,j}$ is the indoor pressure for the jth leakage area (Pa)

$P_{o,j}$ is the outdoor pressure for the jth leakage area, which is calculated by using weather data (Pa)

$sgn\left(P_{i,j} - P_{o,j}\right)$ is to determine flow direction, either infiltration or exfiltration, which is defined as:

$$sgn\left(P_{i,j} - P_{o,j}\right) = \begin{cases} -1, when\ \left(P_{i,j} - P_{o,j}\right) < 0 \\ 1, when\ \left(P_{i,j} - P_{o,j}\right) > 0 \end{cases} \qquad (3.11)$$

After both outside and indoor pressure fields are available, the infiltration or exfiltration condition at a specific wall/roof section can be determined.

When a section is determined to be experiencing infiltration, the RH of infiltrating air is then calculated as its temperature reaches the target layer temperature, which will be described later. The vapor pressure of outdoor air and the saturation vapor pressure at the target layer temperature are calculated by the following equations [64]

$$P_w = 0.6108 * exp(\frac{17.27*T_{dew}}{237.3+T_{dew}}) \quad (3.12)$$

where:

P_w is vapor pressure of outdoor air (kPa)

T_{dew} is dew point (°C), and

$$P_s = 0.6108 * exp(\frac{17.27*T_s}{237.3+T_s}) \quad (3.13)$$

where:

P_s is saturation vapor pressure at temperature T_s (kPa)

T_s is the target layer temperature (°C)

RH of infiltrating air at the target layer, RH_T, is then calculated by the following equation:

$$RH_T = P_w/P_s \quad (3.14)$$

The equation for decreasing or increasing mold growth is then applied to calculate the mold index change.

3.3 Building Configuration and Walls Modeled

The Typical Meteorological Year data set (TMY3) of hourly weather data from Easterwood Airport (College Station, TX) is utilized as the local weather data. Hence the data is examined every hour and can potentially switch from a positive mold index derivative to a negative derivative and vice versa as often as every hour. The building modeled is assumed to be a cubic structure 3 meters high, facing South-East. In the initial simulation (Case 1), the building wall is assumed to have three layers: concrete, fiberglass insulation, and gypsum board from outside to inside, respectively. This matches the wall configuration of the building in which wall temperature measurements were made. Similarly, the second (Case 2) and the third (Case 3) simulations are performed with the TMY3 datasets from Dallas-Fort Worth International Airport and from Atlanta Hartsfield International Airport, respectively, to evaluate the effect of different weather conditions. In addition to the wall configuration described above, the fourth simulation (Case 4) is performed with the following wall configuration: face brick, air gap, OSB sheathing, fiberglass insulation, and gypsum board from outside to inside, respectively. The fifth (Case 5) simulation assumes that the target layer temperature T_{surf} is always equal to the indoor air temperature. A final (Case 6) simulation is the same as Case 1 except having an insulation layer with wood studs placed 16 in. apart to evaluate the thermal bridge effect. Table 3-3 is a summary of all six simulated conditions.

No.	TMY3 Dataset	Wall Configuration
Case 1	College Station, TX	7.5 in. Concrete 3.5 in. Fiberglass insulation 0.5 in. Gypsum board
Case 2	Fort Worth, TX	7.5 in. Concrete 3.5 in. Fiberglass insulation 0.5 in. Gypsum board
Case 3	Atlanta, GA	7.5 in. Concrete 3.5 in. Fiberglass insulation 0.5 in. Gypsum board
Case 4	College Station, TX	4.0 in. Face brick 0.375 in. Air gap 0.5 in. OSB sheathing 3.5 in. Fiberglass insulation 0.5 in. Gypsum board
Case 5	College Station, TX	Fixed target layer temp. (either 22°C or 24°C)
Case 6	College Station, TX	Non-Thermal Bridge Area: 7.5 in. Concrete 3.5 in. Fiberglass insulation 0.5 in. Gypsum board Thermal Bridge Area: 7.5 in. Concrete 3.5 in. Wood stud 0.5 in. Gypsum board

Table 3-3 Description of simulation cases (one floor)

As described previously, the inner gypsum board layer is the target layer. To calculate the hourly target layer temperature, a 1-dimensional transient heat transfer analysis is performed in ANSYS® 16.1 for each case except Case 6, which requires a 2-dimensional analysis. The material parameters in ANSYS® 16.1 are set as shown in Table 3-4.

Material	Thickness mm(in)	Density (kg/m^3)	Thermal Conductivity (W/m °C)	Specific Heat (J/kg °C)
Concrete	190.5(7.5)	2,400	2.03	880
Insulation	88.9(3.5)	21	0.04	800
Gypsum Board	12.7(0.5)	800	0.17	1090
Face Brick	101.6(4.0)	2,000	1.33	920
Air Gap	9.53(0.375)	1.23	0.024	1005
OSB Sheathing	12.7(0.5)	650	0.13	1550
Wood Stud	88.9(3.5)	650	0.13	1550

Table 3-4 Wall material parameters in ANSYS®

The outdoor convective heat transfer coefficient is determined by the following equations: [65, 66]

$$h_w = 5.8 + 3.95 * V\,,\ \ V \leq 5m/s \qquad (3.15)$$

$$h_w = 7.13 * V^{0.78}\,,\ \ V > 5m/s \qquad (3.16)$$

where:

h_w is outdoor convective heat transfer coefficient ($W/m^2 * °C$)

V is the actual wind speed

The procedure used for calculating the solar radiation incident on the wall is based on the approach proposed by Gunerhan and Hepbasli [67]. The absorptivity of the concrete layer and face brick layer are both assumed to be 0.65. The indoor combined (convection and radiation) heat transfer coefficient is determined based on measured temperature data from an existing building. Temperature sensors were placed between the concrete and insulation layers, between the insulation and gypsum board layers, and taped on the gypsum board surface facing the interior, with thermal grease applied in each case. The outdoor air temperature data from Easterwood Airport (~ 1 km from the subject building) is used and indoor air temperature is measured by another temperature sensor placed inside the room air. It is found that the error between the measured and predicted target layer temperatures is minimized when the indoor combined heat transfer coefficient is set to $3.5 W/m^2 * °C$. This value is then applied to the model for a year-long simulation.

The building is assumed to be operating continuously with mechanical ventilation; it is also assumed that the system is capable of providing adequate outside air flow to positively pressurize the building up to 2 Pa, as well as having adequate heating / cooling capacity to maintain indoor temperature at the desired level (either 22°C or 24°C). .

Figure 3-2 is a flow chart showing how the mold index level change is calculated.

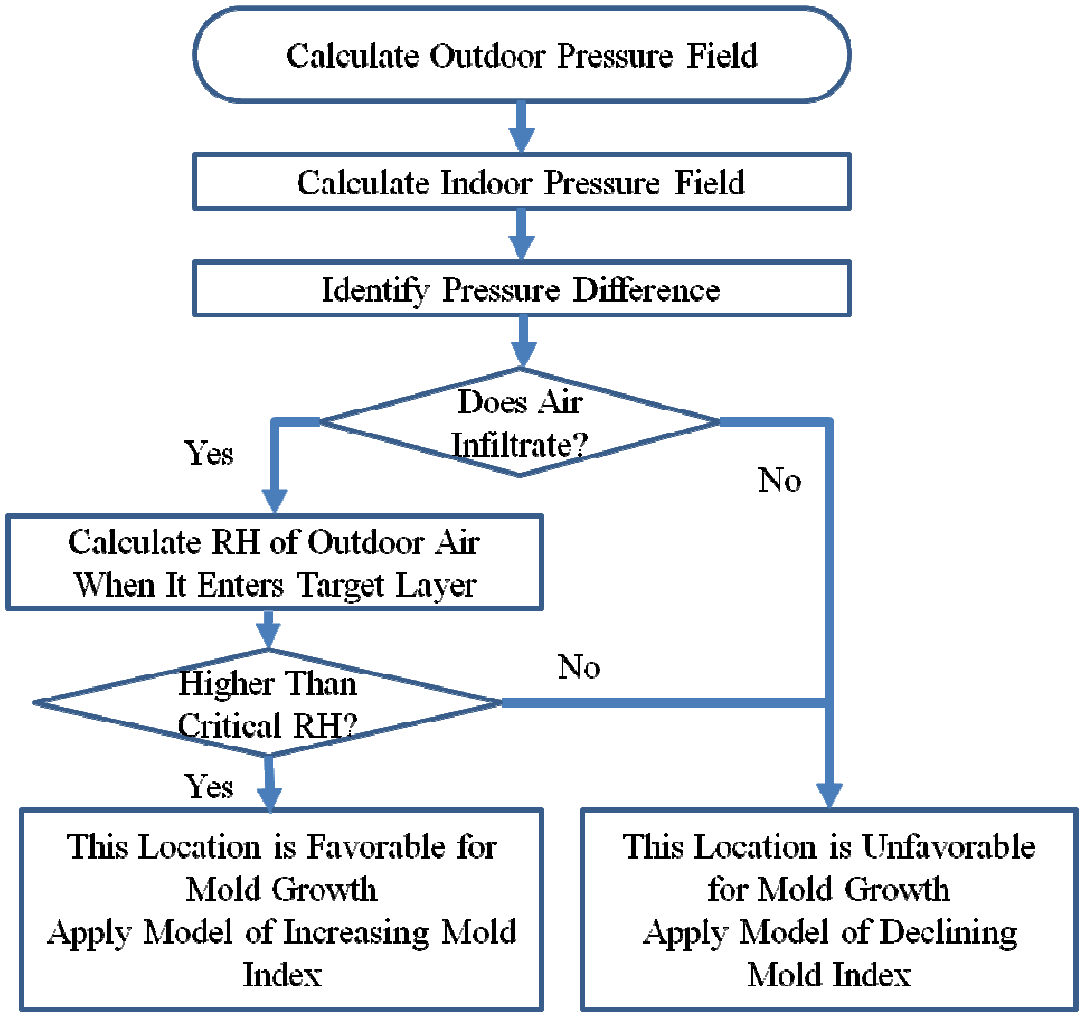

Figure 3-2 Flow chart showing how the mold index change is computed

The building envelope is divided into 9 sections, Top South West, Top South East, Top North West, Top North East, Bottom South West, Bottom South East, Bottom North West, Bottom North East, and Roof; all sections are assumed to have the same specific leakage area. Figure 3-3 is an illustration of the configuration modeled.

The hourly mold index level changes throughout the year are summed up to show the predicted mold index level change for a year, as well as the percentage of time a particular exposure experiences infiltration (denoted as "infiltration time."). Conditions for both 22°C and 24°C are simulated.

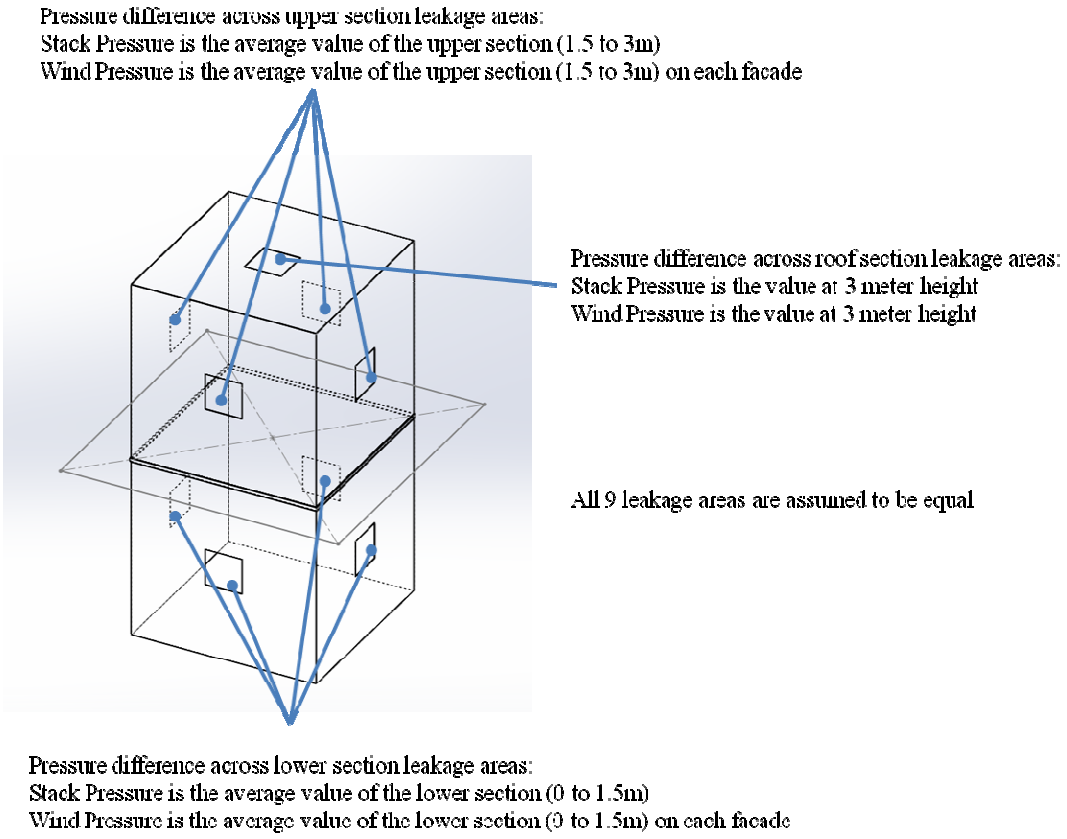

Figure 3-3 An illustration of the building configuration modeled

3.3.1 Modified Mold Growth Index for Multi Floor Buildings

The mold growth prediction model described above is applicable only on single-floor buildings due to the assumptions made. Some modifications should be made to

extend the model to cover multi floor buildings. One of the required changes is the equation utilized to obtain shielding coefficient since equation 3.8 is appropriate only for low-rise buildings. For high-rise buildings, a graphical method can be utilized [4, 68]. Figure 3-4 represents the graphical chart utilized for obtaining shielding coefficient of high-rise buildings.

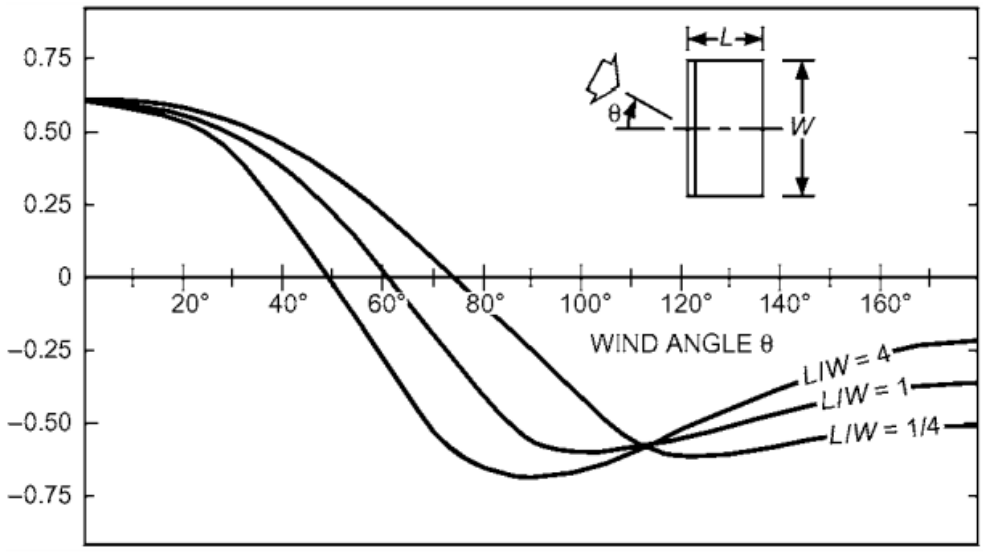

Figure 3-4 Surface-averaged wall pressure coefficients for tall buildings [68]

The above graphical chart is then processed in Excel to acquire shielding coefficient corresponding to different wind angles. Data for wind angle ranging from 0° to 180°, with a 5° increment, is fitted as shown in Figure 3-5. The fitted data points are listed in Table 3-5. (L/W ratio =1):

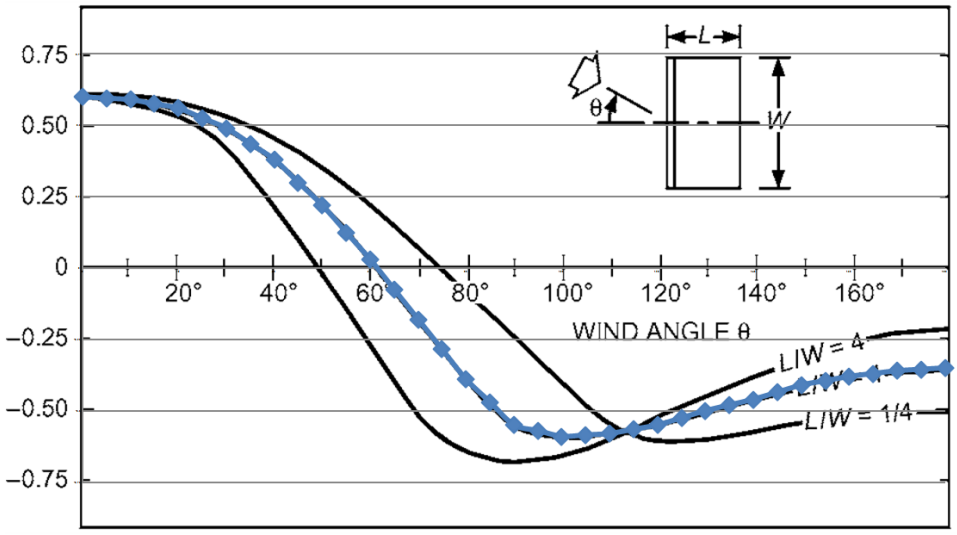

Figure 3-5 Data fitting on wind angle-shielding coefficient chart for tall buildings with 1:1 length-width ratio

Wind Angle θ	Shielding Coefficient	Wind Angle θ	Shielding Coefficient
0	0.6	**95**	-0.57
5	0.595	**100**	-0.59
10	0.59	**105**	-0.585
15	0.575	**110**	-0.58
20	0.56	**115**	-0.565
25	0.525	**120**	-0.55
30	0.49	**125**	-0.525
35	0.435	**130**	-0.5
40	0.38	**135**	-0.48
45	0.3	**140**	-0.46
50	0.22	**145**	-0.435
55	0.125	**150**	-0.41
60	0.03	**155**	-0.395
65	-0.075	**160**	-0.38
70	-0.18	**165**	-0.37
75	-0.285	**170**	-0.36
80	-0.39	**175**	-0.355
85	-0.47	**180**	-0.35
90	-0.55		

Table 3-5 Fitted data points for tall buildings with 1:1 length-width ratio

Two additional simulations, Case 7 and Case 8, are made by using the modified mold growth index based on pressurization levels for a multi-floor building. Case 7 has configurations similar to Case 4 which is described previously except for the following differences: first, the shielding coefficient for Case 7 is acquired from Table 3-5 instead of calculated by using equation 3.8. Second, the building is assumed to have eight floors and is 33.6 meters high. Third, the leakage area is still assumed evenly distributed but the total number of leakage paths on the walls are expanded from 8 to 32. That is, every floor is assumed having 4 identical leakage areas with one placed on each wall facade. Fourth, the indoor temperature is assumed constant at 24°C.

The building height, floors, and wall configurations for Case 7 correspond to Harrington Tower, an actual building located on the Texas A&M University main campus in College Station, TX. The building essentially has an occupancy schedule from 8AM to 5PM, Monday through Friday; however, the HVAC system has an operating schedule that is typically from 7AM to 7PM. Due to this reason, in Case 7 the building is no longer assumed to be maintained at the same pressurization level 24 hours a day, seven days a week. Instead, it is assumed that the building pressurization system can maintain the whole building at a positive pressure level during operating hours (7AM to 7PM, Monday through Friday), otherwise the whole building is assumed unpressurized. Since TMY3 dataset has no definition of weekdays, January 1st is assumed to be a Monday to make the simulation achievable.

The Case 8 simulation has the same configuration as Case 7 except for the wall configuration. The target layer temperature is assumed the same as the indoor temperature (24°C) instead of using simulated results from ANSYS®.

3.4 Modified Mold Growth Index Results

Four types of results are presented in this section. The "infiltration time" shown in figures such as Figure 3-6 is the percent of time a specific section of wall experiences infiltration. A section is assumed to experience infiltration if the outdoor pressure is higher than the indoor pressure.

The mold index level change shown in figures such as Figure 5 is the net change of the mold index after one year at a specific section. Results are also presented for each of the three different pressurization levels. A negative mold index level has no definition in the original research [40], and this would suggest dM/dt=0 once M=0. The negative values for annual change in mold index in the figures thus implicitly assume that the mold index had a significant positive value at the beginning of the year.

The "mold risk time" shown in figures such as Figure 6 is the percentage of time during each month that infiltration will lead to an increase in the value of the mold index. Infiltration is considered to increase the mold index if the RH of infiltrating air at the target layer, RH_T, is higher than the critical RH. RH_T is calculated based on Eqs. 3.12-3.14. Results are shown for both 22°C and 24°C indoor temperatures. Because different amounts of solar radiation fall on walls facing different directions, each wall orientation has a slightly different mold risk time. The average results for all surfaces analyzed are

presented as bars and the range of values for all surfaces analyzed are presented as whiskers in the mold risk figures.

3.4.1 Results of Case 1 Simulation

For an indoor temperature of 24°C, the results for infiltration time percentage, annual mold index change, and mold risk time percentage are shown in Figure 3-6, Figure 3-7 and Figure 3-8. For an indoor temperature at 22°C, the results are shown in Figure 3-9, Figure 3-10 and Figure 3-11. Significant differences can be found in mold risk time and mold index level change per year when changing the indoor temperature set-point by only 2°C. Figure 3-8 and Figure 3-11 show that the cumulative mold risk time is approximately half as long at 24°C compared to 22°C. The reduced mold risk time at 24°C causes all orientations to show an annual decrease in mold index, even at zero pressurization.

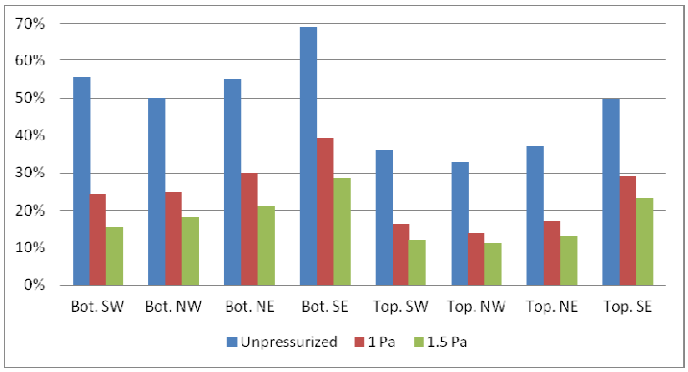

Figure 3-6 Case 1 infiltration time (%) (T_{Indoor}=24°C)

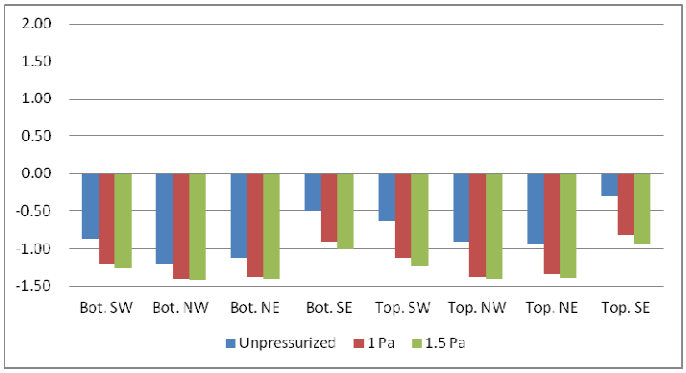

Figure 3-7 Case 1 mold index level change per year (24°C)

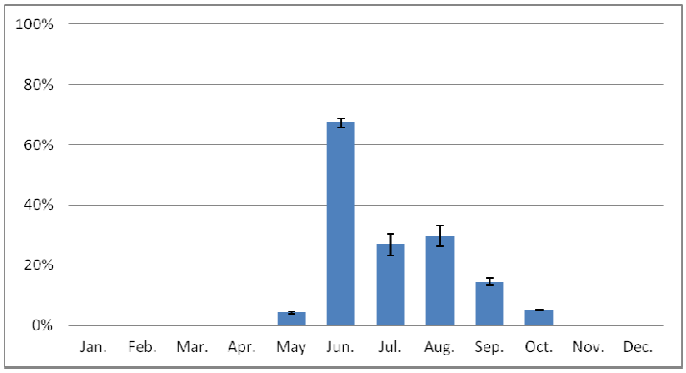

Figure 3-8 Case 1 mold risk time (24°C)

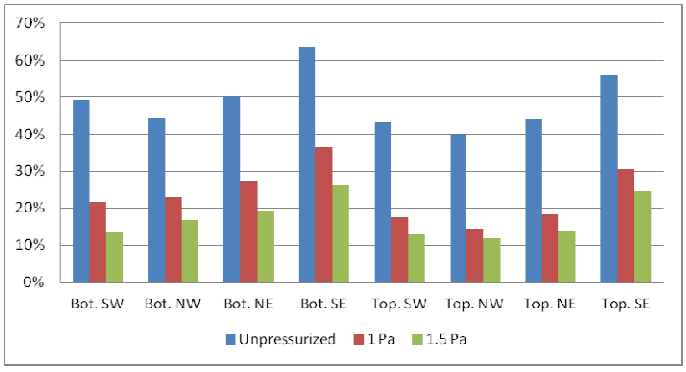

Figure 3-9 Case 1 infiltration time (%) (T_{Indoor}=22°C)

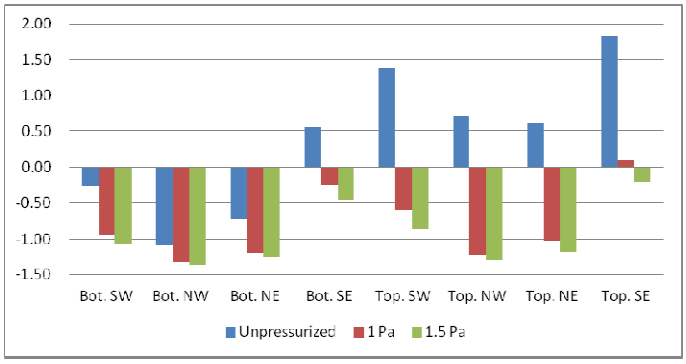

Figure 3-10 Case 1 mold index level change per year (22°C)

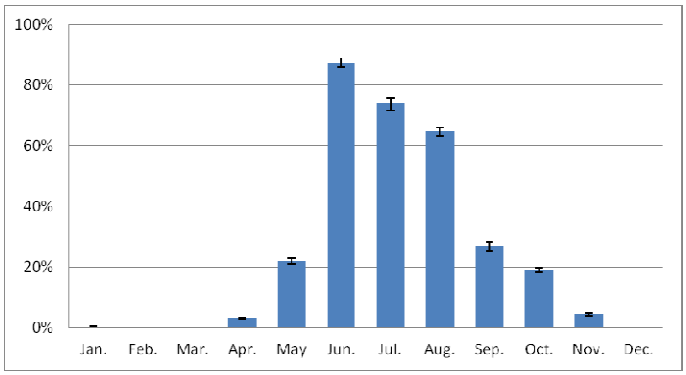

Figure 3-11 Case 1 mold risk time (22°C)

The mold index level change throughout the year for the Top SE section of wall at an indoor temperature set-point of 22°C, with a 1.5 Pa pressurization level is shown in Figure 3-12. The highest and lowest values on the figure are labeled to indicate the maximum and minimum mold index levels when negative values of the mold index level change are computed. The maximum mold index level reaches 0.62 for the case shown

in Figure 3-12 and returns to zero about the first of March. It would show an annual decrease of 0.20 if it had started at a value above 0.82.

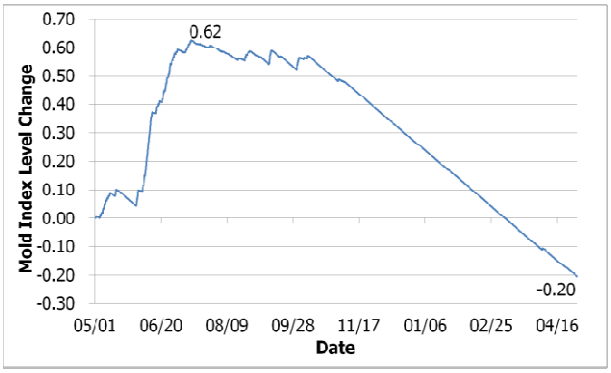

Figure 3-12 Case 1 mold index change as a function of time for one year starting at zero (Top SE, 22°C, 1.5 Pa pressurized)

3.4.2 Results of Case 2 Simulation

The results of the Case 2 simulation (Fort Worth, TX, 3 layer wall configuration) for infiltration time percentage, mold index change per year, and mold risk time percentage are shown in Figure 3-13, Figure 3-14 and Figure 3-15. Fort Worth has slightly more weather above 22ºC than College Station, but is somewhat less humid. Thus only two orientations show positive annual mold index change, even at zero pressurization (vs. five in College Station). The unpressurized case consistently shows substantial reductions in annual mold index relative to College Station, while the differences in the pressurized cases are much smaller. The mold risk time for Fort Worth at 22ºC is much closer to the College Station risk time at 24ºC than at 22ºC.

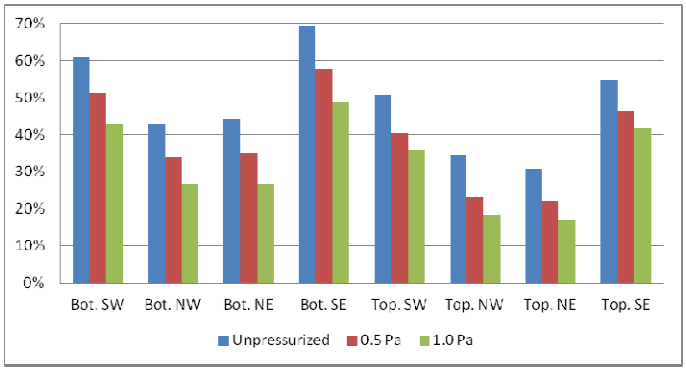

Figure 3-13 Infiltration time (%) (Case 2, 22°C)

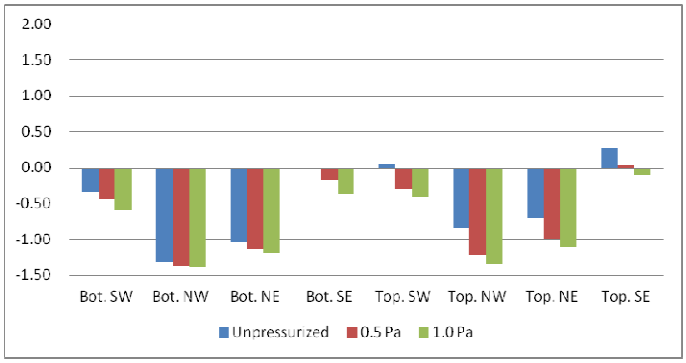

Figure 3-14 Mold index level change per year (Case 2, 22°C)

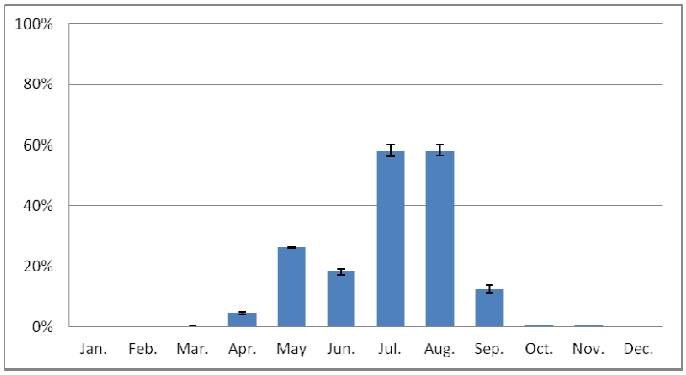

Figure 3-15 Mold risk time (Case 2, 22°C)

3.4.3 Results of Case 3 Simulation

The results of the Case 3 simulation (Atlanta, GA, 3 layer wall configuration) for infiltration time percentage, mold index change per year, and mold risk time percentage are shown in Figure 3-16, Figure 3-17 and Figure 3-18. Atlanta is cooler than College Station and has average relative humidity similar to Fort Worth. It is observed that the mold index level change per year remains negative even under the unpressurized condition, and the mold risk time is significantly less than that in College Station, TX.

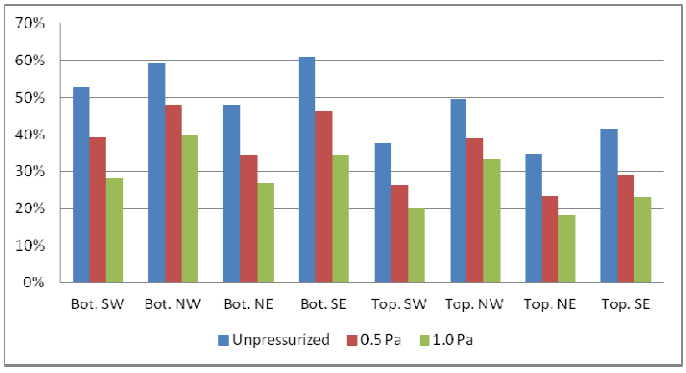

Figure 3-16 Infiltration time (%) (Case 3, 22°C)

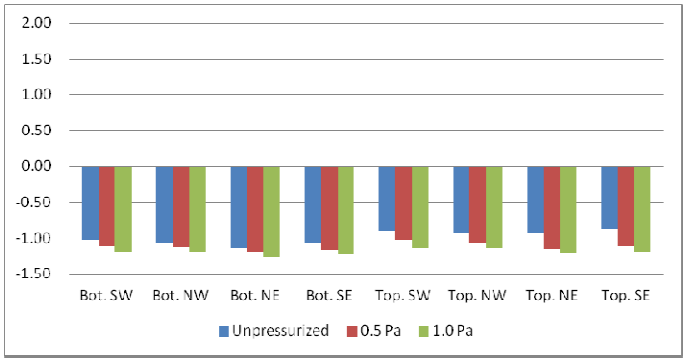

Figure 3-17 Mold index level change per year (Case 3, 22°C)

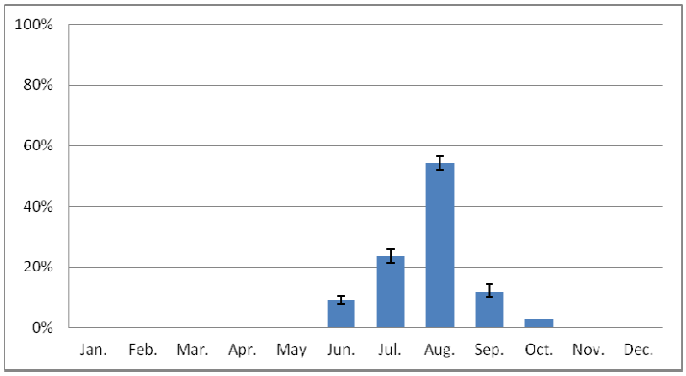

Figure 3-18 Mold risk time (Case 3, 22°C)

3.4.4 Results of Case 4 Simulation

The results of the Case 4 simulation (College Station, TX, 5 layer wall configuration) for mold index change per year and mold risk time percentage are shown in Figure 3-19, Figure 3-20 (24°C), Figure 3-21, and Figure 3-22 (22°C). This case represents another common wall construction in College Station, but the results show no significant differences from that for Case 1.

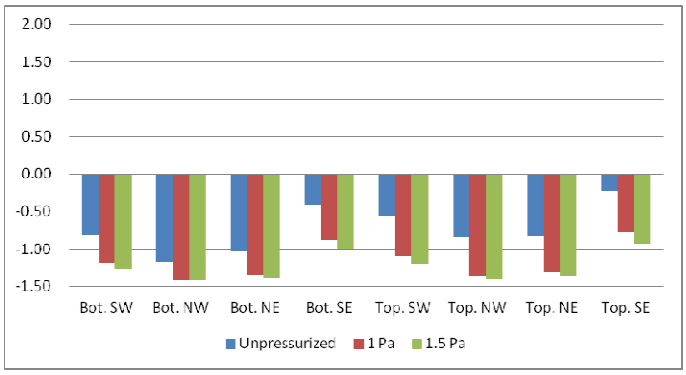

Figure 3-19 Mold index level change per year (Case 4, 24°C)

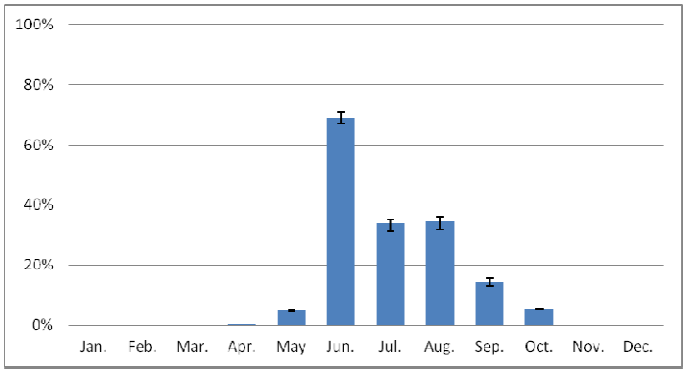

Figure 3-20 Mold risk time (Case 4, 24°C)

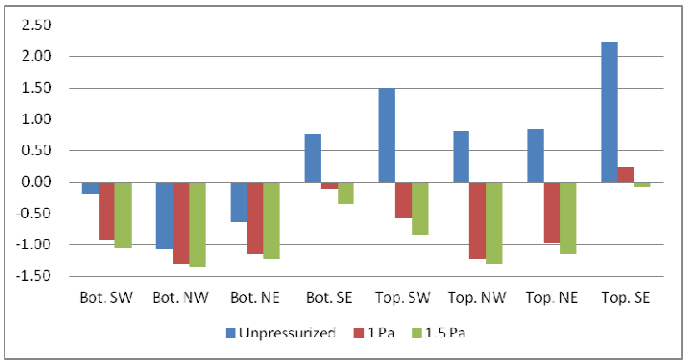

Figure 3-21 Mold index level change per year (Case 4, 22°C)

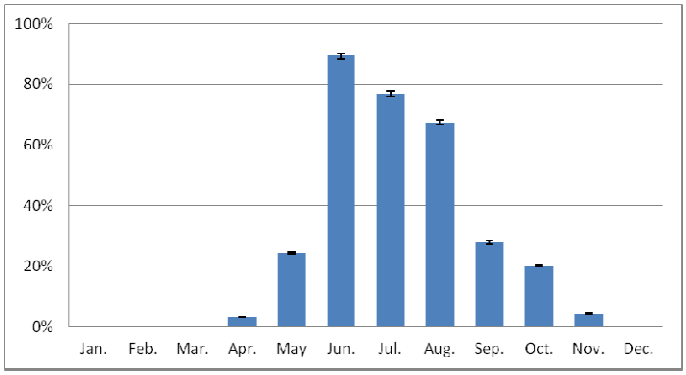

Figure 3-22 Mold risk time (Case 4, 22°C)

3.4.5 Results of Case 5 Simulation

The results of the Case 5 simulation (College Station, TX, fixed target layer temperature) for mold index change per year are shown in Figure 3-23 and Figure 3-24 for indoor temperatures of 24°C and 22°C respectively. This case essentially corresponds to an assumption of perfect wall insulation and changes from Case 1 are observable. Mold index level changes are noticeably less negative for several orientations and at 24°C, two unpressurized orientations show a positive index change, while these same unpressurized orientations showed negative change for Case 1.

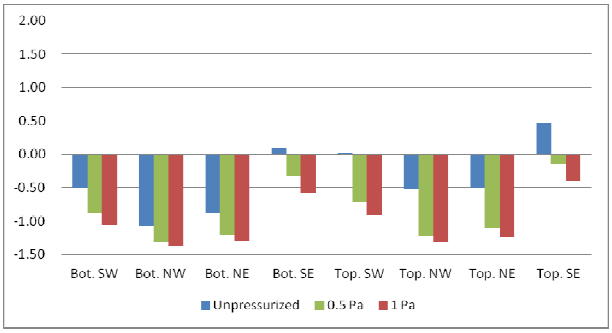

Figure 3-23 Mold index level change per year (Case 5, 24°C)

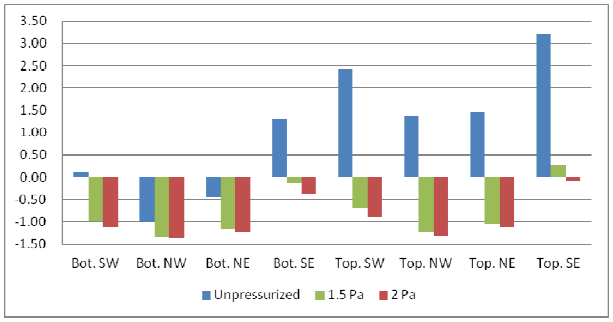

Figure 3-24 Mold index level change per year (Case 5, 22°C)

3.4.6 Results of Case 6 Simulation

The results of the Case 6 simulation (College Station, TX, 3 layer wall with thermal bridge configuration) for mold index change per year are shown in Figure 3-25. Due to the wall configuration, the target layer temperature is no longer uniform but has higher / lower temperature sections at any given time. The results show the mold index change per year for point A and point B. These locations should be the worst case and the best case on this wall in terms of mold growth, respectively. The locations of point A and point B are shown in Figure 3-26. Point A is at the gypsum board section over the wood stud, while point B is 8 in. from point A. In every case modeled, the mold index is slightly more negative at point A than at point B. Hence it is concluded that thermal bridging will decrease the mold index and can generally be ignored.

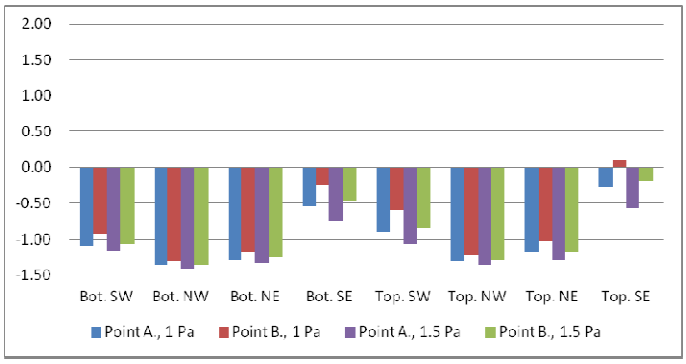

Figure 3-25 Mold index level change per year (Case 6, 22°C)

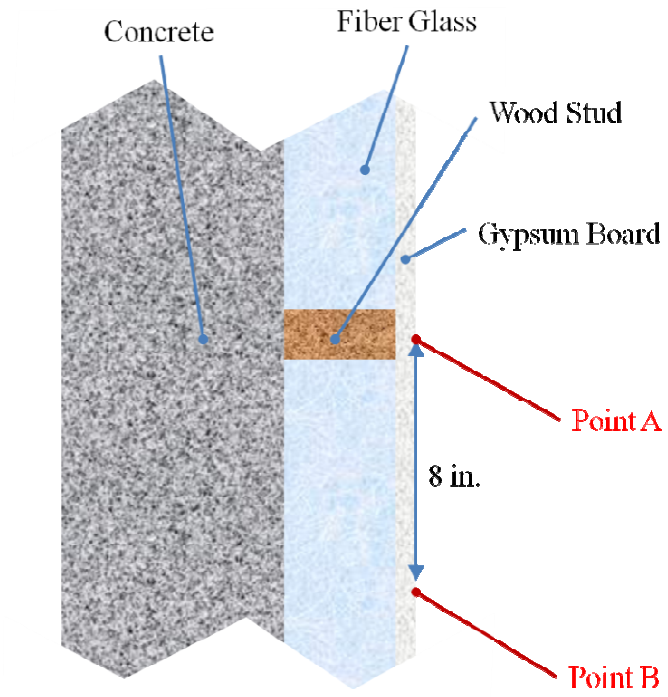

Figure 3-26 Cross section figure showing locations of points A and B (Case 6, 22°C)

3.4.7 Results of Case 7 Simulation

The results of the Case 7 simulation (Harrington Tower, 5 layer wall configuration) for mold index change per year are shown in Figure 3-27. Note that this time only the mold index change of top section (8th floor) walls are shown since these are expected to have the highest mold index change. For the unpressurized case, the results are similar to those for Case 1 and Case 4 at the unpressurized condition. All orientations show an annual decrease in mold index, but the margin is smaller than it is in Case 1 and Case 4. For the 7AM to 7PM, Mon. to Fri. pressurization case, all facades have an annual mold index change of approximately -0.8 except Top SE's is approximately -0.6. If the

pressurization scheme is switched to 24 hours, Mon. to Fri., all facades will have an annual mold index change below -1.

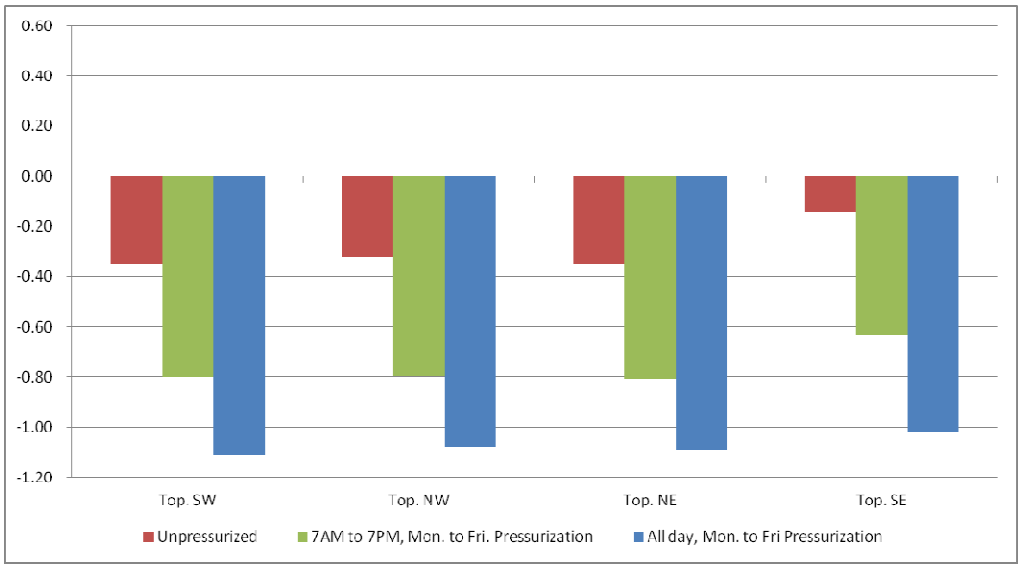

Figure 3-27 Mold index level change per year (Case 7, 24°C)

3.4.8 Results of Case 8 Simulation

The results of the Case 8 simulation (Harrington Tower, fixed target layer temperature) for mold index change per year are shown in Figure 3-28. Similarly, only the mold index change of top section (8th floor) walls are shown in the Figure. For the unpressurized case, the results are a little bit different from those in Case 5 at the unpressurized condition. All orientations of the Top section show an annual increase in mold index in Case 8 at the unpressurized condition but in Case 5, only SW and SE facades have a positive mold index change. The 7AM to 7PM, Mon. to Fri. pressurization, scheme is able to keep all facades with slightly negative annual mold

index changes, while the 24 hour, Mon. to Fri. pressurization scheme can further decrease the annual mold index.

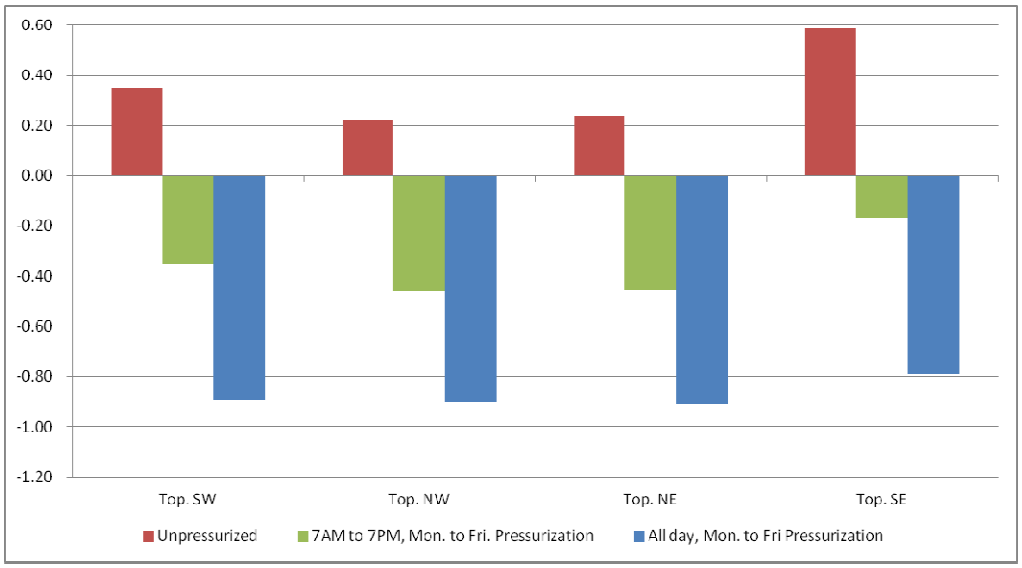

Figure 3-28 Mold index level change per year (Case 8, 24°C)

3.4.9 Weather Statistics

Annual and warm season (June, July and August) wind direction distributions show statistically how often, as a percent of time, the wind blows from different directions over a year and during the warm season, respectively. The results using average wind data for College Station, TX, Fort Worth, TX and Atlanta, GA are shown in Figure 3-29, Figure 3-30, and Figure 3-31, respectively (Extracted from TMY3 data). College Station and Ft. Worth do not show large seasonal differences in wind direction, but Atlanta shows twice as large a frequency of south winds in the warm season as annually, and twice as great a NW wind frequency annually as in the warm season.

Outdoor dry bulb temperature statistics as well as average wind speed and average RH for the three selected cities are shown using IECC/Building America climate region information in Table 3-6.

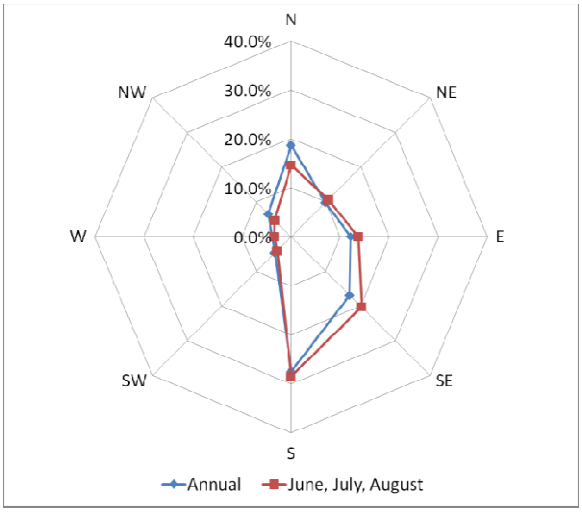

Figure 3-29 Wind direction distribution (College Station, TX)

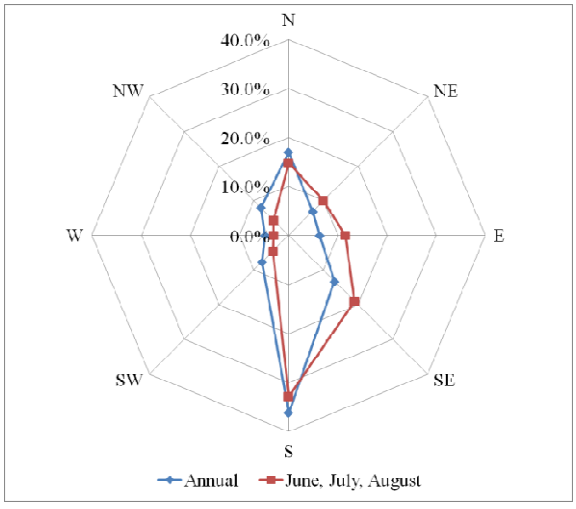

Figure 3-30 Wind direction distribution (Fort Worth, TX)

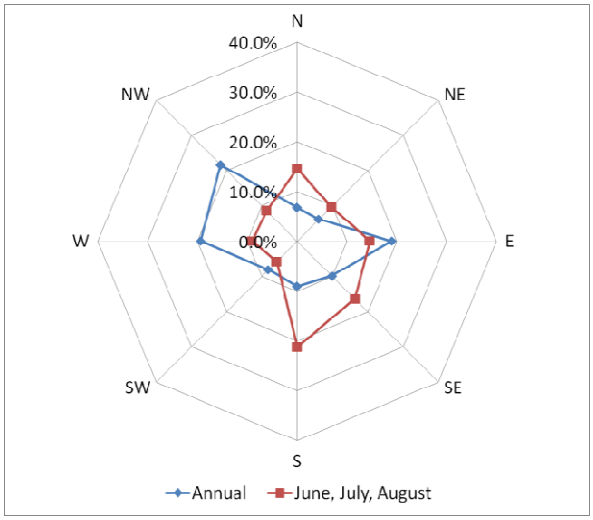

Figure 3-31 Wind direction distribution (Atlanta, GA)

City	College Station, TX		Fort Worth, TX		Atlanta, GA	
Climate Region by Building America	Hot and Humid		Hot and Humid		Mixed and Humid	
Climate Region by IECC	2A		3A		3A	
Time Frame	Yearly	June - August	Yearly	June - August	Yearly	June - August
Time % OA Temp. Above 24°C	31%	75%	34%	84%	22%	59%
Time % OA Temp. Above 22°C	44%	98%	43%	93%	32%	80%
Average Wind Speed (m/s)	3.18	2.44	4.56	4.52	4.04	3.49
Average RH	72%	75%	64%	64%	65%	69%

Table 3-6 Climate region classification, temperature, RH, and wind statistics for three cities. [69, 70]

3.5 Discussion of the Modified Mold Growth Index

The results of the mold index modeling for all cases are summarized in Table 3-7. The left-most column shows the case number and the temperature for which it was analyzed in °C. The second column shows the location and wall-type for each case

number/ inside temperature combination while the third column gives the minimum pressurization required (in 0.5 Pa increments) for which the annual M is negative for the wall section in that row.

Case/ Temp	Location/Wall Type	Min Pressure (Pa) for all M<0
#1 at 24°C	**College Station 3-layer**	**0.0**
#1 at 22°C	**College Station 3-layer**	**1.5**
#2 at 22°C	**Ft. Worth 3-layer**	**1.0**
#3 at 22°C	**Atlanta 3-layer**	**0.0**
#4 at 24°C	**College Station 5-layer**	**0.0**
#4 at 22°C	**College Station 5-layer**	**1.5**
#5 at 24°C	**College Station Fixed T_{surf}**	**0.5**
#5 at 22°C	**College Station Fixed T_{surf}**	**2.0**
#6 at 22°C	**College Station 3-layer Wood stud (Point A)**	**1.0**
#6 at 22°C	**College Station 3-layer-Fiberglass (Point B)**	**1.5**
#7 at 24°C	**College Station 5-layer**	**0.0**
#8 at 24°C	**College Station Fixed T_{surf}**	***M<0 with 7AM~7PM, Mon. to Fri. Pressurization**

*The pressurization level of Case 8 in the table doesn't not represent the minimum requirement since only three conditions are simulated.

Table 3-7 Minimum pressurization required to yield negative annual mold index change for all wall sections analyzed

Table 3-7 shows that only Case #1, Case #4, and Case #7 at 24°C and Case #3 at 22°C require no pressurization to achieve a negative annual mold index change on all wall sections. The other cases require pressurization ranging from 0.5 to 2.0 Pa to achieve this result.

This dissertation computes the nominal minimum values of positive pressurization required to produce a negative annual mold index value change due to infiltration induced moisture. Consideration of the capillary effect is beyond the scope of this investigation, because this issue, if a problem, cannot be resolved by raising the pressurization level. Per the U.S. Department of Energy, air movement accounts for more than 98% of all water vapor movement in building cavities [73]. Vapor diffusion through materials combined with heat transfer induced vapor transport accounts for only a tiny portion of vapor movement; thus these factors are neglected in this dissertation.

Thermally bridged areas like studs between wall insulation have lower thermal resistance than the insulated regions; thus higher indoor surface temperatures can be expected in the warm season where thermal bridges are present compared to non-bridged areas. These higher temperatures lower the RH and hence the amount of time the mold index will increase relative to the insulated areas during the warm season. It is true that lower thermal resistance may increase the mold index in colder weather. However, the risk of mold growth during these seasons comes from internally generated moisture and exfiltration which is not treated in this dissertation. Case 6 is a 2D thermal analysis evaluating the effect of thermal bridges. The results indicate that when the thermal bridge effect considered, the part of the wall section over the thermal bridge requires a

lower pressurization level to achieve a negative annual mold index change. It can be observed in Figure 3-25 that point A needs only 1 Pa pressurization to achieve the goal instead of 1.5 Pa However, keeping the annual mold index change negative for the whole wall area instead of just a partial area is a more reasonable goal. Thus in summary, the required pressurization level should remain unchanged when thermal bridges are present.

The strategy evaluated here does not eliminate the risk of mold growth, but identifies a minimum pressurization level that keeps net annual mold index change negative if the initial mold index is sufficiently positive that it does not drop to zero after one year. For all such cases, the annual mold index change will be zero if the initial mold index is zero. Hence mold growth may be controlled as intended by the wide-spread practice of positively pressurizing buildings in the humid regions of the U.S. There will still be periods favorable for mold growth during the warm season. As an example, Figure 3-12 shows the mold index level change over the year for a top SE section of a building in College Station, TX with a 22°C indoor temperature and 1.5 Pa pressurization level. The difference between the highest (early July) and lowest (end of April) value is 0.82 that is below 1, which means that the mold growth activity should be limited to the range M<1 continuously. It is noted that mold growth only becomes detectable by the naked eyes when M reaches 3 per the definition of M.

For all facades of a building in College Station, TX the bottom wall sections always have higher infiltration time than the top section of the same facade. This can be explained by the fact that even for a city in a hot and humid climate zone like College

Station, TX, TMY3 data indicates that only 2,699 hours of outdoor dry bulb temperature are above 24°C during a year, or 31% of the year. These values go up to 3,875 hours and 44% if the indoor air temperature set-point is lowered to 22°C; however, they are still below 50%. As a result, outside air tends to infiltrate through the bottom section more often due to the stack effect on an annual basis.

It may be noted that infiltration during the warm season (e.g. June, July, and August) is the main contributor to mold growth in these climates. During these months, the outdoor air temperature is above 24°C 75% of time and 98% of the time it is above 22°C. As a result, moist outdoor air goes in from the top and goes out from the bottom during these seasons. This explains why mold growth is more severe in the top sections even though they experience less infiltration time during the year.

The wind direction distribution data for College Station explains why the South-East facade experiences the most infiltration time as well as the most severe mold growth. The wind comes from the South, South-East, and East over 60% of the time during the warm season. This increases the amount of time moist air infiltrates into the building through the South-East facade. The annual and warm season wind direction distribution statistics are quite similar in College Station and Fort Worth, TX, but are quite different in Atlanta, GA. It may be more appropriate to use only warm season data wind data to analyze mold growth potential.

It may be observed that the same pressurization level has different effects on limiting infiltration time in different cities. 1 Pascal pressurization cuts off more than 40% of the infiltration time for a top South-East section compared to the unpressurized

case shown in Figure 3-6 (College Station, TX). However, the same pressurization level only reduces this infiltration time by 25% in Figure 3-13 (Fort Worth, TX). One of the reasons for this behavior is the wind speed difference. The average wind speed measured in Fort Worth, TX is 4.56 m/s, which is 43% higher than the 3.18 m/s measured in College Station, TX. Stronger wind results in a larger pressurization requirement to offset the pressure difference.

By comparing the results of Case 1 and Case 4, it is found that wall configuration effects the mold index level change. As expected, Case 4 has a higher mold index level change because its wall configuration has higher overall thermal resistance; thus the target layer temperature will be lower in the warm season. However, for the two wall configurations simulated, the mold index level change difference is small enough that the required pressurization level to control mold growth remains unchanged at the 0.5 Pa increments evaluated.

Case 5 assumes that the target layer temperature, T_{surf}, always equals the indoor air temperature. This approximates the behavior that would be expected from a wall with infinite thermal resistance and / or an "infinite" indoor combined heat transfer coefficient. When the outside air temperature is higher than the indoor air temperature, this also represents the worst-case scenario. As expected, this case has the highest net mold index level change; however, the model indicates a 2 Pa pressurization level is able to keep the annual net change negative for a 22°C indoor air temperature set-point.

The percentage of mold risk time is strongly influenced by site location, time of year and indoor air temperature set-point. In Atlanta, GA, infiltration is risk free for

mold growth from November to May even when indoor air temperature is set at 22°C. With the same set-point applied to a building in College Station, TX, there is risk of mold growth for more than 70% of the time in June, July and August. However, when the set-point rises to 24°C, this mold risk time drops below 40% except during June.

It is worth mentioning that wind direction and intensity are strongly influenced by local building geometry and terrain. Thus using the nearest airport wind data may not be accurate in a specific case. On the other hand, outdoor air temperature from a nearby weather station should be close to that experienced by the building except in cases where the building has large amounts of reflected solar radiation incident, or is surrounded by many surfaces that are highly solar absorptive. To validate the usage of temperature data the outdoor air temperature was measured on site in College Station, TX. Good agreement was found between the data on-site and that gathered from the weather station. The difference is generally less than 1°C. Other uncertainties like the evenly distributed leakage area assumption may not be true in practical cases and will influence the pressure field.

Mold growth is strongly dependent on the dry / wet pattern under the model utilized. Note that a continuous 24-hour dry time has the same effect as 6 hours of dry time per the model, which means that the average mold index level decline can range from -0.001333/hour (when the dry time duration is less than 6 hours) to -0.000333/hour (when the dry time duration is exactly 24 hours). Longer duration dry times will have an average decline close to -0.000667/hour; these are the values before multiplying by the material dependent coefficient C_{mat}.

Consider the example shown in Figure 3-12. During November to April the mold index level declines almost continuously and there is an approximately a straight line with a slope of -0.00066/hour. This can be explained by Figure 3-11 since infiltration has a lower risk of mold growth during these months. For the declining hours that occur during May to October, Table 3-8 represents the percentage by number of times and hours that fall into specific dry time durations.

Duration of Dry Time	% by number of times	% by total hours	Average Hourly M Change
1-6 hours	60.6%	7.8%	-0.00133
7-18 hours	20.2%	13.4%	-0.000433~ -0.00114
19-48 hours	11.5%	17.6%	-0.000333~ -0.0005
48+ hours	8.7%	61.2%	Incline to -0.00067

Table 3-8 Duration of dry time distribution during May to October (Case 1, Top SE, 22°C, 1.5 Pa pressurized)

In terms of number of incidents, the studied case suffers from frequent changes in dry / wet pattern where over 60% of the times when drying occurs are shorter than 6 hours in duration. However, in terms of total drying hours, long-duration drying times (48+ hours) account for over 60% of the total drying time even during May - October. This can be again explained by Figure 3-11 since in May, September and October, the

mold risk time remains well below 30%, so most of the drying time during these months consists of 48-hour or longer periods. As a result, the average mold index level decline from the May to October months is found to be -0.00064/hour. The duration of drying time during these months is effected by many factors. A worst-case scenario would assume the mold index level decline rate remains at -0.00066/hour from November to April and that all drying times during May to October fall in the range 19-48 hours and having an average mold index level decline of -0.00043/hour instead of -0.00064/hour. With the material dependent coefficient involved, the difference on annual mold index level change compared to the original case is +0.199; as a result, the 1.5Pa pressurization is still valid to keep the annual mold index change negative, but the margin shrinks from -0.20 to -0.001.

4. SCALE-MODEL OPERATION

4.1 Introduction

Following the concept of Internal Fan Balancing System described in the Introduction, a three-floor scale-model is built to demonstrate how the Internal Fan Balancing System can help reduce the required air flow to maintain building pressurization. The experiment results in this section will show the difference in required flow rate with and without Internal Balancing Fan Modules.

4.2 Methodology

The model built has three major sections as shown in Figure 4-1. There is a three floor “building” in the middle of the Figure; on left hand side there are three make-up air devices, one for each floor. Each of the make-up air devices consists of a PVC tube and a fan to pull air to pressurize the model building floor. On the right hand side of the Figure it can be observed that the 2nd and 3rd floors of the building are each connected to an individual chamber, while 1st floor is connected to ambient.

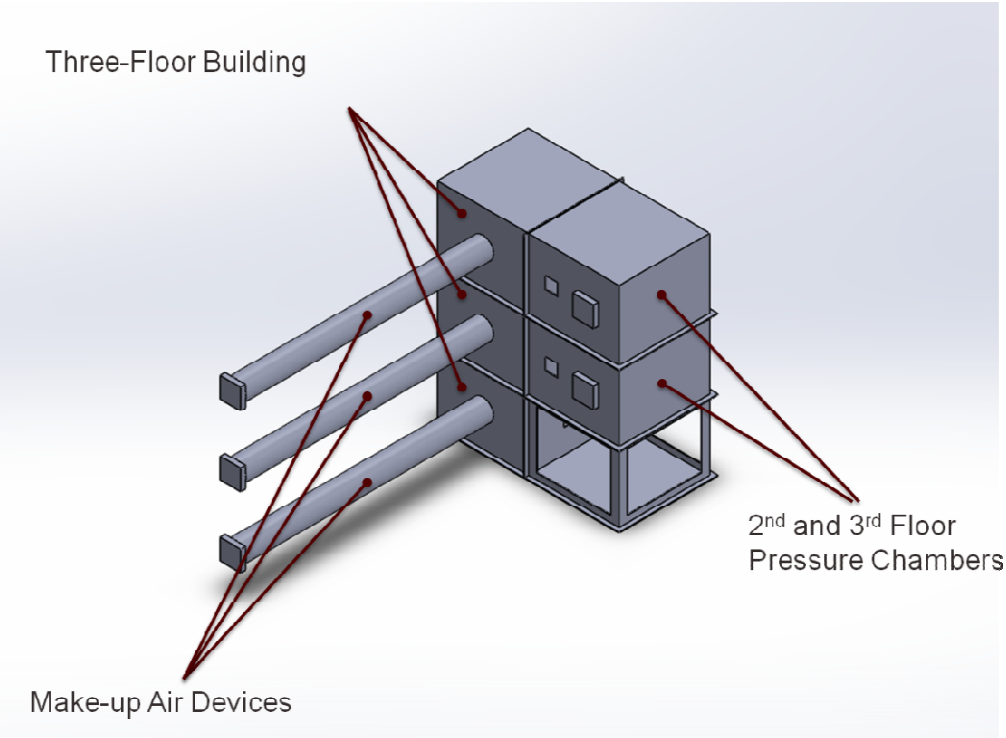

Figure 4-1 The scale-model consisting of three major parts

The purpose of these chambers is to simulate the stack effect. Since the stack effect is a function of height and temperature difference, the stack effect in the scale model with a 20°F temperature difference will be too small to detect. Although increasing the temperature difference can increase the stack effect, the indoor temperature would need to be raised to 300° F which may be unsafe. For this reason another approach is taken. As shown in Figure 4-2, each of the 2nd and 3rd floors of the model building has a 60mm x 60mm leakage area connected to a "chamber" acting as the outdoor environment that has a pressure relief area and a variable speed fan attached to control the chamber pressure while the 1st floor is connected directly to the ambient. When the

higher floor's chamber is set at higher pressure than the lower chamber, the air will tend to flow from the higher chamber to the higher floor and from the lower floor to the lower chamber assuming no make-up air is pulled in. This is similar to what happens in a real building in the warm season, where air tends infiltrate on higher floors and exfiltrate on lower floors.

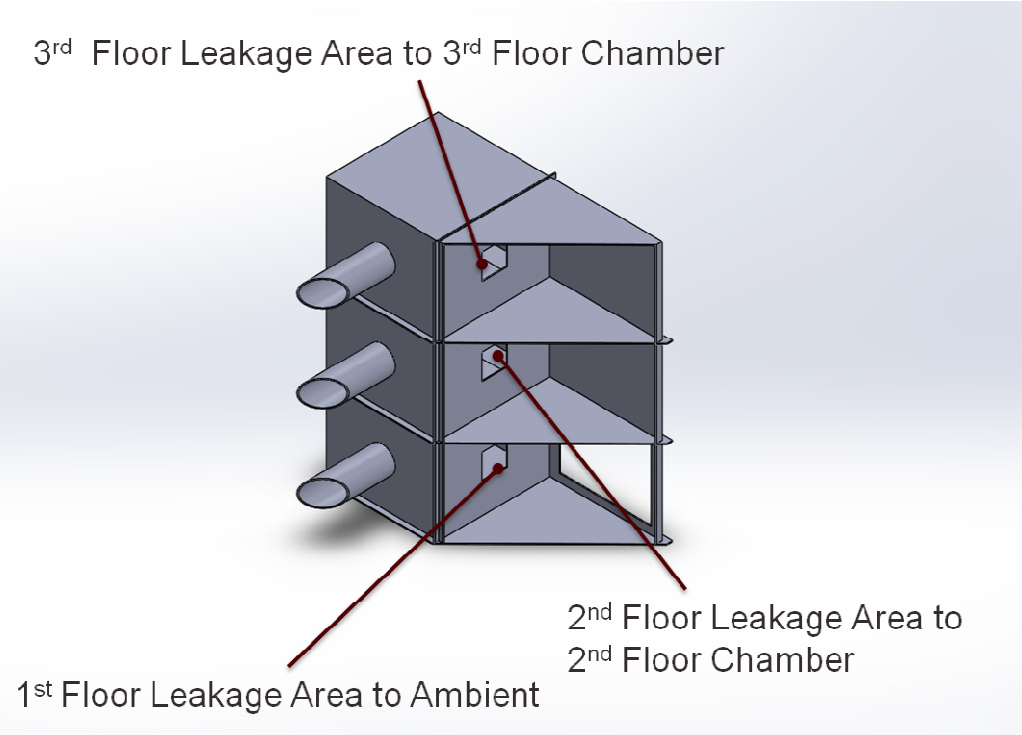

Figure 4-2 Cross-section figure showing the leakage area connecting to individual chambers except 1st floor

All seven fans used in the scale model (three make-up air fans, two internal balancing fans, and two chamber pressure control fans) are identical 60mm x 60mm

x15mm ADDA Inc. model number AD0612MS-D70GL axial fans. These are 12V fans with a current rating 110mA. The fan curve and detailed specification provided by the manufacturer are shown in Figure 4-3 and Figure 4-4, respectively.

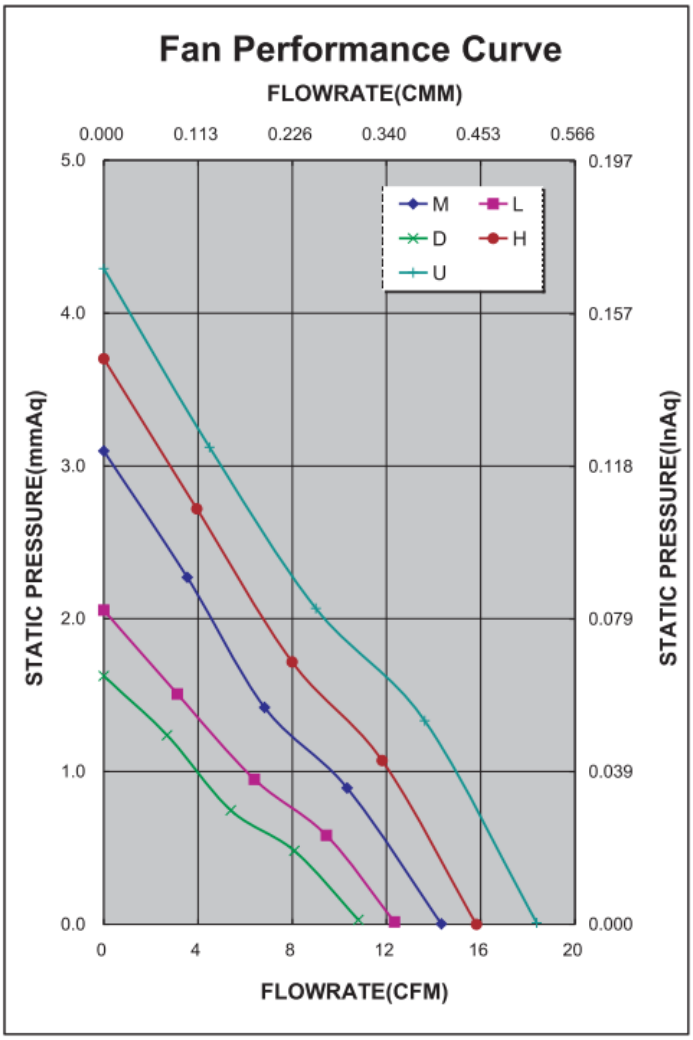

Figure 4-3 Manufacturer provided fan curve of the fan used on scale-model (the blue curve is by default for the model AD0612MS-D70GL)

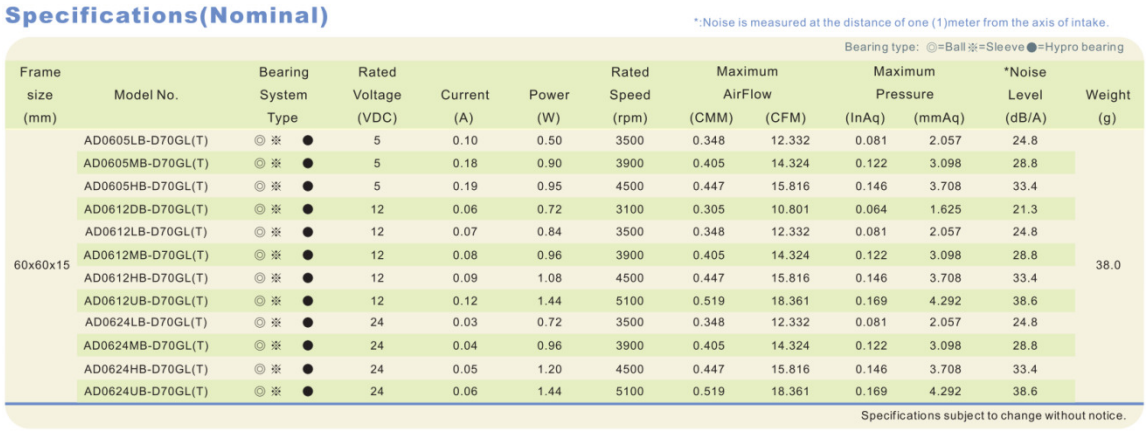

Specifications(Nominal)

*:Noise is measured at the distance of one (1)meter from the axis of intake.

Bearing type: ◎=Ball ❄=Sleeve ●=Hypro bearing

Frame size (mm)	Model No.	Bearing System Type	Rated Voltage (VDC)	Current (A)	Power (W)	Rated Speed (rpm)	Maximum AirFlow (CMM)	Maximum AirFlow (CFM)	Maximum Pressure (InAq)	Maximum Pressure (mmAq)	*Noise Level (dB/A)	Weight (g)
60x60x15	AD0605LB-D70GL(T)	◎ ❄ ●	5	0.10	0.50	3500	0.348	12.332	0.081	2.057	24.8	38.0
	AD0605MB-D70GL(T)	◎ ❄ ●	5	0.18	0.90	3900	0.405	14.324	0.122	3.098	28.8	
	AD0605HB-D70GL(T)	◎ ❄ ●	5	0.19	0.95	4500	0.447	15.816	0.146	3.708	33.4	
	AD0612DB-D70GL(T)	◎ ❄ ●	12	0.06	0.72	3100	0.305	10.801	0.064	1.625	21.3	
	AD0612LB-D70GL(T)	◎ ❄ ●	12	0.07	0.84	3500	0.348	12.332	0.081	2.057	24.8	
	AD0612MB-D70GL(T)	◎ ❄ ●	12	0.08	0.96	3900	0.405	14.324	0.122	3.098	28.8	
	AD0612HB-D70GL(T)	◎ ❄ ●	12	0.09	1.08	4500	0.447	15.816	0.146	3.708	33.4	
	AD0612UB-D70GL(T)	◎ ❄ ●	12	0.12	1.44	5100	0.519	18.361	0.169	4.292	38.6	
	AD0624LB-D70GL(T)	◎ ❄ ●	24	0.03	0.72	3500	0.348	12.332	0.081	2.057	24.8	
	AD0624MB-D70GL(T)	◎ ❄ ●	24	0.04	0.96	3900	0.405	14.324	0.122	3.098	28.8	
	AD0624HB-D70GL(T)	◎ ❄ ●	24	0.05	1.20	4500	0.447	15.816	0.146	3.708	33.4	
	AD0624UB-D70GL(T)	◎ ❄ ●	24	0.06	1.44	5100	0.519	18.361	0.169	4.292	38.6	

Specifications subject to change without notice.

Figure 4-4 Manufacturer provided detailed specification of the fan used (AD0612MS-D70GL)

In general, it is more difficult to measure the air flow rate precisely than to measure the static pressure. To solve this problem, the make-up air device is designed following AMCA Standard 210-99 "Laboratory Method of Testing Fans for Aerodynamic Performance Rating" [71], which is also the standard adopted by the fan manufacturer to prepare the fan curve. By doing this, the air flow can be determined by measuring the fan speed and the static pressure rather than measuring the air flow directly. The make-up air devices are made from Polyvinyl Chloride (PVC) pipe and the fan mentioned above except the flow straightener is made by Polylactic Acid (PLA) using 3D printing technology. The actual dimensions of the make-up air device are shown in Figure 4-5.

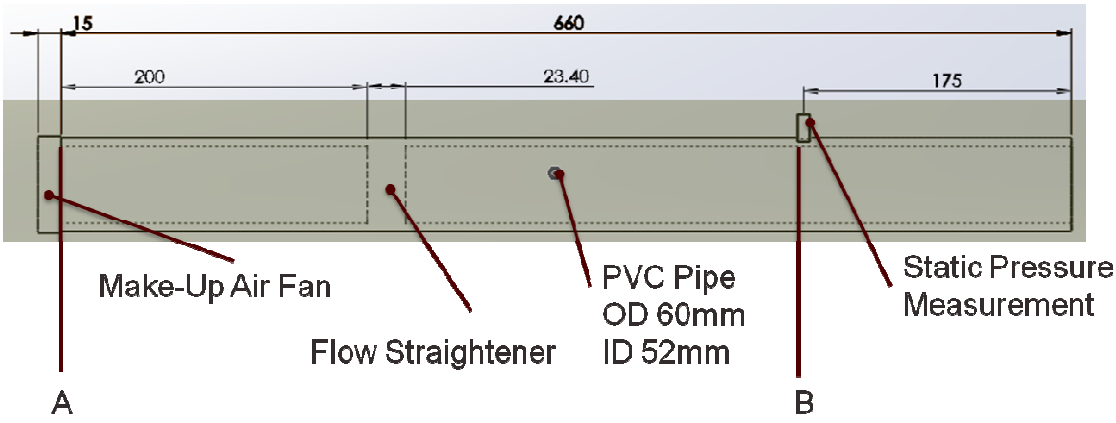

Figure 4-5 The dimensions of the make-up air device (units: mm)

By following AMCA Standard 210-99, it is necessary to compensate the measured static pressure to determine "true" static pressure of the fan. Equations 4.1 – 4.5 from the standard are applied to do the compensation [71]: (Plane A and plane B are shown in Figure 4-5)

$$P_{static} = P_{s,B} + f\left(\frac{L_{A,B}}{D_h} + \frac{L_e}{D_h}\right)P_{v,B} \quad (4.1)$$

$$f = \frac{0.14}{Re^{0.17}} \quad (4.2)$$

$$Re = \frac{\rho V D_h}{\mu} \quad (4.3)$$

$$\frac{L_e}{D_h} = \frac{15.04}{\left[1-26.65\left(\frac{y}{D}\right)+184.6\left(\frac{y}{D}\right)^2\right]^{1.83}} \quad (4.4)$$

$$P_{v,B} = \frac{\rho V^2}{2} \quad (4.5)$$

where:

P_{static} is the compensated static pressure (Pa)

$P_{s,B}$ is the static pressure measured at plane B (Pa)

f is the friction coefficient

$L_{A,B}$ is the length between plane A and plane B (Figure 4-5) (m)

D_h is the hydraulic diameter (m)

L_e is the flow straightener equivalent length (m)

$P_{v,B}$ is the mean velocity pressure at plane B (Pa)

Re is the Reynolds Number

ρ is the density of air (kg/m^3)

V is the mean velocity of air (m/s)

μ is the dynamic viscosity (Pa · s)

y is the element thickness of the flow straightener (m)

D is the equivalent diameter of the flow straightener (m)

Figure 4-3 shows that the fan curve consists of several generally linear relationships between static pressure and flow rate. Three linear regions are 0%-25%, 25%-50%, and 75%-100% of the maximum flow rate (where static pressure equals zero). In the 50-75% region the relation between static pressure and flow rate is less linear due to the turning point. However, this region can be expressed approximately by two linear lines, one for 50%-62.5% and the other for 62.5%-75% of the maximum flow rate. The curve fitting process is done in Excel and the results suggest that the fan curve with fan speed at 3,500 RPM can be expressed by equations 4.6 – 4.10:

$$Q_{fan} = C1 * P_{static} + C2 \ (when \ 0 < P_{static} \leq P_{s,75\%}) \qquad (4.6)$$

$$Q_{fan} = C3 * P_{static} + C4 \ (when \ P_{s,75\%} < P_{static} \leq P_{s,62.5\%}) \qquad (4.7)$$

$$Q_{fan} = C5 * P_{static} + C6 \ (when \ P_{s,62.5\%} < P_{static} \leq P_{s,50\%}) \quad (4.8)$$

$$Q_{fan} = C7 * P_{static} + C8 \ (when \ P_{s,50\%} < P_{static} \leq P_{s,25\%}) \quad (4.9)$$

$$Q_{fan} = C9 * P_{static} + C10 \ (when \ P_{s,25\%} < P_{static} \leq P_{s,0\%}) \quad (4.10)$$

where:

Q_{fan} is the fan air flow to be determined (m^3/s)

P_{static} is the compensated static pressure (Pa)

$P_{s,0\%}$ is the static pressure matching the 0% of the max. flow rate (20.11 Pa)

$P_{s,25\%}$ is the static pressure matching the 25% of the max. flow rate (14.72 Pa)

$P_{s,50\%}$ is the static pressure matching the 50% of the max. flow rate (9.42 Pa)

$P_{s,62.5\%}$ is the static pressure matching the 62.5% of the max. flow rate (7.46 Pa)

$P_{s,75\%}$ is the static pressure matching the 75% of the max. flow rate (5.98 Pa)

C1= -0.0002445, C2= 0.0058528

C3= -0.000417, C4= 0.006884907

C5= -0.00433, C6= 0.00700448

C7= -0.0002762, C8= 0.005527644

C9= -0.0002712, C10= 0.005453745

As mentioned above, the equations are valid when the fan speed is at 3,500 RPM. When the fan is running at a different speed, the following fan laws are applied:

$$k = (N_{new} / N_{old}) \quad (4.11)$$

$$(P_{new} / P_{old}) = k^2 \quad (4.12)$$

$$(Q_{new} / Q_{old}) = k \quad (4.13)$$

where:

k is the fan speed ratio

N_{old} is the original fan speed (3,500 RPM)

N_{new} is the new fan speed in RPM

P_{old} is the static pressure when the fan is running at 3,500 RPM

P_{new} is the static pressure when the fan is running at new speed

Q_{old} is the flow rate when the fan is running at 3,500 RPM

Q_{new} is the flow rate when the fan is running at new speed

By equations 4.11, 4.12 and 4.13, new equations for determining the air flow rate when the fan is running at different speeds can be derived from equations 4.6-4.10:

$$Q_{fan} = \frac{C1*P_{static}}{k} + C2 * k \ (when\ 0 < P_{static} \leq k^2 * P_{s,75\%}) \quad (4.14)$$

$$Q_{fan} = \frac{C3*P_{static}}{k} + C4 * k \ (when\ k^2 * P_{s,75\%} < P_{static} \leq k^2 * P_{s,62.5\%}) \quad (4.15)$$

$$Q_{fan} = \frac{C5*P_{static}}{k} + C6 * k \ (when\ k^2 * P_{s,62.5\%} < P_{static} \leq k^2 * P_{s,50\%}) \quad (4.16)$$

$$Q_{fan} = \frac{C7*P_{static}}{k} + C8 * k \ (when\ k^2 * P_{s,50\%} < P_{static} \leq k^2 * P_{s,25\%}) \quad (4.17)$$

$$Q_{fan} = \frac{C9*P_{static}}{k} + C10 * k \ (when\ k^2 * P_{s,25\%} < P_{static} \leq k^2 * P_{s,0\%}) \quad (4.18)$$

The main building model consists of three identical floors, each floor is 11in by 11in by 8.5in. As illustrated in Figure 4-1, each floor is connected to a make-up air device as described previously. Besides, each of the second and third floors is connected to a pressure chamber that has the same size as a building floor. On each chamber there

exists a chamber pressure control fan and a square pressure relief hole that is 40mm x 40mm. Figure 4-6 illustrates the location of pressure relief holes and chamber pressure control fans.

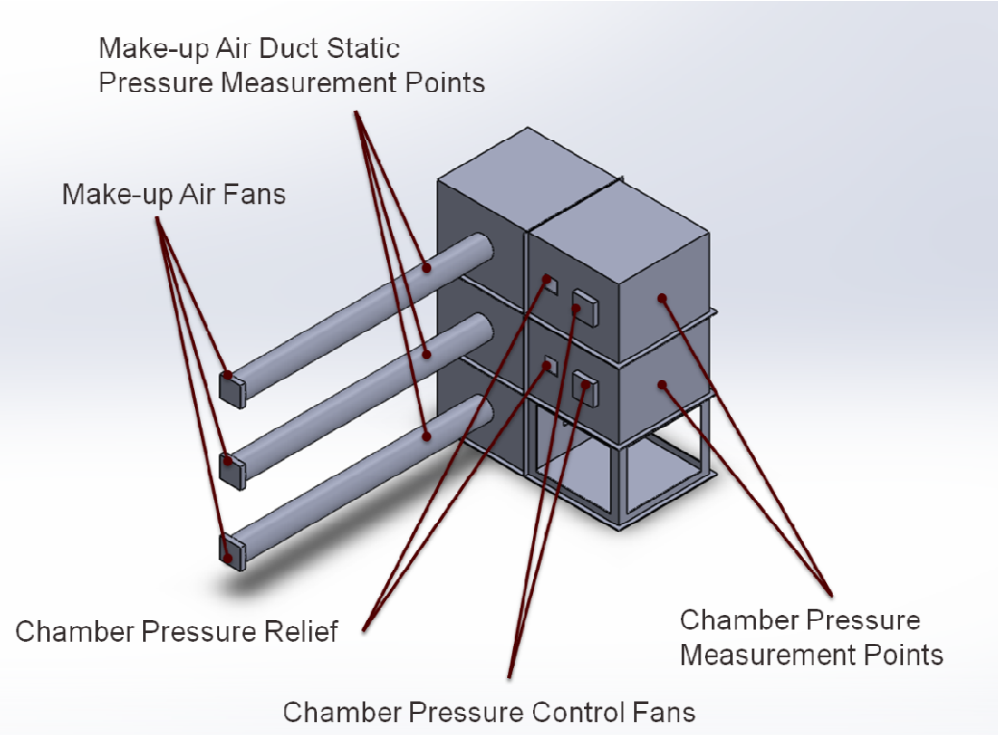

Figure 4-6 Locations of chamber pressure relief holes and pressure control fans

On each of the 2nd and 3rd floors, an internal balancing fan and a leakage area connect to the 1st floor and the 2nd floor, respectively. The leakage area is a 35mm. diameter round hole. Figure 4-7 illustrates the location of the internal balancing fan and the leakage area.

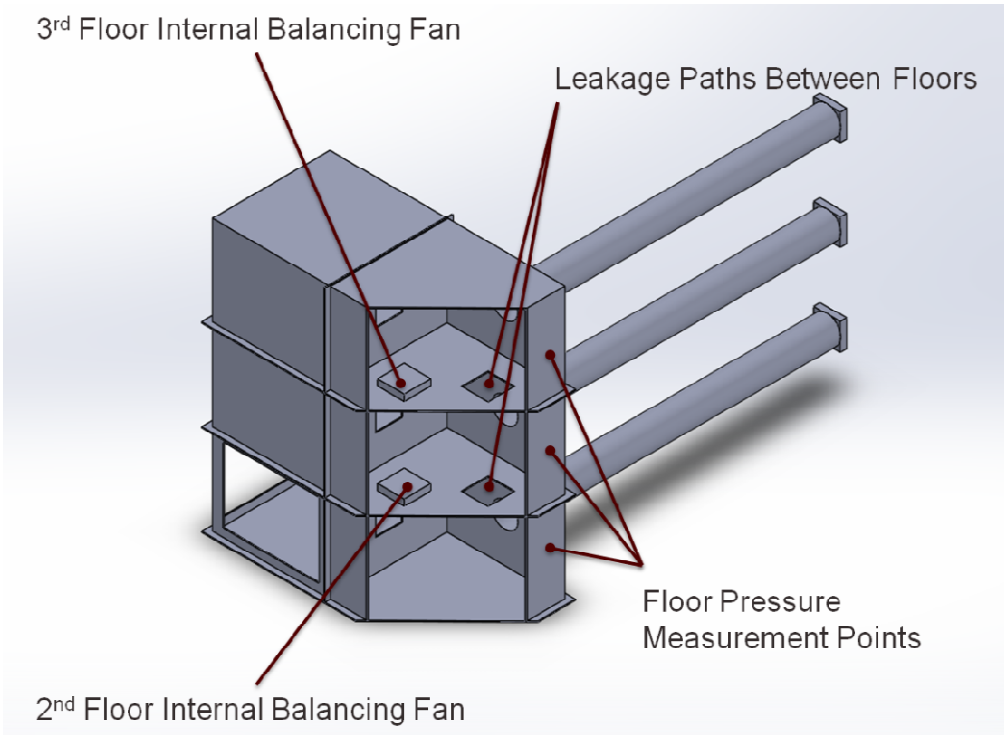

Figure 4-7 Different angle of cross-section figure showing the location of the internal balancing fans and leakage areas

Eight Setra® model 264 bi-directional differential pressure sensors are installed to monitor the pressure differences. The low port of each pressure senor is connected to the ambient and the high ports are connected to varied locations, thus all pressure readings are differential compared to ambient pressure. Five "virtual" pressure readings that are not directly measured but derived from actual readings are defined for further usage. For example, Virtual pressure P_{second} is defined as the second floor pressurization level, which is the value of the 2nd floor building pressure P2 minus 2nd floor chamber pressure P7 (indoor minus outdoor). Table 4-1 is a summary of the pressure sensors'

usage and the locations of measurement points can be found in Figure 4-1, Figure 4-6, and Figure 4-7. Table 4-2 is a summary of the virtual pressure readings and Figure 4-8 illustrates the definition of virtual pressure readings.

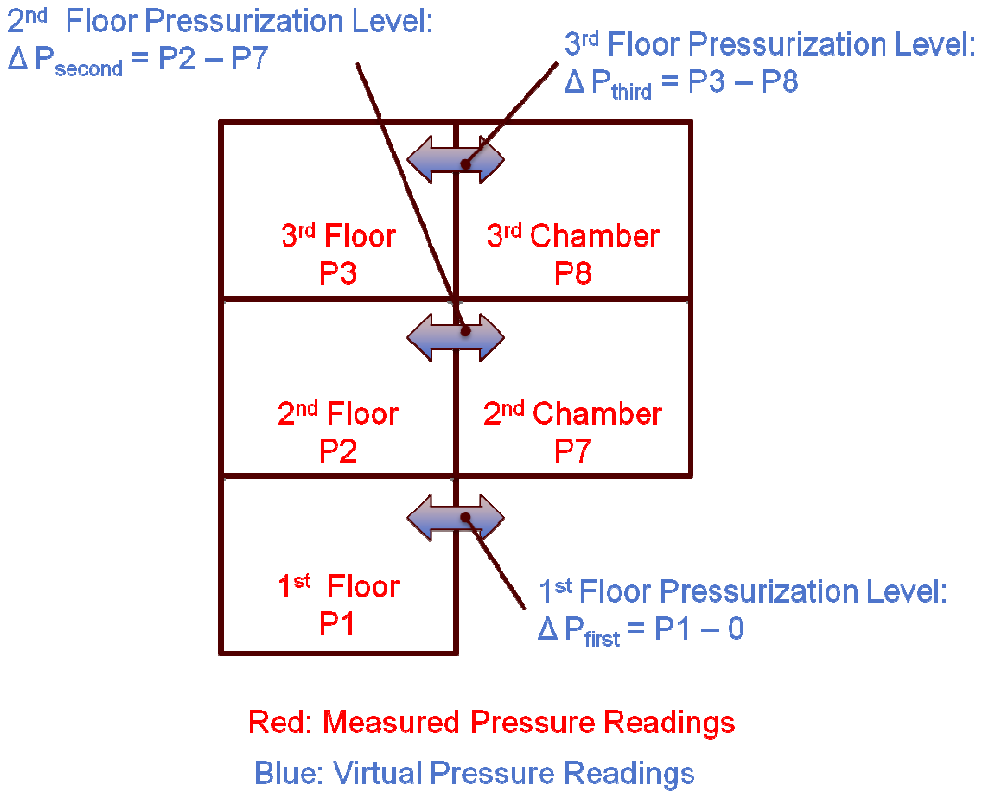

Figure 4-8 Explanation of virtual pressure readings

Pressure Sensor No.	Pressure Sensor Usage
P1	1st floor of the building
P2	2nd floor of the building
P3	3rd floor of the building
P4	1st floor's make-up air device
P5	2nd floor's make-up air device
P6	3rd floor's make-up air device
P7	2nd floor's pressure chamber
P8	3rd floor's pressure chamber

Table 4-1 A summary of pressure sensors' usage

Name	Definition	Calculation
ΔP_{first}	First Floor Pressurization Level	P1
ΔP_{second}	Second Floor Pressurization Level	P2-P7
ΔP_{third}	Third Floor Pressurization Level	P3-P8
$\Delta P_{2nd-1st}$	Second Floor Pressurization Level minus First Floor Pressurization Level	$\Delta P_{second} - \Delta P_{first}$
$\Delta P_{3rd-2nd}$	Third Floor Pressurization Level minus Second Floor Pressurization Level	$\Delta P_{third} - \Delta P_{second}$

Table 4-2 A summary of virtual pressure readings

Both the main building and the pressure chambers are mainly constructed from 1.5mm chipboard; PLA frames printed by a 3D printer are utilized on the chipboard junctions to make tighter connections. Hot glue and duct tape are utilized to seal the possible leakage path at the junctions of chipboard as well as the junctions of PVC pipes and fans.

4.3 Scale-Model Controller Configuration and Operation

An Arduino Leonardo compatible control board (Part Number:DFR0321) manufactured by DFROBOT with two SMAKN® PWM motor driver shields stacked on top as shown in Figure 4-9 are utilized in the central control unit. Each of the shields has four channels which are able to control up to four DC fans with a rating of 4.5VDC to 13.5VDC and 1.2A per channel. The shield is capable of using Pulse Width Modulation (PWM) control to adjust voltage applied on each channel (fan), the resolution of the PWM control is 8-bit, ranging 0-255. Here it means that the voltage applied to the fans can be modulated in a range from 0V to 12V with a minimum 0.047V increment or decrement.

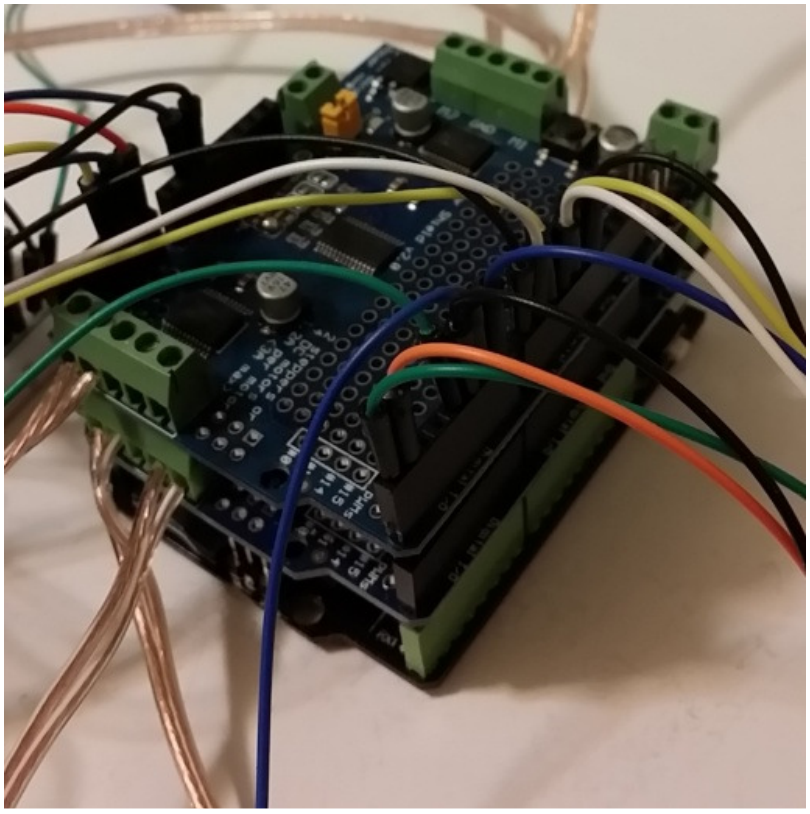

Figure 4-9 Central control unit: top: motor shield board A, middle: motor shield board B, bottom: Arduino Leonardo compatible control board

Each of the fans, including make-up air fans, internal balancing fans, and chamber pressure adjusting fans, is connected to an individual channel on the motor shields. Each of the fans is controlled by a unique feedback signal. In this dissertation, the P controller as shown in Figure 4-10 is utilized and defined by Equations 4.19 and 4.20. The proportional gain is set at 2 and the controller output is rounded up to an integer value because the controller only accepts integer signals (0 to 255)

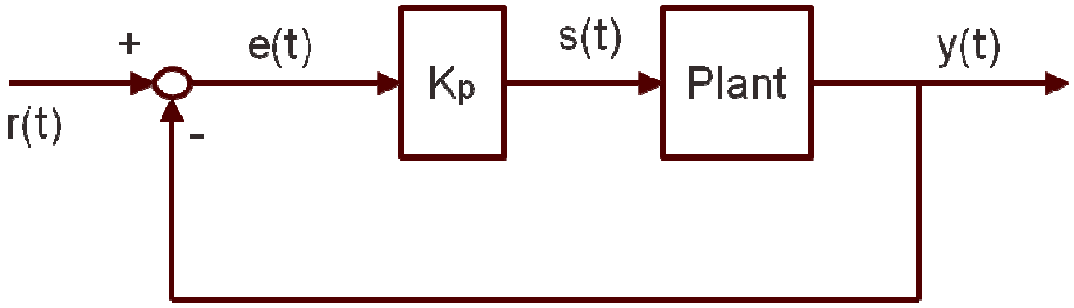

Figure 4-10 P control diagram

$$s(t) = K_P * e(t) \quad (4.19)$$

$$e(t) = r(t) - y(t) \quad (4.20)$$

where:

$s(t)$ is the controller output

K_P is the proportional gain

$e(t)$ is the error

$r(t)$ is the reference signal (pressure set-point)

$y(t)$ is the output signal (actual pressure)

The control sequence is shown in Figure 4-11, while the matching motor shield channels and the control logic are listed in Table 4-3 and the default pressure set points are listed in Table 4-4. The control codes are written under Arduino IDE 1.6.3 environment.

Fan Name	Motor Channel	Control Logic
1F_Make-Up Air Fan	A3	Increase Fan Speed if: Any of ΔP_{first}, ΔP_{second}, or ΔP_{third} is Below $SP_{MIN,BLDG}$ Decrease Fan Speed if: All of ΔP_{first}, ΔP_{second}, and ΔP_{third} are Above $SP_{MAX,BLDG}$
2F_Make-Up Air Fan	A2	
3F_Make-Up Air Fan	A1	
1F-2F Internal Balancing Fan	B1	Increase Fan Speed if: $\Delta P_{2nd-1st}$ is Below $SP_{MIN,2-1}$ Decrease Fan Speed if: $\Delta P_{2nd-1st}$ is Above $SP_{MAX,2-1}$
2F-3F Internal Balancing Fan	B2	Increase Fan Speed if: $\Delta P_{3rd-2nd}$ is Below $SP_{MIN,3-2}$ Decrease Fan Speed if: $\Delta P_{3rd-2nd}$ is Above $SP_{MAX,3-2}$
2F_Pressure Chamber Fan	B3	Increase Fan Speed if: P7 is Below $SP_{MIN,2FOD}$ Decrease Fan Speed if: P7 is Above $SP_{MAX,2FOD}$
3F_Pressure Chamber Fan	B4	Increase Fan Speed if: P8 is Below $SP_{MIN,3FOD}$ Decrease Fan Speed if: P8 is Above $SP_{MAX,3FOD}$

Table 4-3 The motor channel and the control logic of fans

Pressure Set-Point Description	Name	Default (Pa)
Min. Building Pressurization Level	$SP_{MIN,BLDG}$	0
Max. Building Pressurization Level	$SP_{MAX,BLDG}$	+0.2
Min. 2F-1F Pressure Difference	$SP_{MIN,2-1}$	-0.1
Max. 2F-1F Pressure Difference	$SP_{MAX,2-1}$	+0.1
Min. 3F-2F Pressure Difference	$SP_{MIN,3-2}$	-0.1
Max. 3F-2F Pressure Difference	$SP_{MAX,3-2}$	+0.1
Min. 2F Chamber Pressure	$SP_{MIN,2FOD}$	+3.4
Max. 2F Chamber Pressure	$SP_{MAX,2FOD}$	+3.6
Min. 3F Chamber Pressure	$SP_{MIN,3FOD}$	+6.9
Max. 3F Chamber Pressure	$SP_{MAX,3FOD}$	+7.1

Table 4-4 Default value of pressure set-points

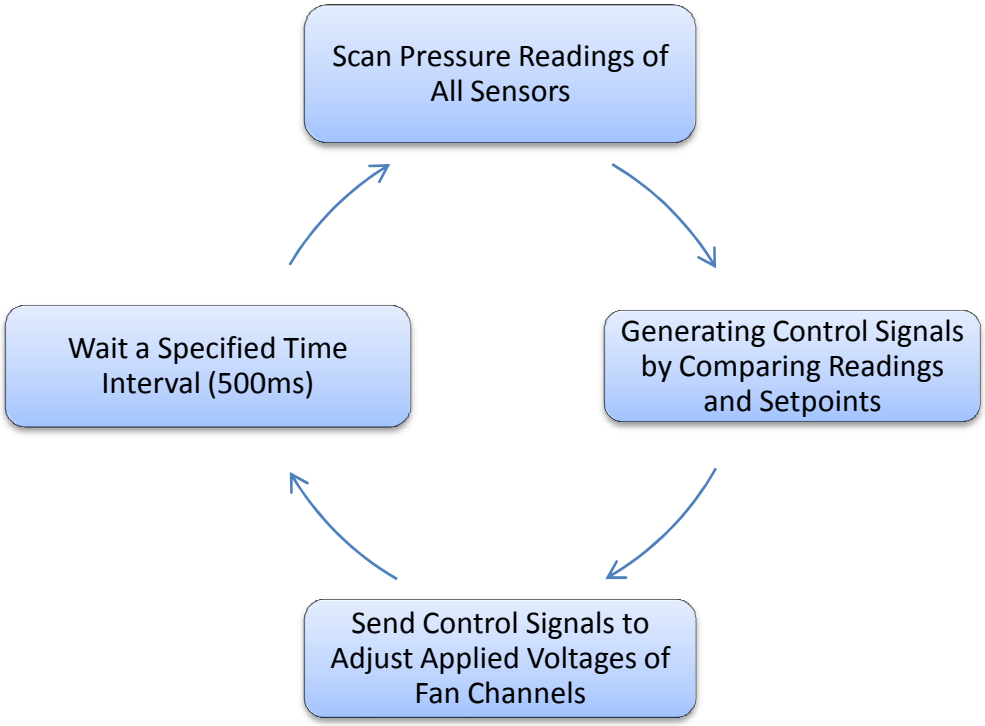

Figure 4-11 The control sequence of the scale-model

To determine the fan speed at different applied voltages, an experiment is done on the make-up air device described previously. Here one end of the make-up air device that was supposed to connect to a building floor is sealed by duct tape, and a Setra® model 260 (Part Number: 260GMS1D) bi-directional differential pressure sensor is connected to do the pressure measurement. By doing this, the static pressure measured is expected to correspond to the point of zero flow, thus the fan speed can be calculated by using equation 4.12. Here the fan running speed with 12V applied voltage is defined as 100% and the fan speed percentage versus applied voltage is shown in Figure 4-12.

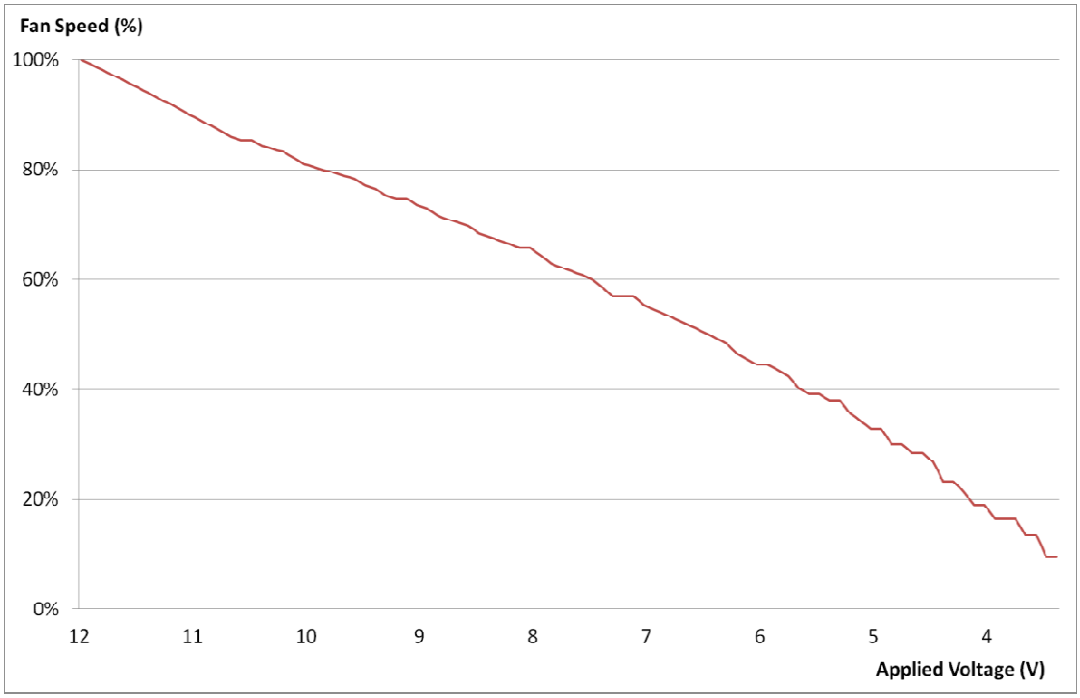

Figure 4-12 Fan speed percentage versus applied voltage

4.4 Scale-Model Operation Results

The total airflow coming out of the building through openings connected either to ambient or to pressure chambers is calculated by following equation:

$$Q_{out,total} = Q_{L,1F} + Q_{L,2F} + Q_{L,3F} \quad (4.21)$$

$$Q_{L,1F} = C(\Delta P_{first})^n \quad (4.22)$$

$$Q_{L,2F} = C(\Delta P_{second})^n \quad (4.23)$$

$$Q_{L,3F} = C(\Delta P_{third})^n \quad (4.24)$$

where:

$Q_{out,total}$ is the total airflow leaked out through openings (m^3/s)

$Q_{L,1F}$ is the airflow leaked out through the 1st floor opening to ambient

$Q_{L,2F}$ is the airflow leaked out through the 2nd floor opening to the 2nd pressure chamber

$Q_{L,3F}$ is the airflow leaked out through the 3rd floor opening to the 3rd pressure chamber

C and n are constants to be determined

Consider the building model as a control volume; then the following equation should apply:

$$Q_{out,total} = Q_{in,total} \tag{4.25}$$

where:

$Q_{in,total}$ is the total make-up airflow provided by three make-up air devices.

Each of the make-up air devices' flow rate is determined by the following procedure:

1. Use the applied voltage on the make-up air fans to determine the fan speed by Figure 4-12.
2. Use Eqs. 4.1- 4.5 and the measured static pressure of the make-up air device to determine the compensated static pressure
3. Once fan speed and compensated static pressure are available, use Eqs. 4.11-4.18 to determine the make-up air devices' flow rate

Per equation 4.25, the constants C and n existing in $Q_{out,total}$ can be determined once experimental data $Q_{in,total}$ is available. The experiment is done with internal

balancing fan disabled and by using settings described in Table 4-4, except chamber pressures are changed gradually to get different data points. By OLS regression analysis, it is determined that C=0.00375 and n=0.5. The experimental results are listed in Table 4-5 and $Q_{out,total}$ versus $Q_{in,total}$ is shown as Figure 4-13. Note that n=0.5 is as expected due to the shape of leakage area and these C and n values are applied to experiments which will be described next.

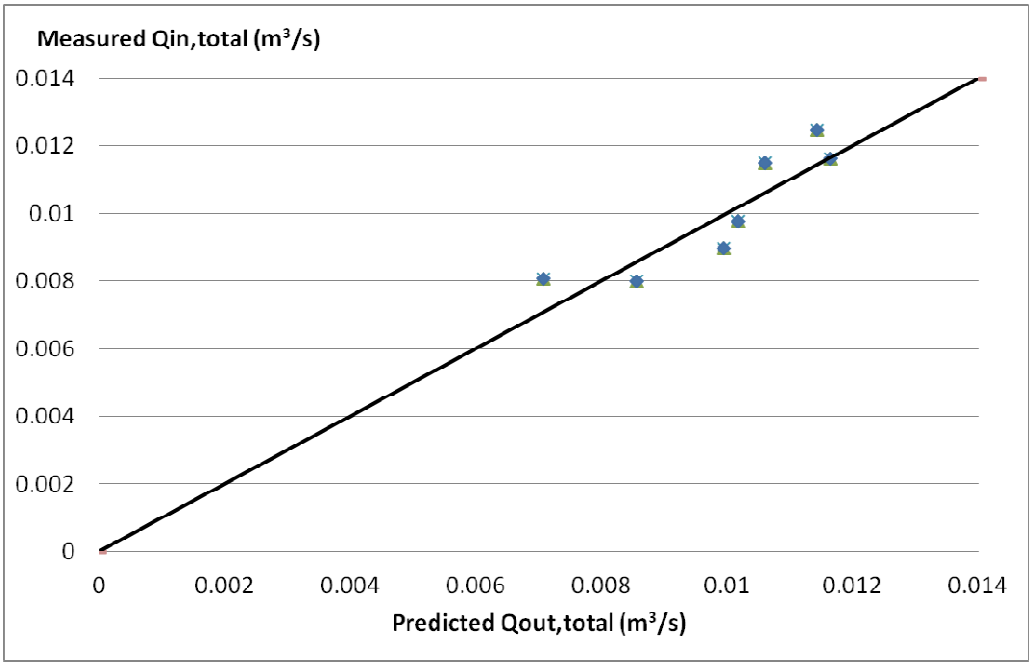

Figure 4-13 Measured $Q_{in,total}$ versus calculated $Q_{out,total}$ (C=0.00375 and n=0.5 are applied)

ΔP_{first} (Pa)	ΔP_{second} (Pa)	ΔP_{third} (Pa)	$Q_{out,total}$ (m^3/s)	$Q_{in,total}$ (m^3/s)
2.79	1.28	0.09	0.01162	0.01163
2.39	1.24	0.15	0.01143	0.01248
2.11	1.05	0.12	0.01059	0.01149
1.83	0.97	0.14	0.01017	0.00997
1.67	0.85	0.19	0.00994	0.00897
1.27	0.79	0.07	0.00855	0.00799
1.19	0.63	0	0.00707	0.00807

Table 4-5 Experimental results of $Q_{in,total}$ versus calculated $Q_{out,total}$

After constants C and n are determined, three sets of experiments with the same settings except stack effect intensity are performed. Each of the experiments starts with the Internal Balancing Fan disabled. When the system reaches equilibrium, supply fan speed, make-up air device static pressure readings P4, P5, and P6, ΔP_{first}, ΔP_{second}, and ΔP_{third} at that point are recorded. After that, two Internal Balancing Fan are activated, and the readings noted above plus two Internal Balancing Fan speeds are recorded again once the system reaches equilibrium. The total air leaked out before and after activating the Internal Balancing Fan are listed in Table 4-6, Table 4-7, and Table 4-8. In all three cases studied, it can be observed that with the Internal Balancing Fan disabled, the third floor pressurization can be kept barely positive (less than 0.15 Pa) only with first floor and second floor over-pressurized. However, after the Internal Balancing Fan is

activated, it can be observed that all three floors' pressurization level are kept at nearly the same level; the third floor pressurization level is also enhanced from less than 0.15 Pa to at least 0.37 Pa. It can also be observed that the reduction of total leaked air ranges from 28% to 32%.

	Internal Balancing Fan Disabled	**Internal Balancing Fan Activated**
ΔP_{first} (Pa)	2.75	0.5
ΔP_{second} (Pa)	1.37	0.48
ΔP_{third} (Pa)	0.11	0.55
$Q_{out,total}$ (m^3/s)	0.01185	0.00803
Reduction on $Q_{out,total}$ (%)	-	32.3%
Make-Up Air Fan Speed (%)	80%	49.6%
1F-2F Internal Balancing Fan Speed (%)	-	18.1%
2F-3F Internal Balancing Fan Speed (%)	-	54.4%

Table 4-6 Experimental results with disabled / activated internal balancing fan with 7/3.5 Pa at 3F/2F pressure chamber

	Internal Balancing Fan Disabled	Internal Balancing Fan Activated
ΔP_{first} (Pa)	2.21	0.45
ΔP_{second} (Pa)	1.37	0.43
ΔP_{third} (Pa)	0.06	0.4
$Q_{out,total}$ (m^3/s)	0.01088	0.00735
Reduction on $Q_{out,total}$ (%)	-	32.5%
Make-Up Air Fan Speed (%)	70.3%	40.9%
1F-2F Internal Balancing Fan Speed (%)	-	19.8%
2F-3F Internal Balancing Fan Speed (%)	-	25.3%

Table 4-7 Experimental results with disabled / activated internal balancing fan with 5/2.5 Pa at 3F/2F pressure chamber

	Internal Balancing Fan Disabled	Internal Balancing Fan Activated
ΔP_{first} (Pa)	1.53	0.48
ΔP_{second} (Pa)	1.08	0.39
ΔP_{third} (Pa)	0.15	0.37
$Q_{out,total}$ (m^3/s)	0.00999	0.00722
Reduction on $Q_{out,total}$ (%)	-	27.7%
Make-Up Air Fan Speed (%)	56.6%	32.9%
1F-2F Internal Balancing Fan Speed (%)	-	14.1%
2F-3F Internal Balancing Fan Speed (%)	-	15.1%

Table 4-8 Experimental results with disabled / activated internal balancing fan with 3/1.5 Pa at 3F/2F pressure chamber

4.5 Discussions on Scale-Model Operation

It is worth mentioning that the scale-model should be considered a distorted model due to certain differences between the model and a real building and is for verifying the control scheme only.

As mentioned before, two pressure chambers are utilized to create a stack effect like condition , since those chambers' pressure are controlled by fans as well, a duration

of response time is expected from the change of the fan speed to the change of chamber building. Also, due to the chamber's limited size, the pressure readings of the chamber are affected by the flow from the building. However, in a real building the response time should be nearly immediate and the pressure should not be affected by flow from the main building. Due to these differences, the control system's response time might differ significantly from the actual response in a real building.

The scale model experiments suggests that the Internal Fan Balancing System on a three-floor building helps reduce leaked air flow by 28% to 32%. However, per Table 5-1 the savings for a three floor building with flow exponent n=0.5 should be able to reach 42%. One of the reasons is the assumptions made. In Table 5-1 it is assumed that both the conventional pressurization system and the Internal Fan Balancing System are able to control the indoor pressure as low as zero but all at positive levels. However, in the results of scale model operation, it can be found that both systems have a minimum pressurization level slightly higher than zero; these levels are 0.15 Pa for the conventional system and 0.37 Pa for the Internal Fan Balancing System. Since mold growth risk tends to decrease with increased pressurization level, it is not necessarily a bad idea to keep the pressurization level slightly higher than the calculated minimum level despite sacrificing a small portion of potential savings.

Since the stack effect is a function of temperature difference, in theory the same indoor-outdoor temperature difference will induce the same stack effect intensity, plus there should exist an optimal system operating point for each stack effect intensity. That is, the pressure sensors can be utilized to create an operating points versus temperature

difference table; once it is implemented, those expensive sensors can be removed from the field and be redeployed to another building. In summary, the experiments done on the scale model can be used to create a table like Table 4-9:

Corresponding In-Outdoor Temp. Difference Case	Stack Effect (Pa)	Make-Up Air Fan Speed (%)	1F-2F Balancing Fan Speed (%)	2F-3F Balancing Fan Speed (%)
a	7	49.6%	18.1%	19.1%
b	5	40.9%	19.8%	25.3%
c	3	32.9%	14.1%	15.1%

Table 4-9 Operating points versus temperature difference

This table could be expanded to cover more temperature-difference conditions. Once enough data is gathered, the fan operating points can be determined from the table using the current indoor-outdoor temperature difference to achieve temperature based control.

5. PREDICTED ENERGY SAVINGS IN A REAL BUILDING

5.1 Introduction

In the previous section, it is demonstrated that the Internal Fan Balancing System can help reduce the make-up air requirement while maintaining the same level of pressurization compared to a conventional pressurization system. In this section, the energy savings achievable by applying the new system to a real building will be simulated.

5.2 Methodology

5.2.1 Theoretical Reduction on Exfiltration Air Flow

Consider a high-rise building with conventional pressurization. If the whole building is positively pressurized, by definition the indoor-outdoor pressure difference ΔP at any given height should be positive and the following equation should apply:

$$\Delta P(y) = P_{indoor}(y) - P_{outdoor}(y) > 0 \quad when\ y < H \qquad (5.1)$$

where:

ΔP(y) is the indoor-outdoor pressure difference at given height y (Pa)

P_{indoor} (y) is the indoor air pressure at given height y (Pa)

$P_{outdoor}$ (y) is the outdoor air pressure at given height y (Pa)

H is the building height (meters)

Assume both wind effect and building internal flow resistance are negligible. In cooling seasons where indoor temperature is lower than outdoor temperature, Figure 5-1

illustrates the minimum indoor-outdoor pressure difference that can be achieved by a conventional pressurization system while maintaining the whole building positively pressurized.

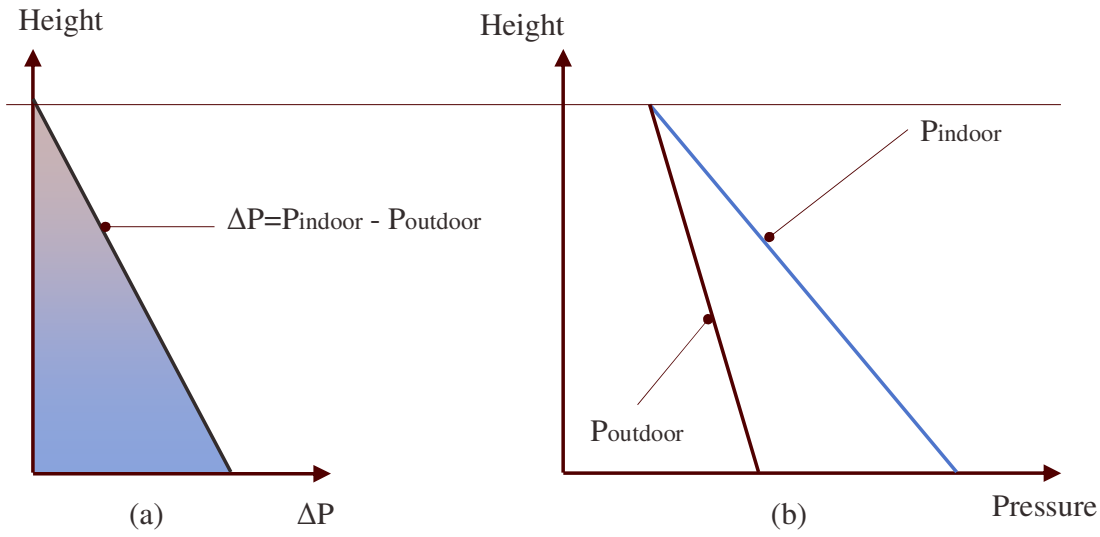

Figure 5-1 Conventional pressurization system, (a) indoor-outdoor pressure difference, (b) indoor and outdoor pressure curves

Similarly, Figure 5-2 illustrates the results of a two-floor building pressurized by the Internal Fan Balancing System and Figure 5-3 illustrates the same results for a four-floor building.

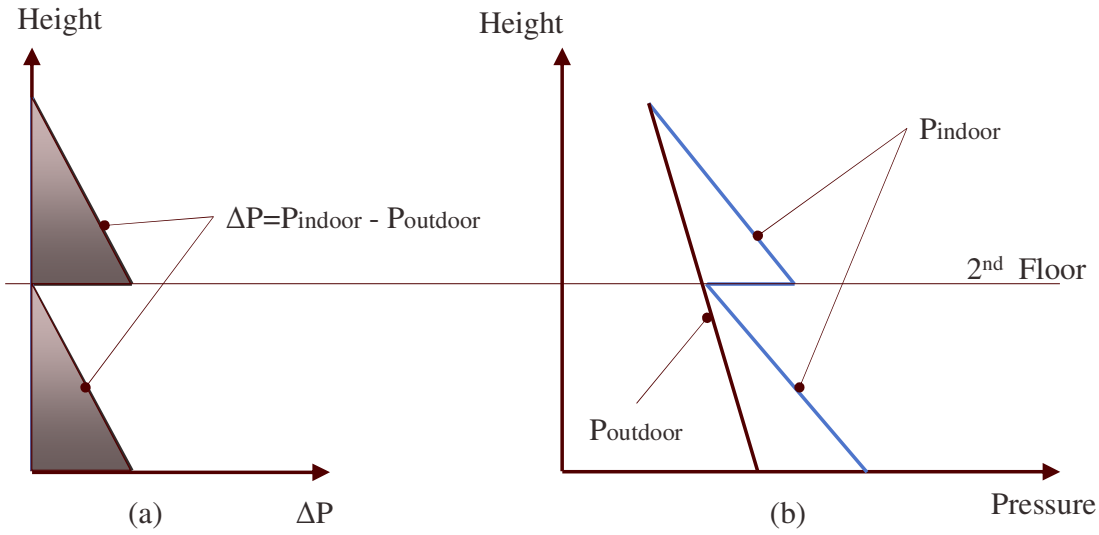

Figure 5-2 Two-floor building with internal fan balancing system, (a) indoor-outdoor pressure difference, (b) indoor and outdoor pressure curves

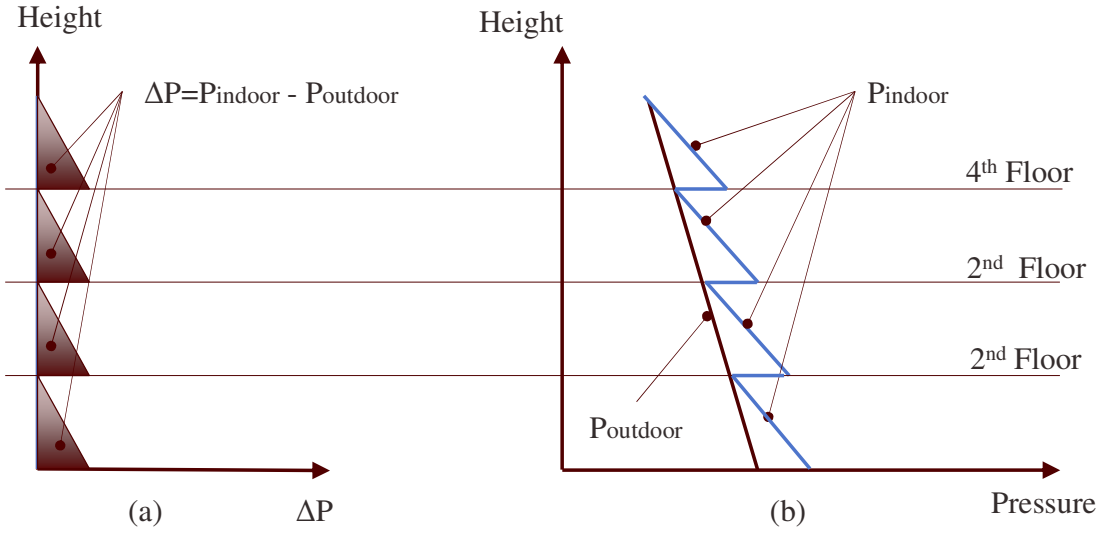

Figure 5-3 Four-floor building with internal fan balancing system, (a) indoor-outdoor pressure difference, (b) indoor and outdoor pressure curves

Since the average indoor-outdoor pressure difference of the whole building is proportional to the area shown on the indoor-outdoor pressure difference figures, all three cases of ΔP figures are illustrated in Figure 5-4 for comparison of average pressure difference. Figure 4 shows that, compared to the baseline (a building under conventional pressurization system), the average pressure is reduced to 50% of baseline for a two-floor building and 25% for a four-floor building. It can also be concluded that the average indoor-outdoor pressure difference can be determined by Equation 5.2 as:

$$\Delta P_{avg} = \Delta P_{base} * \frac{1}{m} \qquad (5.2)$$

where:

ΔP_{avg} is the average indoor-outdoor pressure difference for a building using internal fan balancing system. (Pa)

ΔP_{base} is the average indoor-outdoor pressure difference for the same building using a conventional pressurization system. (Pa)

m is the number of floors

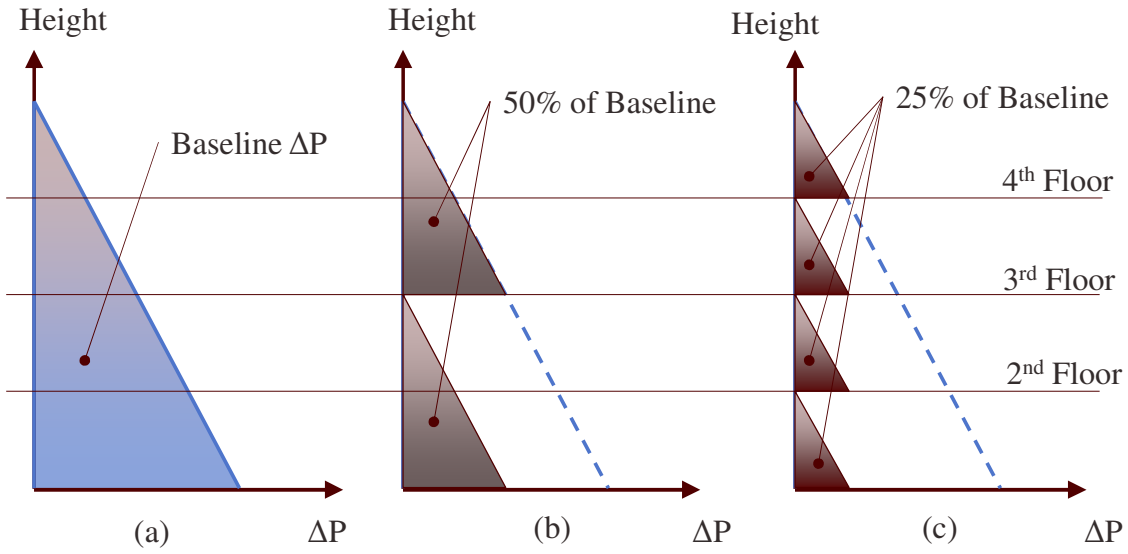

Figure 5-4 ΔP reduction by using internal fan balancing system: (a) conventional system (baseline), (b) two-floor building, and (c) four-floor building

When the whole building is positively pressurized, all leakage paths experience exfiltration and make-up air flow is required to compensate this loss. It is worth mentioning that per power law equation (2.5), the exfiltration air flow is proportional to the pressure difference with an exponent n. As an example, Figure 5-5 illustrates the exfiltration air flow for the three cases described above assuming n=0.65:

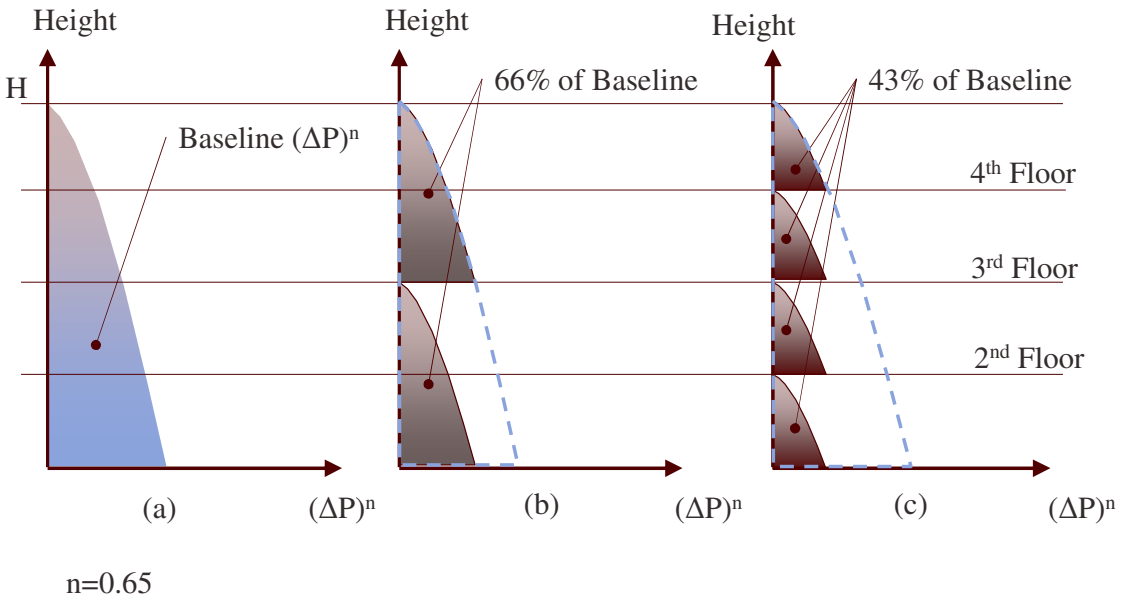

Figure 5-5 Exfiltration air flow reduction by using internal fan balancing system assuming n=0.65: (a) conventional system (baseline), (b) two-floor building, and (c) four-floor building

It can be seen on the figure that, compared to the baseline, the area representing exfiltration air flow is reduced to 66% of the baseline for a two-floor building and 43% for a four-floor building. This is under assumptions that each floor has the same height and the leakage paths are evenly distributed on all building walls. It can also be concluded that the exfiltration air flow can be determined by Equation 5.3 as:

$$Q_{exf} = m * \int_{H-\frac{H}{m}}^{H} C * [\Delta P(y)]^n \, dy \qquad (5.3)$$

where:

Q_{exf} is the exfiltration air flow

m is the number of floors

H is the building height

$\Delta P(y)$ is the indoor-outdoor pressure difference at given height y

C is the flow coefficient

n is the pressure exponent

The results for m=1, 2, or 4 and C=1 are the areas illustrated in Figure 5-5 (a), (b), and (c), respectively, where the m=1 case represents the result for a conventional pressurization system.

When treating the conventional pressurization system case as the baseline, the reduced average indoor-outdoor pressure difference ΔP_{avg} and the reduced exfiltration air flow under different exponent assumptions are shown in Table 5-1. It is assumed that all floors have the same height and the leakage area is evenly distributed on all walls.

Building Floor Number m	**Reduction on Indoor-Outdoor Pressure Difference ΔP_{avg} (% of Baseline)**	**Reduction on Exfiltration air flow Q_{exf} under different exponent n (% of Baseline)**				
		n=0.5	n=0.65	n=0.75	n=0.85	n=1
		Baseline				
2	50%	29%	36%	41%	45%	50%
3	67%	42%	51%	56%	61%	67%
4	75%	50%	59%	65%	69%	75%
5	80%	55%	65%	70%	75%	80%
6	83%	59%	69%	74%	78%	83%
7	86%	62%	72%	77%	81%	86%
8	88%	65%	74%	79%	83%	88%
9	89%	67%	76%	81%	85%	89%
10	90%	68%	78%	82%	86%	90%
11	91%	70%	79%	83%	87%	91%
12	92%	71%	80%	84%	88%	92%
13	92%	72%	81%	85%	89%	92%
14	93%	73%	82%	86%	89%	93%
15	93%	74%	83%	87%	90%	93%
16	94%	75%	84%	88%	91%	94%
17	94%	76%	84%	88%	91%	94%
18	94%	76%	85%	89%	91%	94%
19	95%	77%	85%	89%	92%	95%
20	95%	78%	86%	89%	92%	95%

Table 5-1 Reduction in ΔP_{avg} and Q_{exf} for different flow exponents n (% of baseline)

It can be noted that the reduction percentage of ΔP_{avg} and Q_{exf} increase with building total floor numbers m. However, although maximum energy savings can be achieved by installing a balancing fan module between each pair of floors, it may not always be the best solution when capital cost is taken into consideration. For example, assume there is a 16-floor building with a flow exponent n=0.65. The exfiltration air flow can be reduced by 84% with 15 balancing fan modules installed. However, a 74% reduction of exfiltration air flow can be achieved with only 7 balancing fan modules, with one installed for each two floors. Further calculations are required to determine if it is economic to invest two times as much in balancing systems to gain an extra 10% savings on make-up air.

5.2.2 Target Building Description - Harrington Tower

To perform an energy saving simulation to determine how much savings can be achieved on a real building, Harrington Tower, located on the Texas A&M Campus in College Station, TX, is selected as the target building to study. The physical information of this building described below is gathered from Giebler [72].

The building was completed in 1971 and the building appearance can be seen in Figure 5-6. It houses the College of Education and consists largely of offices, but there are some classrooms and computer labs. The building has eight stories above ground and has an estimated 400 occupants. The occupancy schedule is essentially 8 AM to 5 PM, Monday through Friday. The overall building dimensions are 124 feet by 136 feet by 110 feet high. Harrington Tower receives hot water and chilled water from the Texas

A&M Physical Plant for its HVAC systems. The building was retrofitted in 1995, from a DDCAV system with pre-treated outside air to DDVAV with a temperature economizer. A single DDVAV air handler unit (AHU), located in the basement, serves most of the building. A system diagram can be seen in Figure 5-7. The 200 hp supply fan provides up to 139,000 CFM of air for the second through eighth floors, as well as portions of the basement and first floor. On the upper floors, the hot and cold supply ducts run through a central chase to ducting and then VAV terminal boxes. The first floor has three small constant volume single duct systems to meet its primary heating and cooling requirements. There are five relief fans located on the roof, each with a design flow of 20,670 CFM. However, the relief fans and corresponding relief dampers remain closed unless the building is using the economizer cycle.

Figure 5-6 Harrington Tower on the Texas A&M main campus [72]

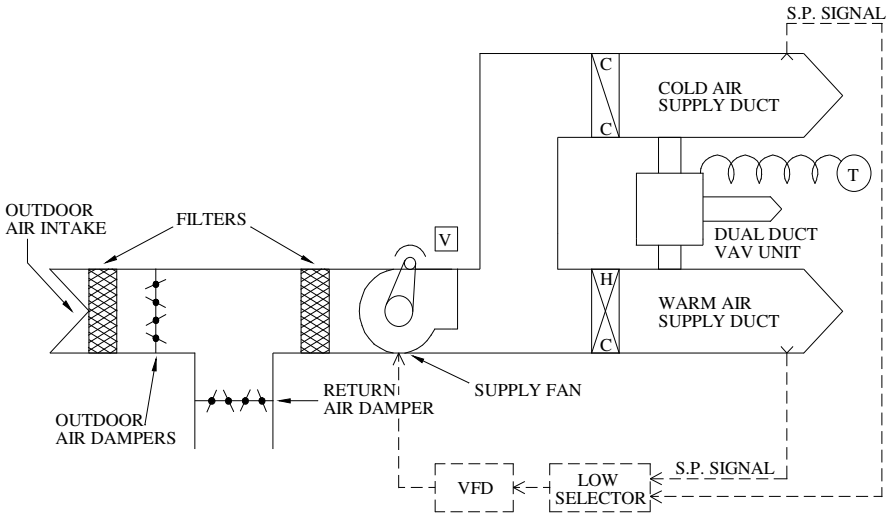

Figure 5-7 Harrington Tower DDVAV AHU system [72]

5.3 Building Energy Saving Simulation

Windows Air Model (WinAM) is utilized to perform the building energy simulation. WinAM is a building energy simulation software program developed by the Energy System Laboratory to rapidly calibrate a simulation and estimate the savings from energy conservation measures to an existing building.

The Harrington Tower building information gathered from previous research [72] is imported to and calibrated by WinAM (version 5.0). As mentioned in the previous section, there is a main DDVAV system and three small SDCAV systems. In the WinAM model the three smaller SDCAV systems are grouped as one single SDCAV system to simplify the simulation. The HVAC system-specific input parameters are listed in Table 5-2 and common building input parameters are listed in Table 5-3 (before calibration). The input range of weather data and consumption data are both from 8/1/2010 to 7/31/2013. To predict savings in US$, local energy unit costs are applied in WinAM as shown in Table 5-4 . As a result, the baseline utility cost is calculated as $313,346 per year. The step by step configurations of calibrating the model in WinAM can be found in Appendix.

Description	DDVAV System	SDCAV System
Serving Area (ft^2)	94,500	7,000
Interior Zone Percentage (%)	60	50
Wall Area (ft^2)	35,000	500
Window Area (ft^2)	15,000	4,500
Roof Area (ft^2)	17,000	0
Supply Air Flow	Variable	Constant
HVAC On/Off Time Schedule	7AM to 7PM	4AM to 11PM
HVAC On/Off Day Schedule	7 Days a Week	7 Days a Week
Minimum Primary Air Flow (CFM/ ft^2)	0.4	N/A
Minimum Outside Air Flow (%)	33	10
Design Primary Air Flow (CFM/ ft^2)	1.5	2
Cold Deck Set Point Reset (°F) **Format:** **(Setpoint Temp. @ OA Temp.)**	Stpt @ OAT 56 @ 50 55 @ 60 53 @ 70 50 @ 80	Stpt @ OAT 55 @ 55 53 @ 70 51 @ 90
Hot Deck Set Point (°F)	115	115
Static Pressure Set Point (in H_2O)	1.5	N/A
Maximum OA (% of Total Flow)	65%	N/A
Using Economizer Between	35°F to 65°F	N/A

Table 5-2 HVAC system-specific input parameters in WinAM

Cold Deck Energy Source	**District Chilled Water**
Hot Deck Energy Source	District Hot Water
Space Temperature Set Point	75°F
Supply Fan Design Total Pressure (in H_2O)	6
Peak Lighting Usage (W/ ft^2)	1.1
Peak Plug Usage (W/ ft^2)	0.65
Peak Occupancy Load (ft^2/person)	200
Sensible Heat Per Person (Btu/h)	250
Latent Heat Per Person (Btu/h)	200
Lighting & Plug Load Schedule	Refer to Figure 5-8
Occupant Load Schedule	Refer to Figure 5-9
Exterior U Value (Btu/ ft^2*h*°F)	
Exterior Walls	0.1
Exterior Windows	1
Roof	0.05

Table 5-3 Common building input parameters in WinAM

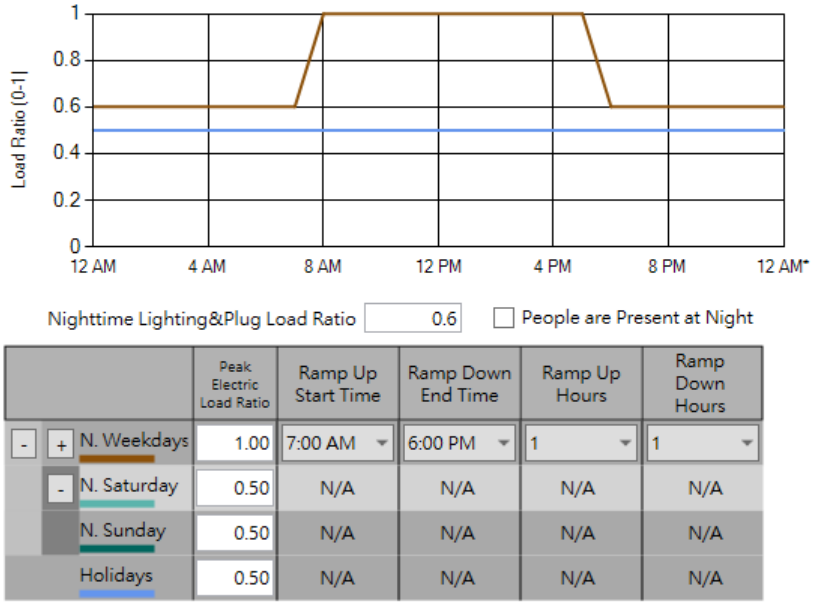

Figure 5-8 Lighting & plug load schedule

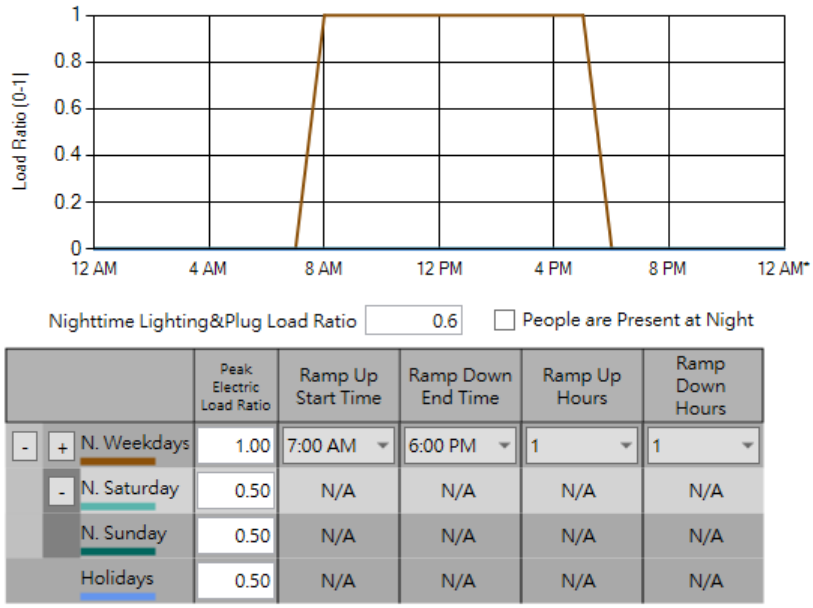

Figure 5-9 Occupant load schedule

Electricity Cost $/kWh	District Chilled Water Cost $/MMBtu	District Hot Water Cost $/MMBtu
0.087	15.26	14.97

Table 5-4 FY2015 local energy unit costs (from Texas A&M University Utilities & Energy Services)

The predicted and measured daily cooling / heating consumption values versus outside air temperature before calibration are shown in Figure 5-10. The total error between measured and predicted consumption of cooling and heating consumption is 23%. The total error percentage is defined by Equations 5.4 and 5.5:

$$Total\ Error\ (\%) = \frac{ERROR_{TOT}}{Mean} \quad (5.4)$$

$$ERROR_{TOT} = (RMSE_{TOT}^2 + MBE_{TOT}^2)^{0.5} \quad (5.5)$$

where:

Total Error (%) is the total error percentage

$ERROR_{TOT}$ is the total error

Mean is the arithmetic mean

RMSE is the root mean square error

MBE is the mean bias error

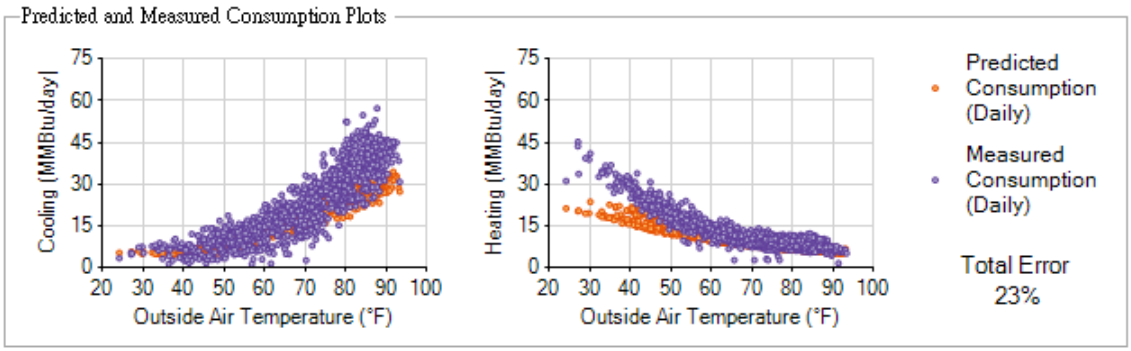

Figure 5-10 Predicted and measured daily consumption vs outside air temperature before calibration. (left) cooling, (right) heating

As suggested by WinAM, multiple parameters are changed to calibrate the model. Table 5-5 represents all parameters changed. After calibration, the total error is reduced from 23% to 12%. The predicted and measured daily cooling / heating consumption versus outside air temperature after calibration are shown in Figure 5-11.

	Before Calibration	After Calibration
Minimum Primary Air Flow (CFM/ ft^2)	0.4	0.55
Minimum Primary Air Flow (% of Design Primary Flow)	27	37
Minimum Outside Air Flow (% of Total Flow)	33	37
Exterior U Value (Btu/ ft^2*h*°F)		
Exterior Walls	0.1	0.1301
Exterior Windows	1	1.3013
Roof	0.05	0.0651

Table 5-5 Parameters changed during calibration

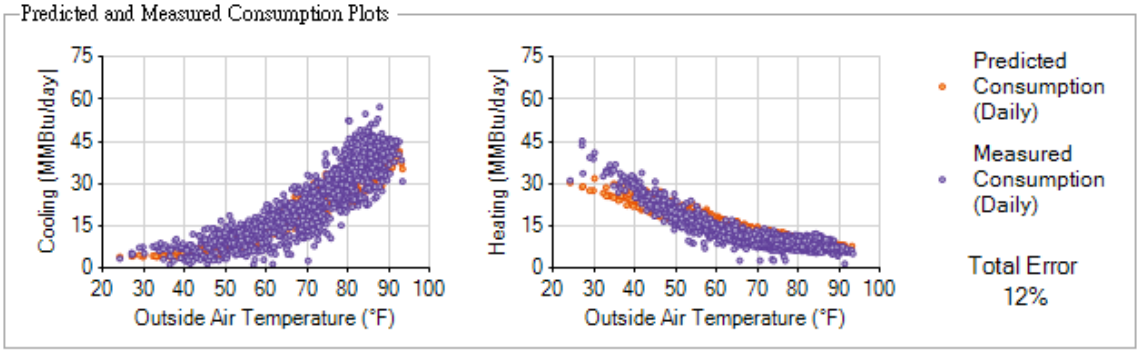

Figure 5-11 Predicted and measured daily consumption vs outside air temperature after calibration. (left) cooling, (right) heating

The calibrated model indicates that the building minimum OA percentage is 37%. As described in the previous section, make-up air flow savings for an eight-floor building can range from 65% (assuming flow exponent n=0.5) to 88% (assuming n=1). However, this does not account for local exhaust air flow - which needs to be compensated by make-up air flow as well. Also, since Harrington Tower is mainly served by a DDVAV system, the outside air flow would also vary with changing supply air flow. In summary, the required outside air flow (make-up air) to positively pressurize a building can be calculated by Equations 5.6 – 5.9 as:

$$Q_{OA} = Q_s * X_{OA} \quad (5.6)$$

$$Q_{exf} = Q_{OA} - Q_e - Q_r \quad (5.7)$$

$$Q'_{exf} = Q_{exf} * (100\% - k) \quad (5.8)$$

$$Q'_{OA} = Q_e + Q_r + Q'_{exf} \quad (5.9)$$

where:

Q_{OA} is the required OA flow under a conventional pressurization system

Q_s is the supply air flow

X_{OA} is the supply air OA flow percentage

Q_{exf} is the exfiltration air flow

Q_{inf} is the infiltration air flow

Q_e is the local exhaust air flow

Q_r is the relief air flow

Q'_{exf} is the reduced exfiltration air flow under Internal Fan Balancing System

k is the exfiltration air flow reduction percentage that can be found in Table 5-1

Q'_{OA} is the required OA flow under an Internal Fan Balancing System

It is worth mentioning that equations described above assume the conventional pressurization system always pulls in just the amount of make air to maintain minimum indoor-outdoor pressure difference as described in the beginning of this section. In practical cases including the Harrington Tower, the conventional pressurization system usually over-pressurized the building. If that is the case, the savings will be even higher. However, here the conservative assumption (the conventional pressurization system always pulls in the perfect amount of make air to maintain minimum indoor-outdoor pressure difference) is made and the result should be treated as a conservative prediction of energy savings. An example calculation assuming the DDVAV system runs at the design supply air flow condition follows.

In the Harrington Tower case, the relief air flow Q_r is zero except in economizer mode. Two exhaust fans used on the restrooms have design flows of 4,725 CFM and 3,550 CFM, respectively. The local exhaust air flow, Q_e, is then calculated as:

$$Q_e = 4{,}275 + 3{,}550 = 7{,}825\ (CFM) \qquad (5.10)$$

As a result 7,825 CFM needs to be compensated. This value should remain unchanged despite using the Internal Fan Balancing System.

At the design condition the DDVAV system delivers 139,000 CFM with 37% OA flow. With three small SDCAV system having a combined outside air flow of 1,300 CFM, the OA flow at the design conditions:

$$Q_{OA} = 139{,}000 * 0.37 + 1{,}300 = 52{,}730\ (CFM) \qquad (5.11)$$

Assuming this OA flow corresponds to the minimum make-up air flow rate to pressurize the Harrington Tower by using the conventional pressurization system, then the exfiltration air flow can be calculated as follows:

$$Q_{exf} = 52{,}730 - 7{,}825 = 44{,}905\ (CFM) \qquad (5.12)$$

Per Table 5-1, assuming the flow exponent is n=0.65, a 74% reduction can be achieved on this part, so the reduced exfiltration air flow can be calculated as follows:

$$Q'_{exf} = 44{,}905 * 0.26 = 11{,}675\ (CFM) \qquad (5.13)$$

The total required OA flow after using Internal Fan Balancing System is then calculated as:

$$Q'_{OA} = 11{,}675 + 7{,}825 = 19{,}500\ (CFM) \qquad (5.14)$$

The reduction percentage on OA flow is then:

$$1 - \frac{Q'_{OA}}{Q_{OA}} = 1 - \frac{19{,}500}{52{,}730} = 63\% \qquad (5.15)$$

This represents the savings on OA flow (make-up air flow) after the constant exhaust flow / constant supply AHUs are taken into consideration. So the new minimum OA flow percentage in WinAM can be calculated as:

$$37\% * (100\% - 63\%) = 13.7\% \qquad (5.16)$$

Additional simulation is then performed in WinAM with adjusted OA flow percentage while all other parameters remain the same. The two simulation results are then compared to determine the energy savings achieved by using the Internal Fan Balancing System. Note that this calculated savings only applies when the system always runs at the design condition and the flow exponent n=0.65. In practical operation

of a DDVAV system, this will not occur. However, in the same manner, savings under minimum supply air flow can also be simulated. Table 5-6 shows a summary of energy savings simulated with a different flow exponent n and DDVAV operating conditions, while Figure 5-12 through Figure 5-21 show predicted savings in terms of electricity, district chilled water, and district hot water in those conditions. These results represent high / low boundaries of the predicted savings since the practical system will operate within the range between design and minimum primary flow condition as well as having a flow exponent n ranging from 0.5 to 1. In summary, the yearly energy cost savings can range from 3.7% to 6.7% depending on different operating conditions and assumptions. In terms of yearly savings in dollars, predicted savings range from $11,461 to 21,018.

Flow Exponent n	**DDVAV Operating Condition**	**Exfiltration Air Flow Reduction %**	**Make-Up Air Flow Reduction %**	**Minimum OA % in WinAM**	**Simulated Yearly Savings %**
0.5	Design	65%	55%	16.5%	**5.0%**
0.5	Minimum	65%	40%	22.3%	**3.7%**
0.65	Design	74%	63%	13.7%	**5.7%**
0.65	Minimum	74%	45%	20.2%	**4.1%**
0.75	Design	79%	67%	12.1%	**6.0%**
0.75	Minimum	79%	48%	19.1%	**4.4%**
0.85	Design	83%	71%	10.8%	**6.4%**
0.85	Minimum	83%	51%	18.2%	**4.6%**
1	Design	88%	75%	9.3%	**6.7%**
1	Minimum	88%	54%	17.1%	**4.9%**

Table 5-6 A summary of energy cost savings in different conditions

		Electricity	District CHW	District HW	Total
		kWh/year	MMBtu/year	MMBtu/year	$/year
Baseline Model Yearly Consumption	Usage	1,304,230	8,677	4,505	
	Cost ($)	$ 113,468	$ 132,439	$ 67,439	$ 313,346
With_ECM Model Yearly Consumption	Usage	1,304,230	7,626	4,528	
	Cost ($)	$ 113,468	$ 116,409	$ 67,785	$ 297,662
Yearly Savings	Usage Savings	-	1,050	(23)	
	Cost Savings ($)	$ -	$ 16,030	$ (347)	$ 15,684
	% Cost Savings	0%	12%	-1%	5.0%

Figure 5-12 Predicted savings (n=0.5, DDVAV running at design flow)

		Electricity	District CHW	District HW	Total
		kWh/year	MMBtu/year	MMBtu/year	$/year
Baseline Model Yearly Consumption	Usage	1,304,230	8,677	4,505	
	Cost ($)	$ 113,468	$ 132,439	$ 67,439	$ 313,346
With_ECM Model Yearly Consumption	Usage	1,304,230	7,909	4,522	
	Cost ($)	$ 113,468	$ 120,722	$ 67,694	$ 301,884
Yearly Savings	Usage Savings	-	768	(17)	
	Cost Savings ($)	$ -	$ 11,717	$ (255)	$ 11,461
	% Cost Savings	0%	9%	0%	3.7%

Figure 5-13 Predicted savings (n=0.5, DDVAV running at minimum flow)

		Electricity	District CHW	District HW	Total
		kWh/year	MMBtu/year	MMBtu/year	$/year
Baseline Model Yearly Consumption	Usage	1,304,230	8,677	4,505	
	Cost ($)	$ 113,468	$ 132,439	$ 67,439	$ 313,346
With_ECM Model Yearly Consumption	Usage	1,304,230	7,488	4,531	
	Cost ($)	$ 113,468	$ 114,300	$ 67,829	$ 295,597
Yearly Savings	Usage Savings	-	1,188	(26)	
	Cost Savings ($)	$ -	$ 18,139	$ (391)	$ 17,749
	% Cost Savings	0%	14%	-1%	5.7%

Figure 5-14 Predicted savings (n=0.65, DDVAV running at design flow)

		Electricity	District CHW	District HW	Total
		kWh/year	MMBtu/year	MMBtu/year	$/year
Baseline Model Yearly Consumption	Usage	1,304,230	8,677	4,505	
	Cost ($)	$ 113,468	$ 132,439	$ 67,439	$ 313,346
With_ECM Model Yearly Consumption	Usage	1,304,230	7,807	4,524	
	Cost ($)	$ 113,468	$ 119,170	$ 67,727	$ 300,365
Yearly Savings	Usage Savings	-	869	(19)	
	Cost Savings ($)	$ -	$ 13,270	$ (288)	$ 12,981
	% Cost Savings	0%	10%	0%	4.1%

Figure 5-15 Predicted savings (n=0.65, DDVAV running at minimum flow)

		Electricity	District CHW	District HW	Total
		kWh/year	MMBtu/year	MMBtu/year	$/year
Baseline Model Yearly Consumption	Usage	1,304,230	8,677	4,505	
	Cost ($)	$ 113,468	$ 132,439	$ 67,439	$ 313,346
With_ECM Model Yearly Consumption	Usage	1,304,230	7,409	4,532	
	Cost ($)	$ 113,468	$ 113,088	$ 67,854	$ 294,411
Yearly Savings	Usage Savings	-	1,268	(28)	
	Cost Savings ($)	$ -	$ 19,351	$ (416)	$ 18,935
	% Cost Savings	0%	15%	-1%	6.0%

Figure 5-16 Predicted savings (n=0.75, DDVAV running at design flow)

		Electricity	District CHW	District HW	Total
		kWh/year	MMBtu/year	MMBtu/year	$/year
Baseline Model Yearly Consumption	Usage	1,304,230	8,677	4,505	
	Cost ($)	$ 113,468	$ 132,439	$ 67,439	$ 313,346
With_ECM Model Yearly Consumption	Usage	1,304,230	7,754	4,525	
	Cost ($)	$ 113,468	$ 118,352	$ 67,744	$ 299,564
Yearly Savings	Usage Savings	-	923	(20)	
	Cost Savings ($)	$ -	$ 14,087	$ (306)	$ 13,781
	% Cost Savings	0%	11%	0%	4.4%

Figure 5-17 Predicted savings (n=0.75, DDVAV running at minimum flow)

		Electricity	District CHW	District HW	Total
		kWh/year	MMBtu/year	MMBtu/year	$/year
Baseline Model Yearly Consumption	Usage	1,304,230	8,677	4,505	
	Cost ($)	$ 113,468	$ 132,439	$ 67,439	$ 313,346
With_ECM Model Yearly Consumption	Usage	1,304,230	7,344	4,534	
	Cost ($)	$ 113,468	$ 112,101	$ 67,875	$ 293,444
Yearly Savings	Usage Savings	-	1,332	(29)	
	Cost Savings ($)	$ -	$ 20,338	$ (436)	$ 19,902
	% Cost Savings	0%	15%	-1%	6.4%

Figure 5-18 Predicted savings (n=0.85, DDVAV running at design flow)

		Electricity	District CHW	District HW	Total
		kWh/year	MMBtu/year	MMBtu/year	$/year
Baseline Model Yearly Consumption	Usage	1,304,230	8,677	4,505	
	Cost ($)	$ 113,468	$ 132,439	$ 67,439	$ 313,346
With_ECM Model Yearly Consumption	Usage	1,304,230	7,710	4,526	
	Cost ($)	$ 113,468	$ 117,681	$ 67,758	$ 298,908
Yearly Savings	Usage Savings	-	967	(21)	
	Cost Savings ($)	$ -	$ 14,758	$ (320)	$ 14,438
	% Cost Savings	0%	11%	0%	4.6%

Figure 5-19 Predicted savings (n=0.85, DDVAV running at minimum flow)

		Electricity	District CHW	District HW	Total
		kWh/year	MMBtu/year	MMBtu/year	$/year
Baseline Model Yearly Consumption	Usage	1,304,230	8,677	4,505	
	Cost ($)	$ 113,468	$ 132,439	$ 67,439	$ 313,346
With_ECM Model Yearly Consumption	Usage	1,304,230	7,269	4,535	
	Cost ($)	$ 113,468	$ 110,961	$ 67,898	$ 292,327
Yearly Savings	Usage Savings	-	1,407	(31)	
	Cost Savings ($)	$ -	$ 21,478	$ (460)	$ 21,018
	% Cost Savings	0%	16%	-1%	6.7%

Figure 5-20 Predicted savings (n=1, DDVAV running design flow)

		Electricity	District CHW	District HW	Total
		kWh/year	MMBtu/year	MMBtu/year	$/year
Baseline Model Yearly Consumption	Usage	1,304,230	8,677	4,505	
	Cost ($)	$ 113,468	$ 132,439	$ 67,439	$ 313,346
With_ECM Model Yearly Consumption	Usage	1,304,230	7,656	4,527	
	Cost ($)	$ 113,468	$ 116,859	$ 67,776	$ 298,102
Yearly Savings	Usage Savings	-	1,021	(23)	
	Cost Savings ($)	$ -	$ 15,580	$ (337)	$ 15,243
	% Cost Savings	0%	12%	0%	4.9%

Figure 5-21 Predicted savings (n=1, DDVAV running at minimum flow)

If flow exponent n is assumed to be 0.65, the projected savings by installing one, three, and seven internal balancing fan modules can be summarized as follows in Table 5-7. Also, Figure 5-22 through Figure 5-25 show predicted savings in terms of electricity, district chilled water, and district hot water when one or three fan modules are installed. Note that the one module is assumed to be installed at the 5th floor and the three modules are assumed to be installed at the 3th, 5th, and 7th floors, respectively.

Fan Module Installed	DDVAV Operating Condition	Exfiltration air flow Reduction %	Make-up Air Flow Reduction %	Minimum OA % in WinAM	Simulated Yearly Savings %
1	Design	36%	31%	25.7%	**2.9%**
1	Minimum	36%	22%	28.9%	**2.2%**
3	Design	59%	50%	18.4%	**4.6%**
3	Minimum	59%	36%	23.6%	**3.4%**
7	Design	74%	63%	13.7%	**5.7%**
7	Minimum	74%	45%	20.2%	**4.1%**

Table 5-7 Summary of energy cost saving with different number of fan modules installed (n=0.65)

		Electricity	District CHW	District HW	Total
		kWh/year	MMBtu/year	MMBtu/year	$/year
Baseline Model Yearly Consumption	Usage	1,304,230	8,677	4,505	
	Cost ($)	$ 113,468	$ 132,439	$ 67,439	**$ 313,346**
With_ECM Model Yearly Consumption	Usage	1,304,230	8,072	4,518	
	Cost ($)	$ 113,468	$ 123,215	$ 67,640	**$ 304,324**
Yearly Savings	Usage Savings	-	604	(13)	
	Cost Savings ($)	$ -	$ 9,224	$ (202)	**$ 9,022**
	% Cost Savings	0%	7%	0%	**2.9%**

Figure 5-22 Predicted savings (n=0.65, one fan module installed, DDVAV operating at design flow)

		Electricity	District CHW	District HW	Total
		kWh/year	MMBtu/year	MMBtu/year	$/year
Baseline Model Yearly Consumption	Usage	1,304,230	8,677	4,505	
	Cost ($)	$ 113,468	$ 132,439	$ 67,439	$ 313,346
With_ECM Model Yearly Consumption	Usage	1,304,230	8,224	4,515	
	Cost ($)	$ 113,468	$ 125,538	$ 67,590	$ 306,596
Yearly Savings	Usage Savings	-	452	(10)	
	Cost Savings ($)	$ -	$ 6,902	$ (151)	$ 6,750
	% Cost Savings	0%	5%	0%	2.2%

Figure 5-23 Predicted savings (n=0.65, one fan module installed, DDVAV operating at minimum flow)

		Electricity	District CHW	District HW	Total
		kWh/year	MMBtu/year	MMBtu/year	$/year
Baseline Model Yearly Consumption	Usage	1,304,230	8,677	4,505	
	Cost ($)	$ 113,468	$ 132,439	$ 67,439	$ 313,346
With_ECM Model Yearly Consumption	Usage	1,304,230	7,720	4,526	
	Cost ($)	$ 113,468	$ 117,830	$ 67,755	$ 299,054
Yearly Savings	Usage Savings	-	957	(21)	
	Cost Savings ($)	$ -	$ 14,609	$ (317)	$ 14,292
	% Cost Savings	0%	11%	0%	4.6%

Figure 5-24 Predicted savings (n=0.65, three fan modules installed, DDVAV operating at design flow)

		Electricity	District CHW	District HW	Total
		kWh/year	MMBtu/year	MMBtu/year	$/year
Baseline Model Yearly Consumption	Usage	1,304,230	8,677	4,505	
	Cost ($)	$ 113,468	$ 132,439	$ 67,439	$ 313,346
With_ECM Model Yearly Consumption	Usage	1,304,230	7,972	4,520	
	Cost ($)	$ 113,468	$ 121,679	$ 67,673	$ 302,820
Yearly Savings	Usage Savings	-	705	(16)	
	Cost Savings ($)	$ -	$ 10,761	$ (235)	$ 10,526
	% Cost Savings	0%	8%	0%	3.4%

Figure 5-25 Predicted savings (n=0.65, three fan modules installed, DDVAV operating at minimum flow)

5.4 Dependence of the Savings on the Temperature Difference

Considering a single duct variable air volume system is pulling in minimum outside air flow (make-up air flow) required to maintain positive pressurization, the flow will be mixed with the return air flow before entering the cooling coil. If the outside air temperature is higher than return air temperature, extra sensible cooling is required to cool the outside air to the return air temperature. Similarly it also requires extra latent cooling when the outside air humidity ratio is higher than return air humidity ratio. The required extra sensible cooling and latent cooling can be calculated by equations:

$$E_S = 1.1 * Q_{OA}(T_{OA} - T_R) \quad (5.17)$$

$$E_L = 4{,}840 * Q_{OA}(w_{OA} - w_R) \quad (5.18)$$

$$E_S{}' = 1.1 * Q_{OA}{}'(T_{OA} - T_R) \quad (5.19)$$

$$E_L{}' = 4{,}840 * Q_{OA}{}'(w_{OA} - w_R) \quad (5.20)$$

where:

E_S is the required extra sensible cooling under a conventional pressurization system (Btu/hr)

E_L is the required extra latent cooling under a conventional pressurization system (Btu/hr)

$E_S{}'$ is the required extra sensible cooling under an Internal Fan Balancing System (Btu/hr)

$E_L{}'$ is the required extra latent cooling under an Internal Fan Balancing System (Btu/hr)

Q_{OA} is the required OA flow under a conventional pressurization system (CFM)

Q_{OA}' is the required OA flow under an Internal Fan Balancing System (CFM)

T_{OA} is the outside air temperature (°F)

T_R is the return air temperature (°F)

w_{OA} is the outside air humidity ratio (lbw/lba)

w_R is the return air humidity ratio (lbw/lba)

The sensible load savings can be calculated by $E_S - E_S'$, the latent load savings can be calculated by $E_L - E_L'$.

Per equation 2.1 the indoor-outdoor pressure difference due to stack effect is proportional to the indoor-outdoor temperature difference. As previously described, the ratio between Q_{OA}' and Q_{OA} is a function of operating condition and flow. As a result, the energy saving can be calculated once outside air and return air condition are available. As a sample calculation, assuming the return air temperature is 75°F and the return air humidity ratio is 0.01 lbw/lba, the outside air temperature is 85°F and the outside air humidity ration is 0.015 lbw/lba, the Q_{OA} is 10,000 CFM and the Q_{OA}' is 50% of Q_{OA}.

The sensible load savings = $E_S - E_S'$= 110,000 - 55,000 = 55,000 (Btu/hr)

The latent load savings = $E_L - E_L'$= 242,000 - 121,000 = 121,000 (Btu/hr)

Assuming the flow exponent n is 0.65, when outside air temperature is raised to 95°F and the humidity ratio remains 0.015, per equation 5.3 the new Q_{OA} under new

indoor-outdoor temperature difference will be 15,690 CFM. If $Q_{OA}{}'$ remains 50% of new Q_{OA}:

The sensible load savings = $E_S - E_S{}'$= 345,185 - 172,590 = 172,590 (Btu/hr)

The latent load savings = $E_L - E_L{}'$= 379,698 - 189,849 = 189,849 (Btu/hr)

It can be found that when the indoor-outdoor temperature difference is doubled, the new sensible load savings is raised to 314% of the original saving. The latent load savings will also be increased by 57% despite the humidity remain the same because of the increased Q_{OA}. It can also be concluded that if the load savings under certain outside air condition is known, the load savings under different outside air conditions can be calculated as follows (assuming return air conditions are equal to space air conditions):

$$\frac{NEW\ sensible\ load\ savings}{BASE\ sensible\ load\ savings} = \left(\frac{T_{OA}{}'-T_R}{T_{OA}-T_R}\right)^{1+n} \qquad (5.21)$$

$$\frac{NEW\ latent\ load\ savings}{BASE\ latent\ load\ savings} = \left(\frac{T_{OA}{}'-T_R}{T_{OA}-T_R}\right)^{n} * \left(\frac{w_{OA}{}'-w_R}{w_{OA}-w_R}\right) \qquad (5.22)$$

where:

$T_{OA}{}'$ is the new outside air temperature (°F)

$w_{OA}{}'$ is the new outside air humidity ratio (lbw/lba)

n is the flow exponent

It is worth mentioning that if the outside air temperature is lower than the return air temperature and/or the outside air humidity ratio is lower than the return air humidity ratio, the system may have a potential energy savings running under economizer mode.

There will be no savings using an Internal Fan Balancing System since pulling in minimum outside air is no longer the most energy efficient system operation point in that condition.

5.5 Discussion of Energy Savings Prediction

In terms of building energy simulation, leakage area information is generally not available. Even a blower door test can only provide a rough estimation on the amount of leakage area, but the distribution profile through the building walls will be still missing. In this dissertation, it is assumed that the leakage area is always evenly distributed on all walls, but the true distribution profile of buildings may vary and needs further investigation since it will affect the simulation results.

In terms of building leakage intensity, large deviations are found between different building cases. Emmerich and Persily [27] summarized air leakage data for the 201 U.S. commercial and institutional buildings studied and found that the air leakage at 75 Pa can range from 2.7 $m^3/h*m^2$ to 168 $m^3/h*m^2$ with an average 28.4 $m^3/h*m^2$ and standard deviation 35.8 $m^3/h*m^2$. Fortunately, with the even leakage area distribution assumption, the savings that can be achieved by the Internal Fan Balancing System are independent of the leakage area; instead, they are a percentage of leakage flow under a conventional pressurization system.

In Table 5-7 it can be observed that an average 2.6% energy savings can be achieved if only one fan module is installed between the 4th and 5th floors. The average energy savings improves to 4.0% with two more fan modules installed and to 4.9% with

six more fan modules installed. The savings achieved by each installed fan module in the eight-floor building case are shown in Table 5-8. The cost of installing four more fan modules to gain an additional ~$2,800 projected annual savings should be considered. Note that the first three fan modules produce ~$12,500 projected savings.

	Baseline	**One Fan Module**	**Three Fan Modules**	**Seven Fan Modules**
Annual Total Savings	$0	$8,147	$12,533	$15,354
Annual Total Savings (%)	-	2.6%	4.0%	4.9%
Fan Modules Installed	0	1	3	7
Additional Modules Installed from Previous Configuration	-	+1	+2	+4
Extra Savings from Previous Configuration	-	$8,147	$4,386	$2,821
Extra Savings from Previous Configuration (%)	-	2.6%	1.4%	0.9%
Extra Savings / Additional Modules Installed	-	$8,147	$2,193	$705
Extra Savings (%) / Additional Modules Installed	-	2.6%	0.7%	0.23%

Table 5-8 Average savings achieved by each additional module and total savings

In this dissertation, it is assumed that the baseline conventional pressurization system always pulls the minimum make-up air that can maintain the whole building positively pressurized. But in practical cases, buildings are usually largely over-pressurized. On the other hand, in this dissertation the internal flow resistance between floors is assumed negligible to simplify the case; if internal flow resistance is very high between floors, the actual savings will be lower than the savings predicted. In an extreme case, if it is initially completely airtight between floors, then no savings will be achieved by installing an Internal Fan Balancing System.

It is worth mentioning that the required OA air flow should be also constrained by ASHRAE 62.1 "Ventilation for Acceptable Indoor Air Quality [74]. That is, even if the Internal Fan Balancing System can help reduce make-up air (OA) flow below the value given by Standard 62.1, it should not be set lower than that amount to maintain indoor air quality. This should always be checked before reducing OA flow. For example, in the Harrington Tower case, the DDVAV system serves 94,500 ft^2 floor area which is essentially offices with estimated 200 ft^2/person occupancy density. Assuming zone air distribution effectiveness Ez=1, the required OA flow can be calculated as follows:

$$Q_{OA} = 94{,}500 * 0.06 + 94{,}500 \div 200 * 5 = 8{,}033\ (CFM) \qquad (5.23)$$

where:

Q_{OA} is the required OA flow per ASHRAE 62.1.

Per Table 5-6, the required OA flow % is estimated to be 9.3% at the design condition and 17.1% at the minimum flow condition. For the design condition cases:

$$Q_{OA,Design} = 139{,}000 * 9.3\% = 12{,}927\ (CFM) \quad (5.24)$$

$$Q_{OA,Minimum} = 139{,}000 * 37\% * 17.1\% = 8{,}795\ (CFM) \quad (5.25)$$

where:

$Q_{OA,Design}$ is the reduced OA flow at the design condition

$Q_{OA,Minimum}$ is the reduced OA flow at the minimum flow condition

Per Eqs. (5.24) and (5.25), both of OA flow are above the required OA flow of 8,033 CFM per ASHRAE 62.1. Thus this issue doesn't not affect the studied case.

It is possible that the flow required by ASHRAE 62.1 is high enough that it will impact the savings that can be achieved by the Internal Fan Balancing System in some cases. However, if this is the case, further savings can still be achieved by installing a heat recovery device connecting the OA intake duct and exhaust duct. By using a conventional pressurization system, the majority of OA flow is exfiltrated from leakage area due to excessive pressurization; by using an Internal Fan Balancing System, the majority of the flow can be exhausted through a dedicated path so a heat recovery system can significantly improve the system efficiency.

6. DISCUSSION AND CONCLUSIONS*

6.1 Discussion on Issues Caused by Conventional Pressurization System

Figure 6-1 represents a 24 hour field measurement of indoor-outdoor pressure difference performed on Harrington Tower in August 2014. Two Setra® Model 264 bi-directional pressure sensors (Part Number: 26410R1WB11A1D) are placed at the ground floor and top floor, respectively. Each pressure sensor is connected to a HOBO® U12-012 data logger for data logging as well as measuring indoor air temperature, which is an integrated function of the logger. The loggers are configured to record indoor air temperature and the pressure difference signal generated by the pressure sensors. The signal is transferred from the pressure sensor to the logger by using accessory cable CABLE-4-20mA purchased from the ONSET website. The ground floor pressure sensor-logger set is placed in Room 121 (North West facade of the building) and the pressure difference through the exterior wall of the room is measured. The top floor pressure sensor-logger set is placed in Room 804-B (South East facade of the building). In Figure 6-1 the recorded ground floor pressure difference is labeled as Ground Delta P, the top floor pressure difference is labeled as Top Delta P. The indoor temperature is the average value of the recorded ground floor and top floor indoor air temperatures, while the outdoor temperature is gathered from the local weather station at Eastwood Airport, College Station, TX.

Several issues can be observed in this case. First, the building is at least partially over-pressurized at any given occupied hour. During the occupied hours the top floor pressurization level reaches its lowest level (on average less than 1 Pa) around 4:00PM while the ground floor still has an average pressurization level around 7 Pa at the same time. Note that this is a building with 37% minimum OA flow per the calibrated model, which substantially exceeds the ventilation air flow required by ASHRAE 62.1. Even so, the positive pressurization level of the entire building is not guaranteed, as one negative reading is recorded around 4:00PM. It may be an unrealistic goal to maintain the whole building positively pressurized at all times due to periodically strong wind effect. On the other hand, if the top floor pressurization level at 4:00PM is high enough, then it doesn't make sense to over pressurize the building at other hours/locations. The conventional pressurization system has limitations and the proposed Internal Fan Balancing System can largely reduce over-pressurization.

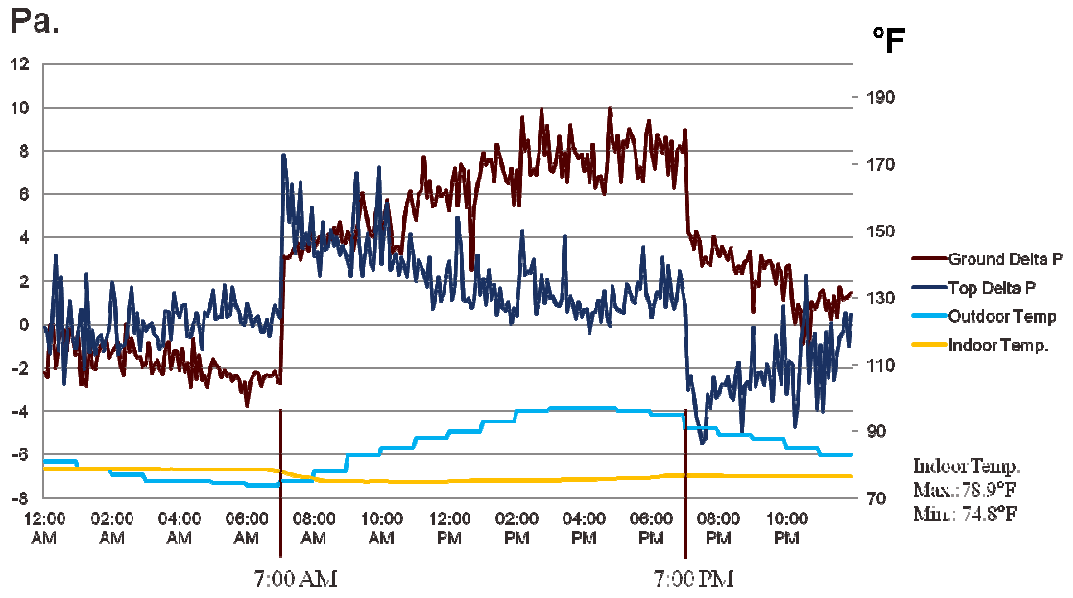

Figure 6-1 A 24-hour field measurement of indoor-outdoor pressure difference (August 2014)

It can also be noted that the building pressurization system is switched off during most unoccupied hours. This is reasonable since thermal comfort is not a concern during unoccupied hours. However, in terms of reducing risk of mold growth, the pressurization system should keep running whether the building is occupied or not because some unoccupied hours favor mold growth and mold does not have a working schedule but rather works 24/7. On the other hand, this building has been operated for over 40 years and no systematic mold growth has been observed yet. This strongly indicates it is not necessary to ensure that the building is positively pressurized continuously. The result from the model suggests that the building's current pressurization schedule is sufficient to maintain the annual mold index change negative so theoretically it should be a

building with low mold growth risk and this matches the reality. This is may be considered a partial validation of the proposed modified mold growth index based on pressurization levels.

6.2 Energy Usage of Internal Fan Balancing System

As described before, the Internal Fan Balancing System utilizes multiple balancing fan modules to adjust the pressure level at each floor. To calculate the energy required to operate these fan modules, Harrington Tower is treated as an example with assumptions shown in Table 6-1. Here, CONTAM (version 3.1.0.3) is utilized to predict the required flow rate of each internal fan module to balance the stack effect. CONTAM is a multi-zone indoor air quality and ventilation analysis computer program developed by the National Institute of Standards and Technology (NIST).

Description	Value	Note
Elevation(ft)	338	College Station, TX
Design Outside Air Temperature (°F)	95	
Design Indoor Air Temperature (°F)	75	
Flow Exponent n	0.65	
Exterior Wall Air Leakage at 75 Pa (CFM / ft^2)	1.562	Mean value from previous studies on 201 buildings [27]
Floor to Floor Air Leakage at 75 Pa (CFM / ft^2)	1.562	Assumed to be the same with Exterior Wall Air Leakage
Floor Height (ft)	13.75	Averaged height
Exterior Wall Area of Each Floor (ft^2)	7,150	Assuming each floor has the same height
Floor Area (ft^2)	17,000	
Number of Floors	8	
Fan Modules Installed	7	
Airflow Element Model (Leakage Path)		$Q=C(dP)^n$
Airflow Element Model (Balancing Fan)		Constant Volume Flow
Airflow Element Model (Mak-Up Air)		Constant Volume Flow

Table 6-1 Key input parameters in CONTAM

The simulation results indicate that to balance the stack effect at the conditions described above, each fan module should run at 2,250 CFM (1.062 m^3/s) with an average pressure difference 1.75 Pascal between each floor. The required fan power can be calculated by the following equation:

$$W_{ideal} = QdP \quad (6.1)$$

$$W_{actual} = W_{ideal}/\eta \quad (6.2)$$

$$W_{total} = W_{actual} * N_{fan} \quad (6.3)$$

Where:

W_{ideal} is the ideal fan power consumption (W)

Q is the fan flow rate (m^3/s)

P is the pressure difference (Pa)

W_{actual} is the actual fan power consumption (W)

η is the fan efficiency (W)

W_{total} is the total fan power consumption of all fan modules (W)

N_{fan} is the number of fan modules installed

As a sample calculation, W_{ideal} is 1.859 W. Assuming the fan efficiency is 1% (12.1CFM / Watt), the W_{actual} will be 0.186 kW. With seven fan modules installed, the total energy consumption of the Internal Fan Balancing System at the design condition is projected to be 1.3 kW. With the electricity cost assumed in Table 5-4 ($0.087/ kWh), the operating cost of the Internal Fan Balancing System at the design condition is projected to be 10 cents per hour, or $493 per year assuming an average of 12 operating

hours per day. Note that in reality the fan modules will rarely run at the design condition; thus in general, the operating cost is small compared to the energy savings achieved.

6.3 Other Approach Besides Internal Fan Balancing System

Since the key factor in reducing the make-up air requirement is to keep each floor's indoor-outdoor pressure difference positive but as low as possible, other methods exist to achieve this goal. For example, a common building design uses space above the ceiling as the return plenum, and the return plenum might be connected to the return air path by a short duct. In this kind of design, a damper can be installed in the short duct to control the flow rate of return air. When the return air of certain floor is limited while supply air remains the same, the pressure of that floor increases. On the other hand, a fan can be installed in the short duct to induce more return air to lower the pressurization level of that floor. As a result a damper or a return boost fan controlled by the pressurization level might be able to achieve a similar goal as using the Internal Fan Balancing System. In summary there are multiple methods to minimize the indoor-outdoor pressure difference and the optimal method for an individual building should be considered case by case.

6.4 Conclusions and Future Research Recommendations

6.4.1 Conclusions

This dissertation focuses on two main goals - the first goal is to develop a modified mold growth index based on pressurization levels to quantify the required pressurization

level to reduce risk of mold growth within a building envelope. Per simulation results of the modified mold growth index based on pressurization levels, to ensure a negative annual change in the mold index within a building envelope, positive pressurization and higher indoor temperature set-points are both effective solutions for the hot and humid climate cases modeled. Maintaining the indoor temperature set-point as high as possible in warmer seasons while still staying within the thermal comfort zone will always reduce the warm-season mold index growth. Pressurization is not necessary during colder months to avoid mold index growth, but is quite necessary from June to August for a building in College Station, TX. However, for a city in a less humid climate such as Atlanta, GA, pressurization is not required to avoid mold index growth according to the model results.

1.5 Pa positive pressurization should ensure that the mold index does not become substantially positive over multiple years when the building is assumed to be in College Station, TX with an indoor temperature set-point as low as 22°C and the 3 or 5 layer wall configurations described in Table 3-3. The pressurization level should be raised to 2 Pa if the building has a very high thermal resistance and/or very high indoor combined heat transfer coefficient. The model also indicates that only 1 Pa pressurization is required to produce negative annual change in mold index if the same building is moved to Fort Worth, TX and no pressurization is required in Atlanta, GA with a 22°C indoor temperature set-point. Similar results were obtained for another wall-construction in College Station, while a wall behaving as if it has infinite thermal resistance in College

Station requires a 2 Pa pressurization to yield an annual decrease in mold index for all orientations.

When assuming a fixed target layer temperature, the simulation results of an eight floor building located in College Station, TX with a 24°C indoor temperature set-point suggest that the current Monday to Friday, 7AM to 7PM pressurization schedule is able to keep a negative annual change in the mold index. When assuming a 5-layer-wall configuration on building envelope, the annual change of mold index remains negative even when building is unpressurized.

When assuming a fixed target layer temperature, the simulation results of an eight floor building located in College Station, TX with a 24°C indoor temperature set-point suggest that the current Monday to Friday, 7AM to 7PM pressurization schedule is able to keep a negative annual change in the mold index. When assuming a 5-layer-wall configuration on building envelope, the annual change of mold index remains negative even when building is unpressurized.

The second goal of this dissertation is to develop an Internal Fan Balancing System that can significantly reduce make-air usage while still maintaining appropriate pressurization level on any part of the building. A field experiment is done on an eight floor building in College Station, TX and the results indicates that the pressurization level of each floor can be quite different especially when the indoor-outdoor temperature difference is large. Under the condition when the indoor temperature is at 75°F and outdoor temperature is around 95°F, it is observed that the ground floor has an eight Pa

average pressurization level while the top floor has only 2 Pa – and is sometimes negatively pressurized.

A series of building energy simulations are performed to predict the annual savings that can be achieved by installing the Internal Fan Balancing System on the building where the field experiment is made. The simulation results indicate that the annual energy cost savings can range from 3.7% to 6.7% of the total utility bill depending on different assumptions made. For an eight floor building, installing seven internal balancing fan modules can maximize the savings. However, installing only one internal balancing fan module is expected to achieve 53% of the maximum savings assuming the flow exponent n is 0.65. The capital cost as well as payback period should be considered when applying this technique.

A three-floor scale-model is built to verify the feasibility of the Internal Fan Balancing System. The experiment made with the scale model shows that the response time of the system is usually within 5 seconds. It is also demonstrated that the system operating point is a function of indoor-outdoor temperature difference, so once enough system operating points are gathered, the on-site pressure sensors can be removed for further usage and the system can run per fan speed-temperature difference table.

6.4.2 Future Research Recommendations

The modified mold growth index based on pressurization levels assumed that the indoor temperature is controlled at a single point, either 22°C to 24°C. However, in practice the indoor temperature is normally controlled within a range. Since the target

layer is in contact with indoor air, the fluctuation of indoor temperature could greatly affect the target temperature but is not addressed in this dissertation. Future study of this issue seems appropriate. Several past studies have focused on mold growth behavior under different dry-time/wet-time cycles. However, most of these studies had a dry/wet switch frequency of a few hours (i.e. 6 hours dry, 6 hours wet cycle). If the indoor temperature is controlled in a range that causes RH of outside air entering the target layer to go up and down at the edge of the critical RH, the dry-time / wet-time of the target layer may switch frequently on the scale of minutes (i.e. 15 minutes dry, 15 minutes wet). Since dry-time/ wet-time duration is also an important factor regarding mold growth, a future study focused on mold growth behavior in an environment that switches rapidly between favorable and unfavorable conditions seem warranted.

The simulation results of modified mold growth index based on pressurization levels could be validated by monitoring real buildings with controlled pressurization levels. A slice of gypsum board could be examined periodically to check the mold index level change and put back to continue the experiment. This could also be accomplished by blowing a dry/wet stream cyclically in test cells maintained at different temperatures. Furthermore, if a building's pressurization schedule and indoor temperature data are readily available, certain validation can be done by observing existing buildings as is done on Harrington Tower described previously.

For the Internal Fan Balancing System, in this dissertation the predicted savings are listed in ranges rather than an amount because the hourly pressurization level and flow exponent n are not available. The required OA flow to maintain whole building is a

function of indoor-outdoor temperature difference but the supply air flow is very complicated with many other factors involved. In the future logged data recording the pressurization level of each floor, supply air flow rate, outside air percentage of the supply air flow, indoor and outdoor temperature will help determine the savings more precisely. Also the flow exponent n can be obtained by blower door test to better predicting the savings.

Wind effect induced control issues are not addressed in the scale-model operation. It is observed that the pressurization level of the scale model building typically can be controlled within ±0.5 Pa and the fan operating points are fairly stable. However, when dealing with a real building, the wind effect can make it difficult to control the pressurization level appropriately since a pressure sensor tells the change of pressure but is not able to tell if the change is due to stack effect or wind effect. Furthermore, a real building could have a "dynamic" leakage area. When someone is entering the building, the temporary opened entrance door will provide additional leakage path and most likely will greatly decrease the ground floor pressurization level. A well designed Internal Fan Balancing System should be able to detect non-stack effect pressure changes and balance only the stack effect. A possible solution is adding an extra procedure: when pressure change is detected, check if indoor and outdoor temperature changed as well; if not then the pressure change should be considered temporary and no pressure balance action should be made.

Wind effect is not considered in energy simulation models discussed in this dissertation, as a result all leakage area is simulated experiencing exfiltration of all time

during opening hours. However, as shown in Figure 6-1, a temporary strong wind effect actually can make the partial building wall under infiltration condition for a short time. This difference can impact the accuracy of energy simulations and further study on this issue seems appropriate.

REFERENCES

[1] ASHRAE S. Standard 90.1-2007, Energy Standard for Buildings Except Low-Rise Residential Buildings. 2007.

[2] Emmerich SJ, Persily AK, McDowell TP. Impact of infiltration on heating and cooling loads in US office buildings. Proceedings of the 26th IEA Conference of the Air Infiltration and Ventilation Center. 2005.

[3] Sherman MH. Infiltration-pressurization correlation: Simplified physical modeling. Conference of the American Society of Heating, Refrigeration and Air Conditioning Engineers, Denver, CO. June 1980.

[4] Handbook AS. ASHRAE handbook–fundamentals. Atlanta, GA. 2009.

[5] Blocken B, Carmeliet J, Stathopoulos T. CFD evaluation of wind speed conditions in passages between parallel buildings—effect of wall-function roughness modifications for the atmospheric boundary layer flow. Journal of Wind Engineering and Industrial Aerodynamics. 2007;95:941-62.

[6] Blocken B, Stathopoulos T, Carmeliet J. CFD simulation of the atmospheric boundary layer: wall function problems. Atmospheric Environment. 2007;41:238-52.

[7] Nozu T, Tamura T, Okuda Y, Sanada S. LES of the flow and building wall pressures in the center of Tokyo. Journal of Wind Engineering and Industrial Aerodynamics. 2008;96:1762-73.

[8] Irminger JOV, Nøkkentved C. Wind-pressure on Buildings: Experimental Researches. Danmarks naturvidenskabelige samfund; 1930.

[9] Reinhold TA. Wind tunnel modeling for civil engineering applications: Proceedings of the International Workshop on Wind Tunnel Modeling Criteria and Techniques in Civil Engineering Applications, Gaithersburg, Maryland. April 1982.

[10] Hölscher N, Niemann H-J. Towards quality assurance for wind tunnel tests: A comparative testing program of the Windtechnologische Gesellschaft. Journal of Wind Engineering and Industrial Aerodynamics. 1998;74:599-608.

[11] Richardson G, Robertson A, Hoxey R, Surry D. Full-scale and model investigations of pressures on an industrial/agricultural building. Journal of Wind Engineering and Industrial Aerodynamics. 1990;36:1053-62.

[12] Levitan ML, Mehta KC, Vann W, Holmes J. Field measurements of pressures on the Texas Tech building. Journal of Wind Engineering and Industrial Aerodynamics. 1991;38:227-34.

[13] Etheridge D. Unsteady flow effects due to fluctuating wind pressures in natural ventilation design—mean flow rates. Building and Environment. 2000;35:111-33.

[14] Younes C, Shdid CA, Bitsuamlak G. Air infiltration through building envelopes: A review. Journal of Building Physics. 2012;35:267-302.

[15] Handbook, A.S.H.R.A.E. ASHRAE Handbook–Fundamentals, IP Edition. Atlanta, GA. 2009.

[16] Sherman MH, Chan WR. Building airtightness: Research and practice. LBNL Report. 2004;53356.

[17] ÄSK AC. Ventilation and air leakage. ASHRAE Journal. 2003;45:28-36.

[18] Persily AK. Myths about building envelopes. ASHRAE Journal. 1999;41:39-48.

[19] Cheong K. Airflow measurements for balancing of air distribution system—tracer-gas technique as an alternative? Building and Environment. 2001;36:955-64.

[20] Lagus P, Persily A. A review of tracer-gas techniques for measuring airflows in buildings. ASHRAE Transactions. 1985;91:1075-87.

[21] Grot RA, Clark RE. Air leakage characteristics and weatherization techniques for low-income housing. Proceedings of the American Society of Heating, Refrigeration, and Air-Conditioning Engineers Conference on Thermal Performance of the Exterior Envelopes of Buildings, Orlando, FL. December 1979.

[22] Niemelä R, Toppila E, Tossavainen A. A multiple tracer gas technique for the measurement of airflow patterns in large industrial premises. Building and Environment. 1987;22:61-6.

[23] Nederhoff E, Van de Vooren J, ten Cate A. A practical tracer gas method to determine ventilation in greenhouses. Journal of Agricultural Engineering Research. 1985;31:309-19.

[24] Montoya MI, Pastor E, Planas E. Air infiltration in Catalan dwellings and sealed rooms: An experimental study. Building and Environment. 2011;46:2003-11.

[25] Labat M, Woloszyn M, Garnier G, Roux JJ. Assessment of the air change rate of airtight buildings under natural conditions using the tracer gas technique. Comparison with numerical modelling. Building and Environment. 2013;60:37-44.

[26] Persily AK, Grot RA. Pressurization testing of federal buildings. Measured air leakage of buildings. ASTM International. 1986:184-200.

[27] Emmerich SJ, Persily AK. Airtightness of commercial buildings in the US. 26th AIVC Conference, Brussels, Belgium. 2005.

[28] Musser A, Persily AK. Multizone modeling approaches to contaminant-based design. ASHRAE Transactions. 2002;108:803-10.

[29] Persily AK, Dols W, Nabinger S, Kirchner S. Preliminary results of the environmental evaluation of the Federal Records Center in Overland Missouri. National Inst. of Standards and Technology (BFRL), Gaithersburg, MD. 1991.

[30] Cummings JB, Tooley JJ, Moyer N, Center FSE. Uncontrolled air flow in non-residential buildings: Final Report: Florida Solar Energy Center. 1996.

[31] Cummings J, Shirey D, Withers C, Raustad R, Moyer N. Evaluating the impacts of uncontrolled air flow and HVAC performance problems on Florida's commercial and institutional buildings, Final Report. FSEC-CR-1210-00. 2000.

[32] Bahnfleth WP, Yuill GK, Lee BW. Protocol for field testing of tall buildings to determine envelope air leakage rate. ASHRAE Transactions. 1999;105:27.

[33] Brennan T, Turner W, Fisher G, Thompson B, Ligman B. Fan pressurization of school buildings. Proceedings of Thermal Performance of the Exterior Envelopes of Buildings V. 1992.

[34] Baker P, Sharples S, Ward I. Air flow through cracks. Building and Environment. 1987;22:293-304.

[35] Fox RW, McDonald AT, Pritchard PJ. Introduction to fluid mechanics. John Wiley & Sons New York. 1985.

[36] Etheridge D. Crack flow equations and scale effect. Building and Environment. 1977;12:181-9.

[37] Sedlbauer K. Prediction of mould growth by hygrothermal calculation. Journal of Building Physics. 2002;25:321-36.

[38] Hens H. Fungal defacement in buildings: A performance related approach. HVAC&R Research. 1999;5:265-80.

[39] Clarke J, Johnstone C, Kelly N, McLean R, Rowan N, Smith J. A technique for the prediction of the conditions leading to mould growth in buildings. Building and Environment. 1999;34:515-21.

[40] Hukka A, Viitanen HA. A mathematical model of mould growth on wooden material. Wood Science and Technology. 1999;33:475-85.

[41] Viitanen H, Ojanen T, Peuhkuri R, Vinha J, Lähdesmäki K, Salminen K. Mould growth modelling to evaluate durability of materials. Proceedings of the 12th DBMC International Conference on Durability of Building Materials and Components, Porto, Portugal. 2011.

[42] Viitanen H, Vinha, J, Salminen, K, Ojanen, T, Peuhkuri, R, Paajanen, L, Lähdesmäki, K. Moisture and bio-deterioration risk of building materials and structures. Journal of Building Physics. 2010;33:201-24.

[43] Viitanen H, Ojanen T. Improved model to predict mold growth in building materials. Proceedings of Thermal Performance of the Exterior Envelopes of Whole Buildings X. 2007.

[44] Johansson S, Wadsö L, Sandin K. Estimation of mould growth levels on rendered façades based on surface relative humidity and surface temperature measurements. Building and Environment. 2010;45:1153-60.

[45] Grant C, Hunter C, Flannigan B, Bravery A. The moisture requirements of moulds isolated from domestic dwellings. International Biodeterioration. 1989;25:259-84.

[46] Burge H. Airborne allergenic fungi: classification, nomenclature, and distribution. Immunology and Allergy Clinics of North America. 1989;9:307-19.

[47] Gill C, Lowry P. Growth at sub-zero temperatures of black spot fungi from meat. Journal of Applied Bacteriology. 1982;52:245-50.

[48] Hocking AD, Miscamble BF, Pitt J. Water relations of alternaria alternata, Cladosporium cladosporioides, Cladosporium sphaerospermum, Curvularia lunata and Curvularia pallescens. Mycological Research. 1994;98:91-4.

[49] Panasenko VT. Ecology of microfungi. The Botanical Review. 1967;33:189-215.

[50] Pelhate J. Recherche des besoins en eau chez quelques moisissures des grains. Mycopathologia. 1968;36:117-28.

[51] Scott W. Water relations of food spoilage microorganisms. Advances in Food Research. 1957;7:83-127.

[52] Sedlbauer K. Vorhersage von Schimmelpilzbildung auf und in Bauteilen: Lehrstuhl fur Bauphysik; 2001.

[53] Sedlbauer K. Prediction of mould fungus formation on the surface of and inside building components. Fraunhofer Institute for Building Physics. 2001.

[54] Vereecken E, Roels S. Review of mould prediction models and their influence on mould risk evaluation. Building and Environment. 2012;51:296-310.

[55] Johansson P, Bok G, Ekstrand-Tobin A. The effect of cyclic moisture and temperature on mould growth on wood compared to steady state conditions. Building and Environment. 2013;65:178-84.

[56] Liu M. Variable speed drive volumetric tracking (VSDVT) for airflow control in variable air volume (VAV) systems. Journal of Solar Energy Engineering. 2002.

[57] Walker I, Wilson D. Evaluating models for superposition of wind and stack effect in air infiltration. Building and Environment. 1993;28:201-10.

[58] Walker IS, Wilson D. The Alberta air infiltration model: AIM-2: Department of Mechanical Engineering, University of Alberta; 1990.

[59] Persily A. Simultaneous measurements of infiltration and intake in an office building. ASHRAE Transactions. 1987;93.

[60] Pang X, Liu M, Zheng B. Building pressure control in VAV system with relief air fan. Proceedings of the Fifth International Conference for Enhanced Building Operations, Pittsburgh, PA. October 2005.

[61] Johansson P, Ekstrand-Tobin A, Svensson T, Bok G. Laboratory study to determine the critical moisture level for mould growth on building materials. International Biodeterioration & Biodegradation. 2012;73:23-32.

[62] Johansson P, Svensson T, Ekstrand-Tobin A. Validation of critical moisture conditions for mould growth on building materials. Building and Environment. 2013;62:201-9.

[63] Hayati A, Mattsson M, Sandberg M. Evaluation of the LBL and AIM-2 air infiltration models on large single zones: Three historical churches. Building and Environment. 2014;81:365-79.

[64] Tetens O. Uber einige meteorologische Begriffe. Z Geophys. 1930;6:297-309.

[65] Palyvos J. A survey of wind convection coefficient correlations for building envelope energy systems' modeling. Applied Thermal Engineering. 2008;28:801-8.

[66] Blocken B, Defraeye T, Derome D, Carmeliet J. High-resolution CFD simulations for forced convective heat transfer coefficients at the facade of a low-rise building. Building and Environment. 2009;44:2396-412.

[67] Gunerhan H, Hepbasli A. Determination of the optimum tilt angle of solar collectors for building applications. Building and Environment. 2007;42:779-83.

[68] Akins R, Peterka J, Cermak J. Averaged pressure coefficients for rectangular buildings. Wind Engineering. 1979;1:369-80.

[69] Council IC. International Energy Conservation Code. International Code Council; 2009.

[70] Baechler MC, Williamson JL, Gilbride TL, Cole PC, Hefty MG, Love PM. Building America best practices series: volume 7.1: Guide to determining climate regions by county. Pacific Northwest National Laboratory (PNNL), Richland, WA (US); 2010.

[71] Standard A.M.C.A. 210-99: Laboratory Methods of Testing Fans for Aerodynamic Performance Rating. AMCA; 1999.

[72] Giebler T. Evaluation of Selected Economizer and Cold Deck Reset Strategies for Dual Duct Single Fan AHUs in Hot and Humid Climates.: M.S. Thesis, Texas A&M University; 2003.

[73] DOE. Moisture Control. http://energygov/energysaver/moisture-control, accessed April 30. 2016.

[74] ASHRAE S. Standard 62.1-2010. Ventilation for Acceptable Indoor Air Quality. 2010

APPENDIX

WinAM Page by Page Configurations

This section presents page by page configurations of the WinAM simulation model described in section 5.3.

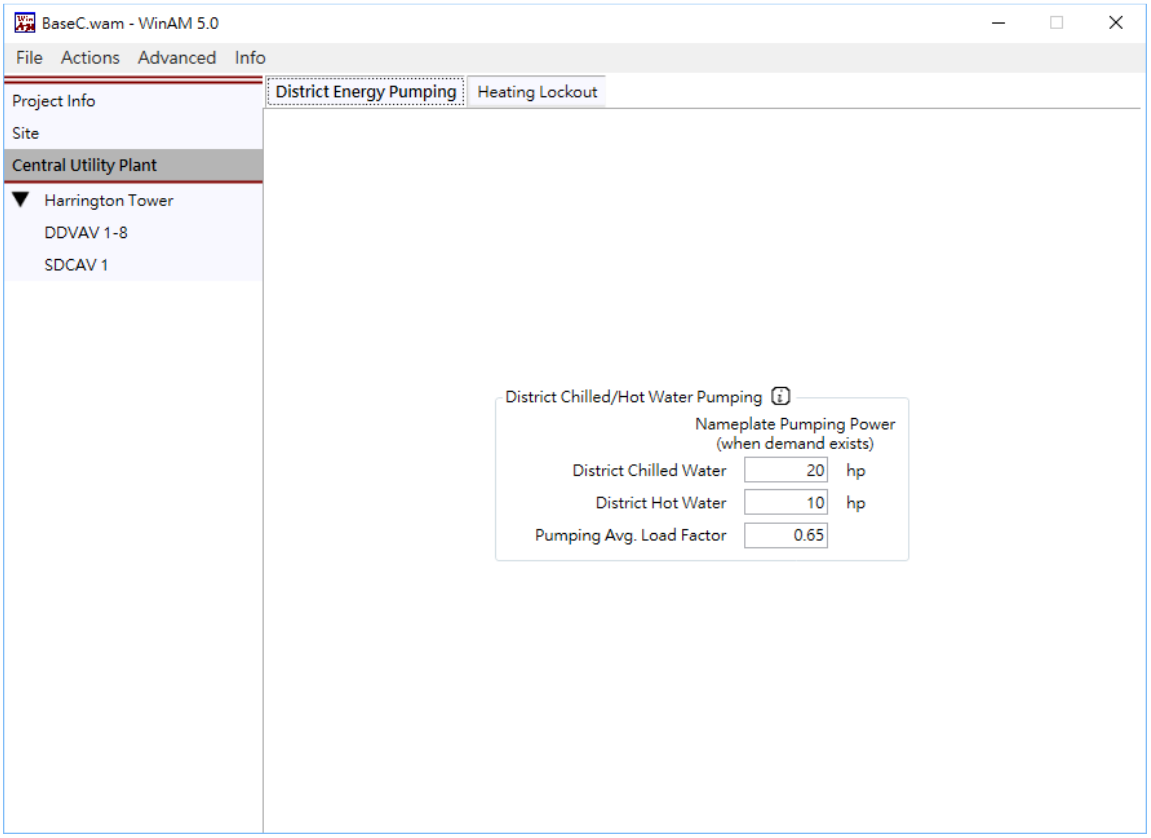

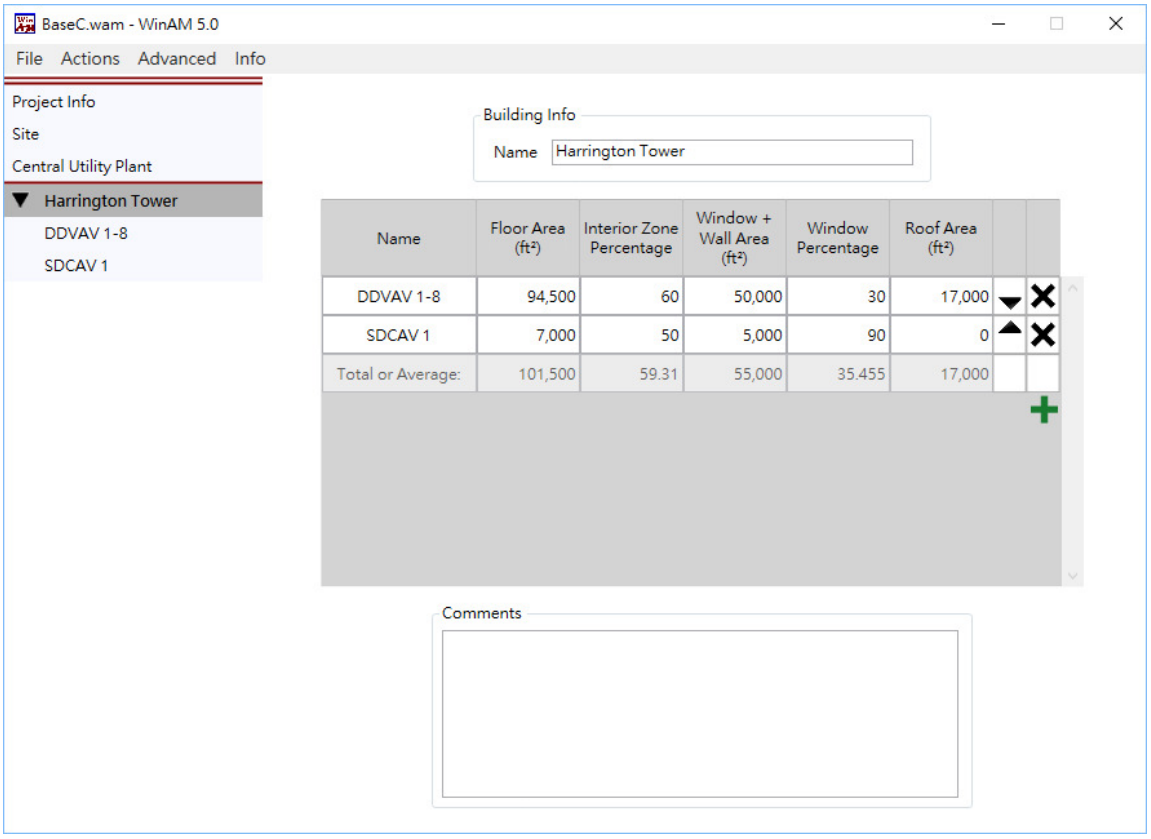
BaseC.wam - WinAM 5.0
File
Actions
Advanced
Info
Project Info
Site
Central Utility Plant
Harrington Tower
DDVAV 1-8
SDCAV 1
Building Info
Name
Harrington Tower
Name
Floor Area (ft²)
Interior Zone Percentage
Window + Wall Area (ft²)
Window Percentage
Roof Area (ft²)
DDVAV 1-8
94,500
60
50,000
30
17,000
SDCAV 1
7,000
50
5,000
90
0
Total or Average:
101,500
59.31
55,000
35.455
17,000
Comments

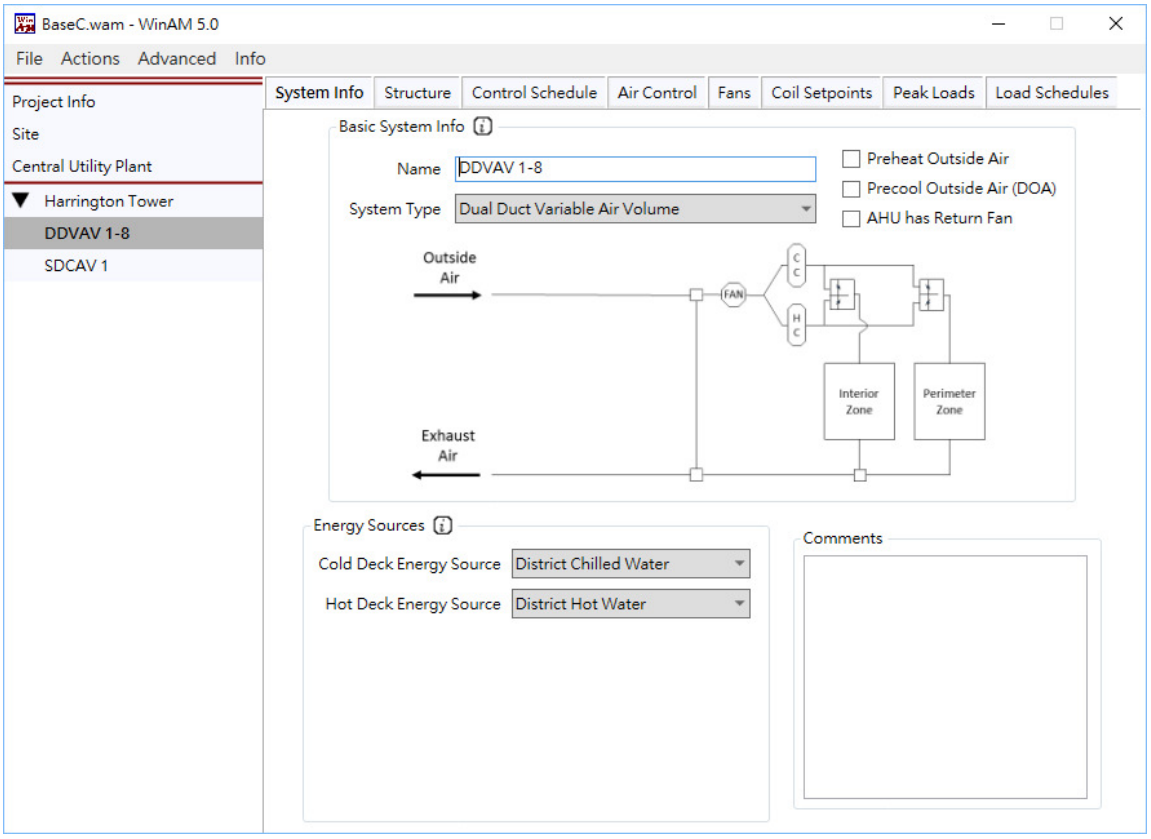
BaseC.wam - WinAM 5.0
File
Actions
Advanced
Info
Project Info
Site
Central Utility Plant
Harrington Tower
DDVAV 1-8
SDCAV 1
System Info
Structure
Control Schedule
Air Control
Fans
Coil Setpoints
Peak Loads
Load Schedules
Basic System Info
Name
DDVAV 1-8
System Type
Dual Duct Variable Air Volume
Preheat Outside Air
Precool Outside Air (DOA)
AHU has Return Fan
Outside Air
FAN
C C
H C
Interior Zone
Perimeter Zone
Exhaust Air
Energy Sources
Cold Deck Energy Source
District Chilled Water
Hot Deck Energy Source
District Hot Water
Comments

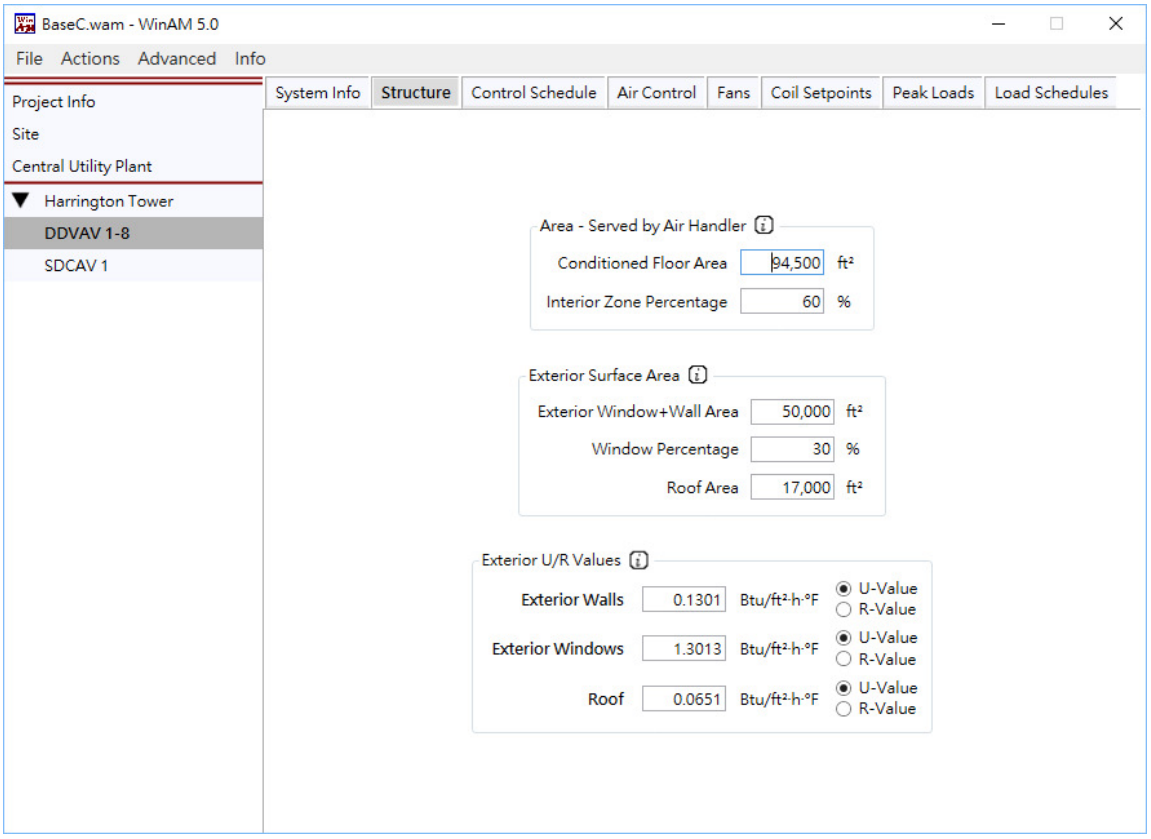
BaseC.wam - WinAM 5.0
File
Actions
Advanced
Info
Project Info
Site
Central Utility Plant
Harrington Tower
DDVAV 1-8
SDCAV 1
System Info
Structure
Control Schedule
Air Control
Fans
Coil Setpoints
Peak Loads
Load Schedules
Area - Served by Air Handler
Conditioned Floor Area
94,500
ft²
Interior Zone Percentage
60
%
Exterior Surface Area
Exterior Window+Wall Area
50,000
ft²
Window Percentage
30
%
Roof Area
17,000
ft²
Exterior U/R Values
Exterior Walls
0.1301
Btu/ft²·h·°F
U-Value
R-Value
Exterior Windows
1.3013
Btu/ft²·h·°F
U-Value
R-Value
Roof
0.0651
Btu/ft²·h·°F
U-Value
R-Value

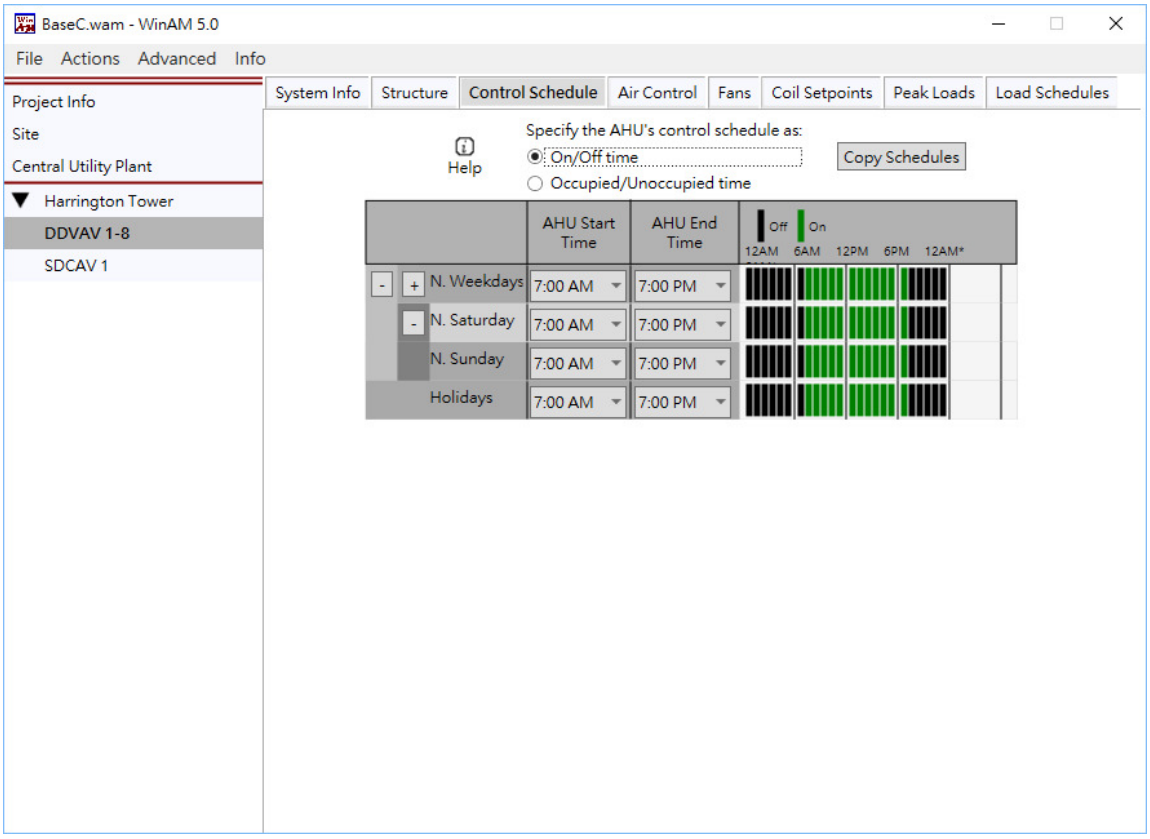
BaseC.wam - WinAM 5.0
File
Actions
Advanced
Info
Project Info
Site
Central Utility Plant
Harrington Tower
DDVAV 1-8
SDCAV 1
System Info
Structure
Control Schedule
Air Control
Fans
Coil Setpoints
Peak Loads
Load Schedules
Help
Specify the AHU's control schedule as:
On/Off time
Occupied/Unoccupied time
Copy Schedules
AHU Start Time
AHU End Time
Off
On
12AM
6AM
12PM
6PM
12AM*
N. Weekdays
N. Saturday
N. Sunday
Holidays
7:00 AM
7:00 PM

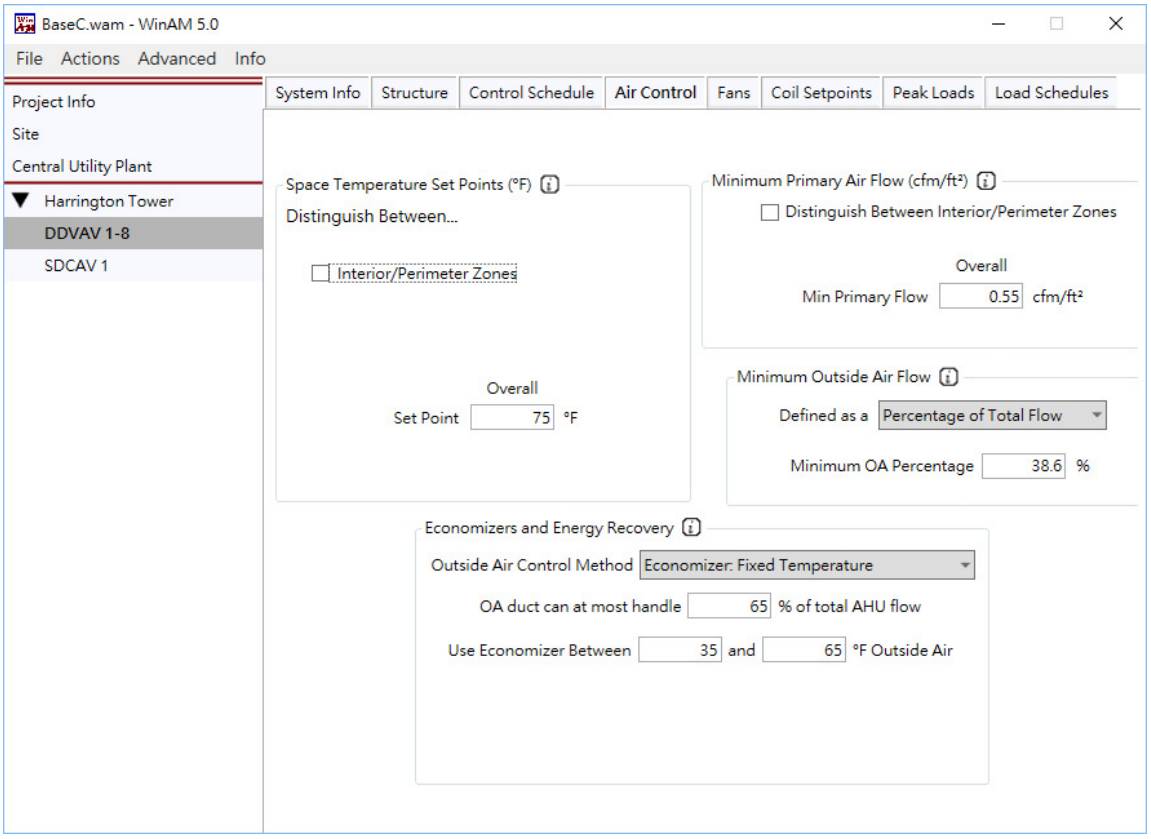
BaseC.wam - WinAM 5.0
File
Actions
Advanced
Info
Project Info
Site
Central Utility Plant
Harrington Tower
DDVAV 1-8
SDCAV 1
System Info
Structure
Control Schedule
Air Control
Fans
Coil Setpoints
Peak Loads
Load Schedules
Space Temperature Set Points (°F)
Distinguish Between...
Interior/Perimeter Zones
Overall
Set Point
75
°F
Minimum Primary Air Flow (cfm/ft²)
Distinguish Between Interior/Perimeter Zones
Overall
Min Primary Flow
0.55
cfm/ft²
Minimum Outside Air Flow
Defined as a
Percentage of Total Flow
Minimum OA Percentage
38.6
%
Economizers and Energy Recovery
Outside Air Control Method
Economizer: Fixed Temperature
OA duct can at most handle
65
% of total AHU flow
Use Economizer Between
35
and
65
°F Outside Air

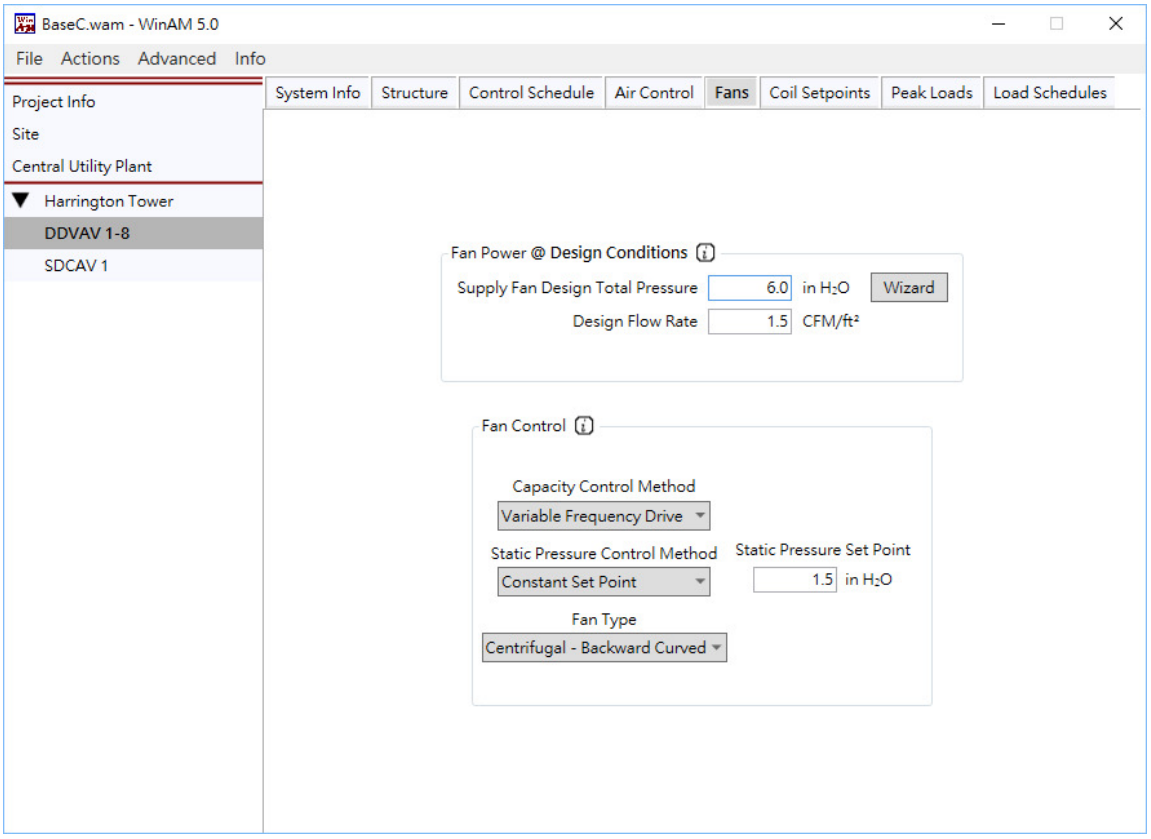
BaseC.wam - WinAM 5.0
File
Actions
Advanced
Info
Project Info
Site
Central Utility Plant
Harrington Tower
DDVAV 1-8
SDCAV 1
System Info
Structure
Control Schedule
Air Control
Fans
Coil Setpoints
Peak Loads
Load Schedules
Fan Power @ Design Conditions
Supply Fan Design Total Pressure
6.0
in H2O
Wizard
Design Flow Rate
1.5
CFM/ft²
Fan Control
Capacity Control Method
Variable Frequency Drive
Static Pressure Control Method
Constant Set Point
Static Pressure Set Point
1.5
in H2O
Fan Type
Centrifugal - Backward Curved

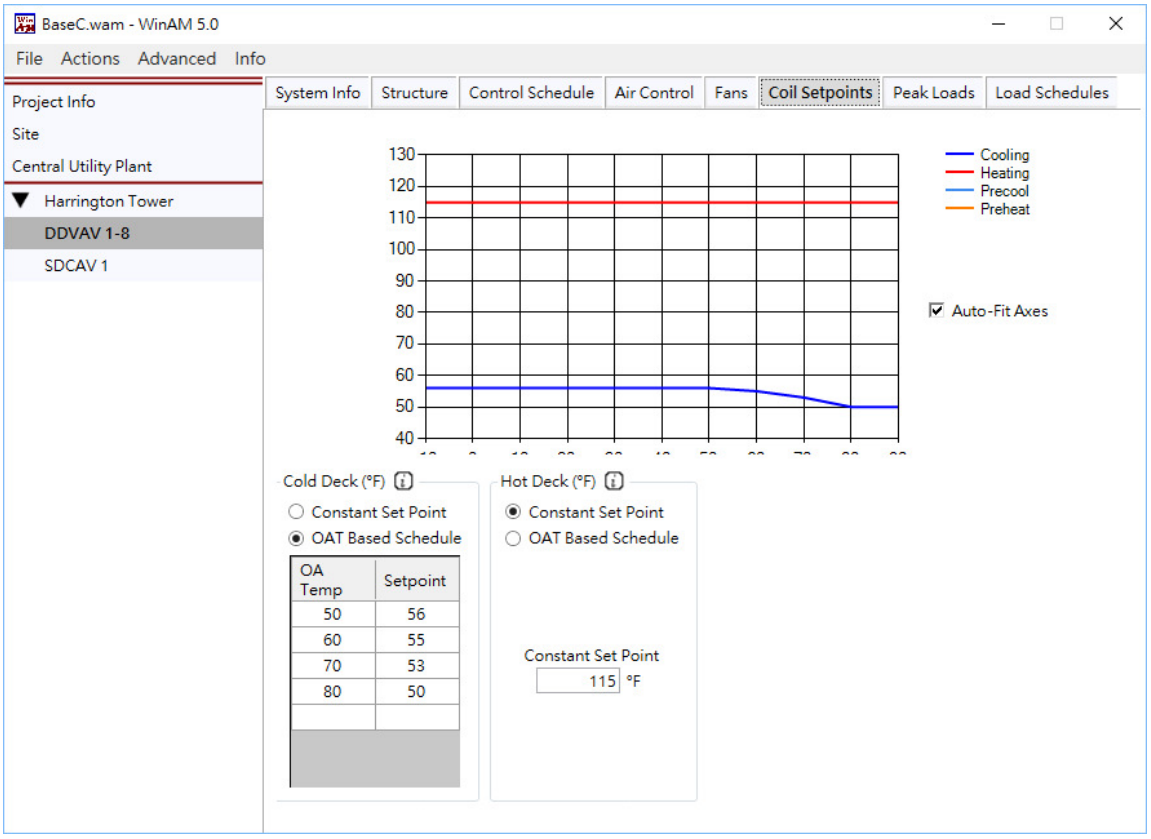
BaseC.wam - WinAM 5.0
File
Actions
Advanced
Info
Project Info
Site
Central Utility Plant
Harrington Tower
DDVAV 1-8
SDCAV 1
System Info
Structure
Control Schedule
Air Control
Fans
Coil Setpoints
Peak Loads
Load Schedules
130
120
110
100
90
80
70
60
50
40
Cooling
Heating
Precool
Preheat
Auto-Fit Axes
Cold Deck (°F)
Constant Set Point
OAT Based Schedule
OA Temp
Setpoint
50
56
60
55
70
53
80
50
Hot Deck (°F)
Constant Set Point
OAT Based Schedule
Constant Set Point
115
°F

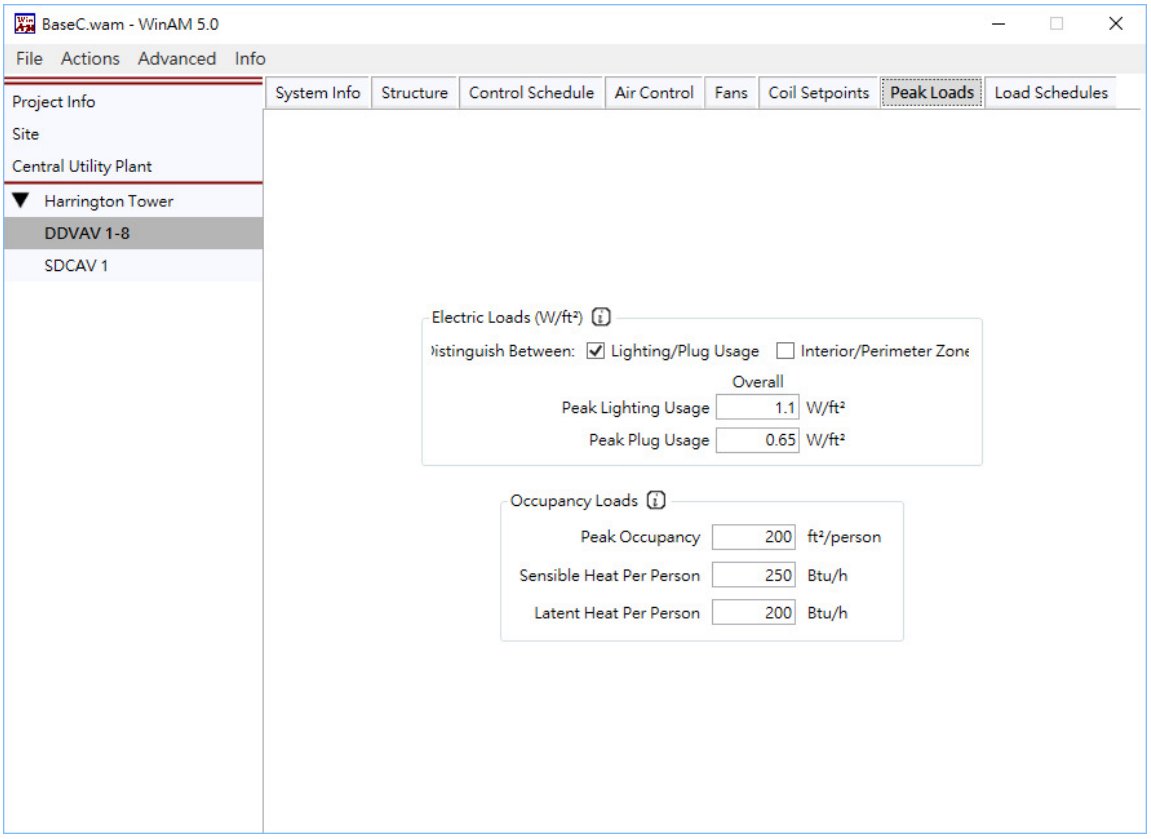
BaseC.wam - WinAM 5.0
File
Actions
Advanced
Info
Project Info
Site
Central Utility Plant
Harrington Tower
DDVAV 1-8
SDCAV 1
System Info
Structure
Control Schedule
Air Control
Fans
Coil Setpoints
Peak Loads
Load Schedules
Electric Loads (W/ft²)
istinguish Between:
Lighting/Plug Usage
Interior/Perimeter Zone
Overall
Peak Lighting Usage
1.1
W/ft²
Peak Plug Usage
0.65
W/ft²
Occupancy Loads
Peak Occupancy
200
ft²/person
Sensible Heat Per Person
250
Btu/h
Latent Heat Per Person
200
Btu/h

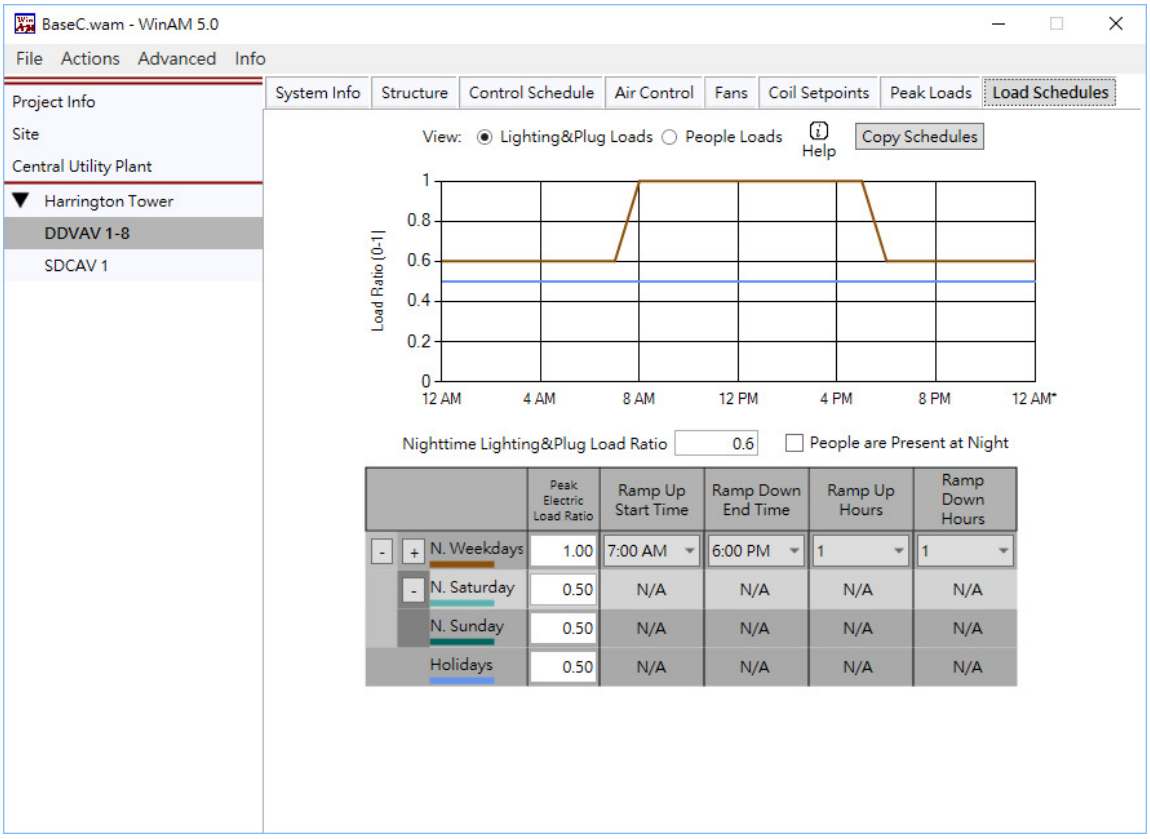
BaseC.wam - WinAM 5.0
File
Actions
Advanced
Info
Project Info
Site
Central Utility Plant
Harrington Tower
DDVAV 1-8
SDCAV 1
System Info
Structure
Control Schedule
Air Control
Fans
Coil Setpoints
Peak Loads
Load Schedules
View:
Lighting&Plug Loads
People Loads
Help
Copy Schedules
Load Ratio [0-1]
1
0.8
0.6
0.4
0.2
0
12 AM
4 AM
8 AM
12 PM
4 PM
8 PM
12 AM*
Nighttime Lighting&Plug Load Ratio
0.6
People are Present at Night
Peak Electric Load Ratio
Ramp Up Start Time
Ramp Down End Time
Ramp Up Hours
Ramp Down Hours
N. Weekdays
1.00
7:00 AM
6:00 PM
1
1
N. Saturday
0.50
N/A
N/A
N/A
N/A
N. Sunday
0.50
N/A
N/A
N/A
N/A
Holidays
0.50
N/A
N/A
N/A
N/A

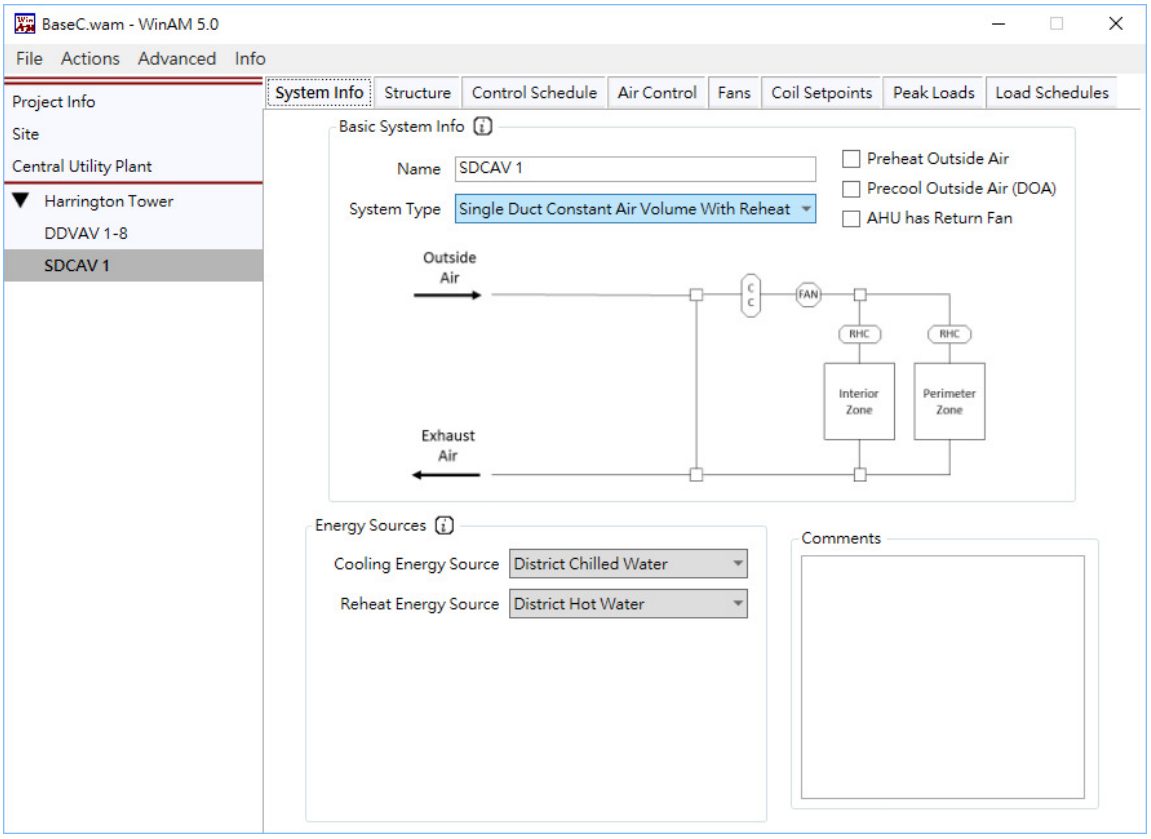
BaseC.wam - WinAM 5.0
File
Actions
Advanced
Info
Project Info
Site
Central Utility Plant
Harrington Tower
DDVAV 1-8
SDCAV 1
System Info
Structure
Control Schedule
Air Control
Fans
Coil Setpoints
Peak Loads
Load Schedules
Basic System Info
Name
SDCAV 1
System Type
Single Duct Constant Air Volume With Reheat
Preheat Outside Air
Precool Outside Air (DOA)
AHU has Return Fan
Outside Air
C C
FAN
RHC
RHC
Interior Zone
Perimeter Zone
Exhaust Air
Energy Sources
Cooling Energy Source
District Chilled Water
Reheat Energy Source
District Hot Water
Comments

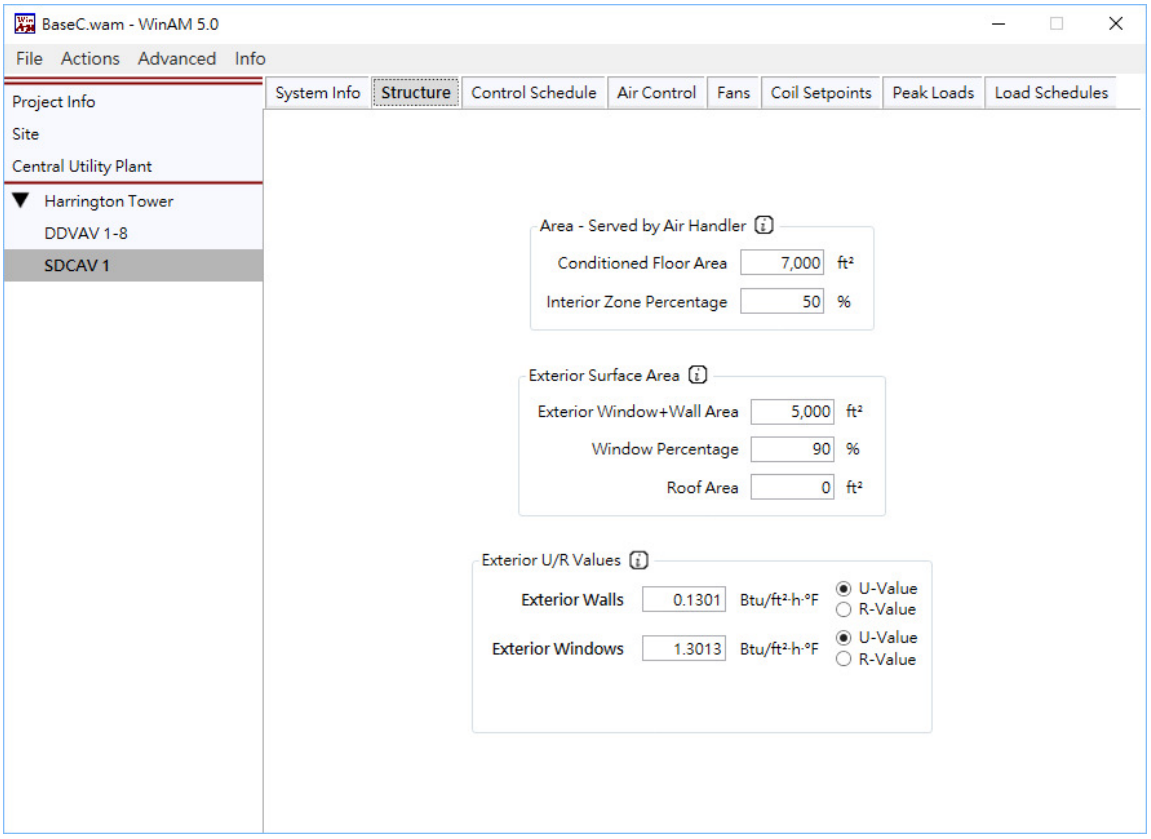
BaseC.wam - WinAM 5.0
File
Actions
Advanced
Info
Project Info
Site
Central Utility Plant
Harrington Tower
DDVAV 1-8
SDCAV 1
System Info
Structure
Control Schedule
Air Control
Fans
Coil Setpoints
Peak Loads
Load Schedules
Area - Served by Air Handler
Conditioned Floor Area
7,000
ft²
Interior Zone Percentage
50
%
Exterior Surface Area
Exterior Window+Wall Area
5,000
ft²
Window Percentage
90
%
Roof Area
0
ft²
Exterior U/R Values
Exterior Walls
0.1301
Btu/ft²·h·°F
U-Value
R-Value
Exterior Windows
1.3013
Btu/ft²·h·°F
U-Value
R-Value

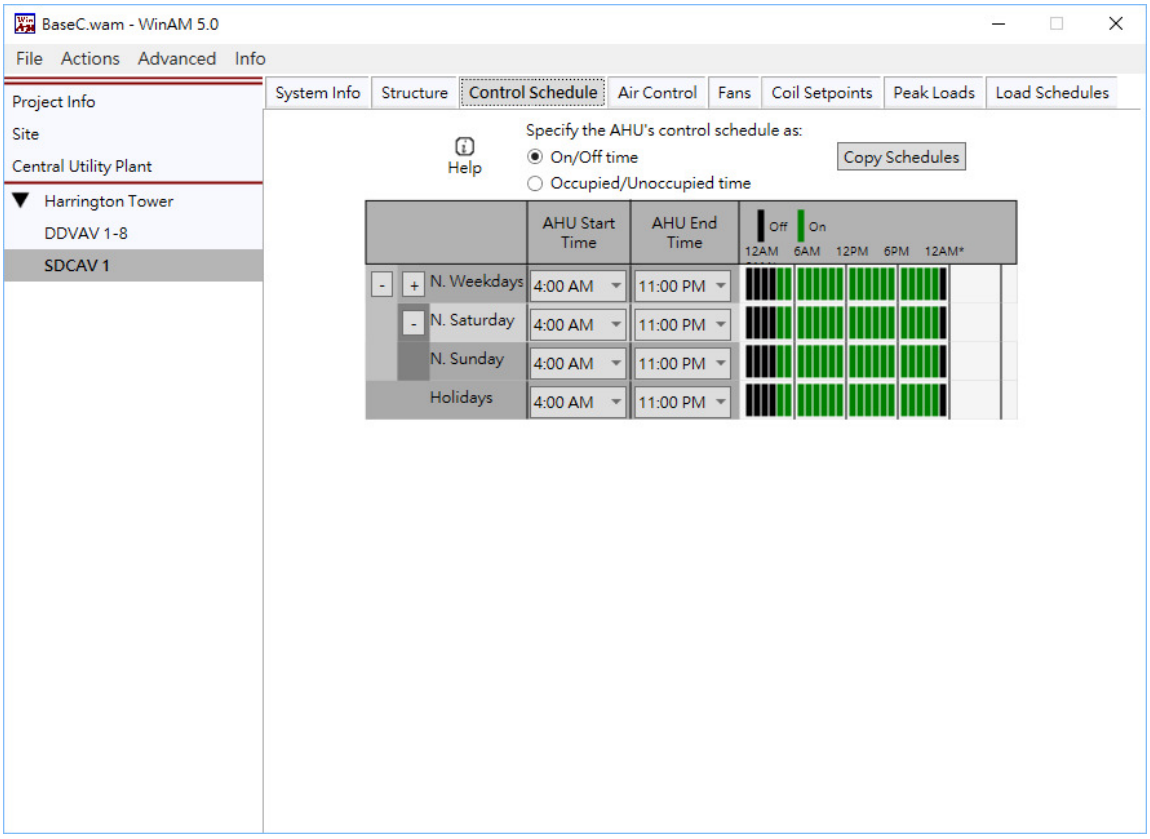
BaseC.wam - WinAM 5.0
File
Actions
Advanced
Info
Project Info
Site
Central Utility Plant
Harrington Tower
DDVAV 1-8
SDCAV 1
System Info
Structure
Control Schedule
Air Control
Fans
Coil Setpoints
Peak Loads
Load Schedules
Help
Specify the AHU's control schedule as:
On/Off time
Occupied/Unoccupied time
Copy Schedules
AHU Start Time
AHU End Time
Off
On
12AM
6AM
12PM
6PM
12AM*
N. Weekdays
N. Saturday
N. Sunday
Holidays
4:00 AM
11:00 PM

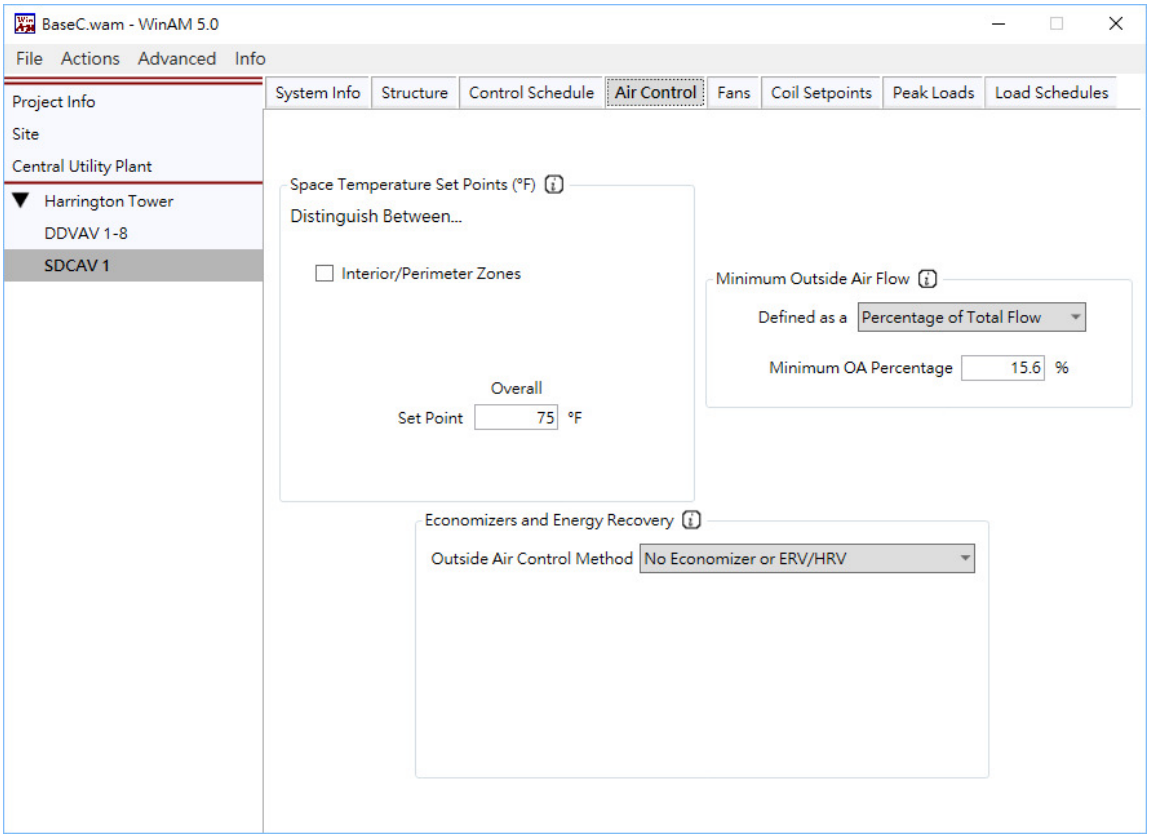
BaseC.wam - WinAM 5.0
File
Actions
Advanced
Info
Project Info
Site
Central Utility Plant
Harrington Tower
DDVAV 1-8
SDCAV 1
System Info
Structure
Control Schedule
Air Control
Fans
Coil Setpoints
Peak Loads
Load Schedules
Space Temperature Set Points (°F)
Distinguish Between...
Interior/Perimeter Zones
Overall
Set Point
75
°F
Minimum Outside Air Flow
Defined as a
Percentage of Total Flow
Minimum OA Percentage
15.6
%
Economizers and Energy Recovery
Outside Air Control Method
No Economizer or ERV/HRV

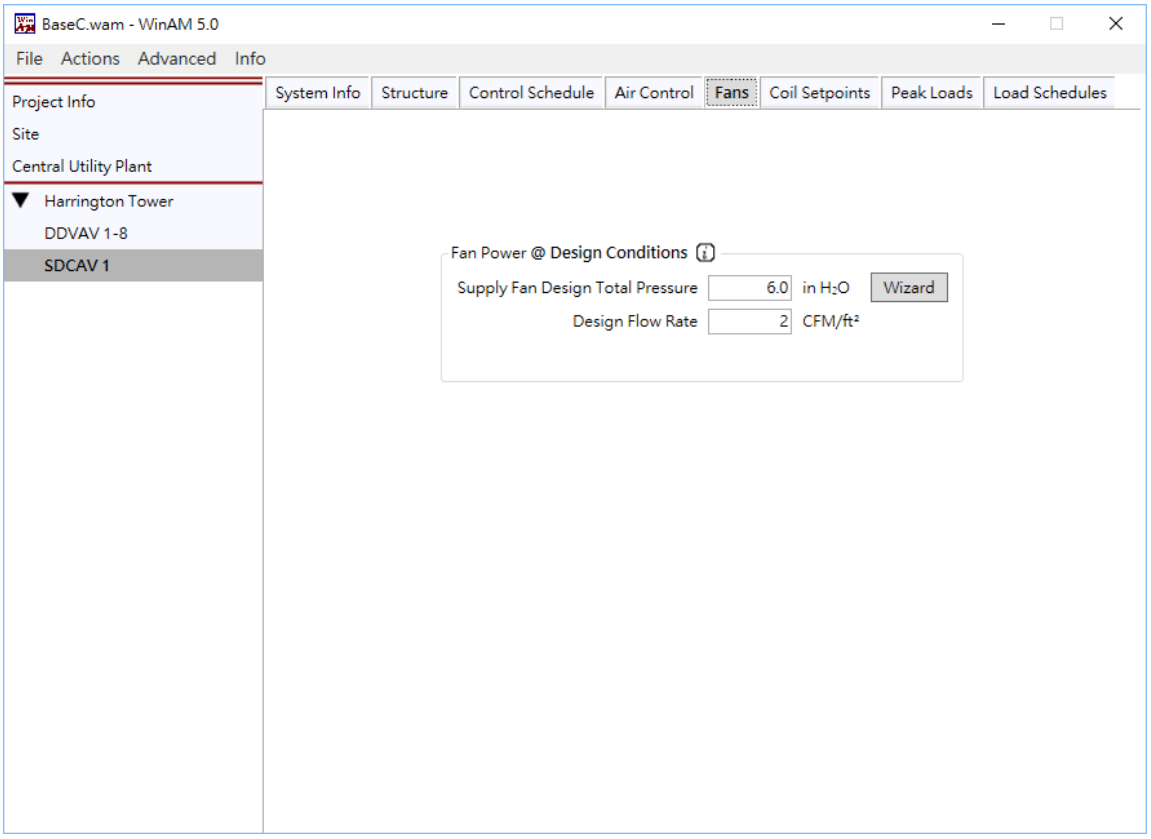
BaseC.wam - WinAM 5.0
File
Actions
Advanced
Info
Project Info
Site
Central Utility Plant
Harrington Tower
DDVAV 1-8
SDCAV 1
System Info
Structure
Control Schedule
Air Control
Fans
Coil Setpoints
Peak Loads
Load Schedules
Fan Power @ Design Conditions
Supply Fan Design Total Pressure
6.0
in H2O
Wizard
Design Flow Rate
2
CFM/ft²

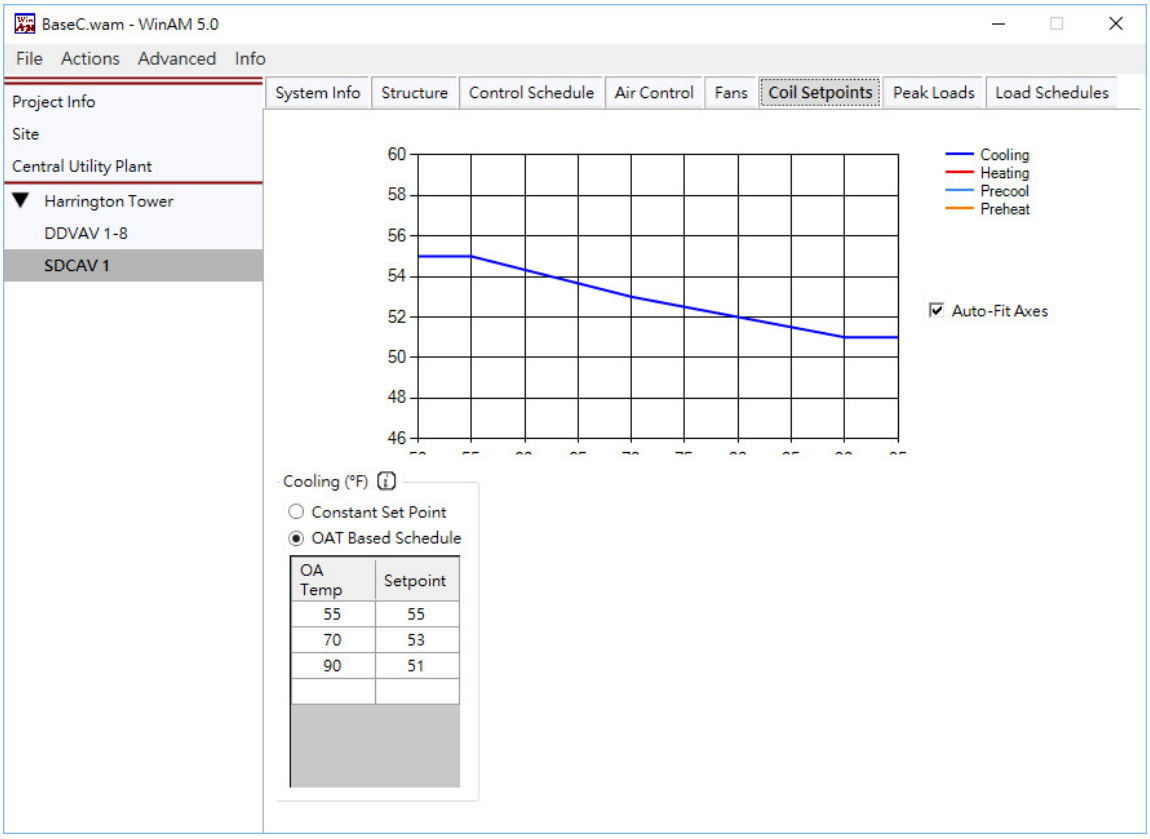
BaseC.wam - WinAM 5.0
File
Actions
Advanced
Info
Project Info
Site
Central Utility Plant
Harrington Tower
DDVAV 1-8
SDCAV 1
System Info
Structure
Control Schedule
Air Control
Fans
Coil Setpoints
Peak Loads
Load Schedules
60
58
56
54
52
50
48
46
Cooling
Heating
Precool
Preheat
Auto-Fit Axes
Cooling (°F)
Constant Set Point
OAT Based Schedule
OA Temp
Setpoint
55
55
70
53
90
51

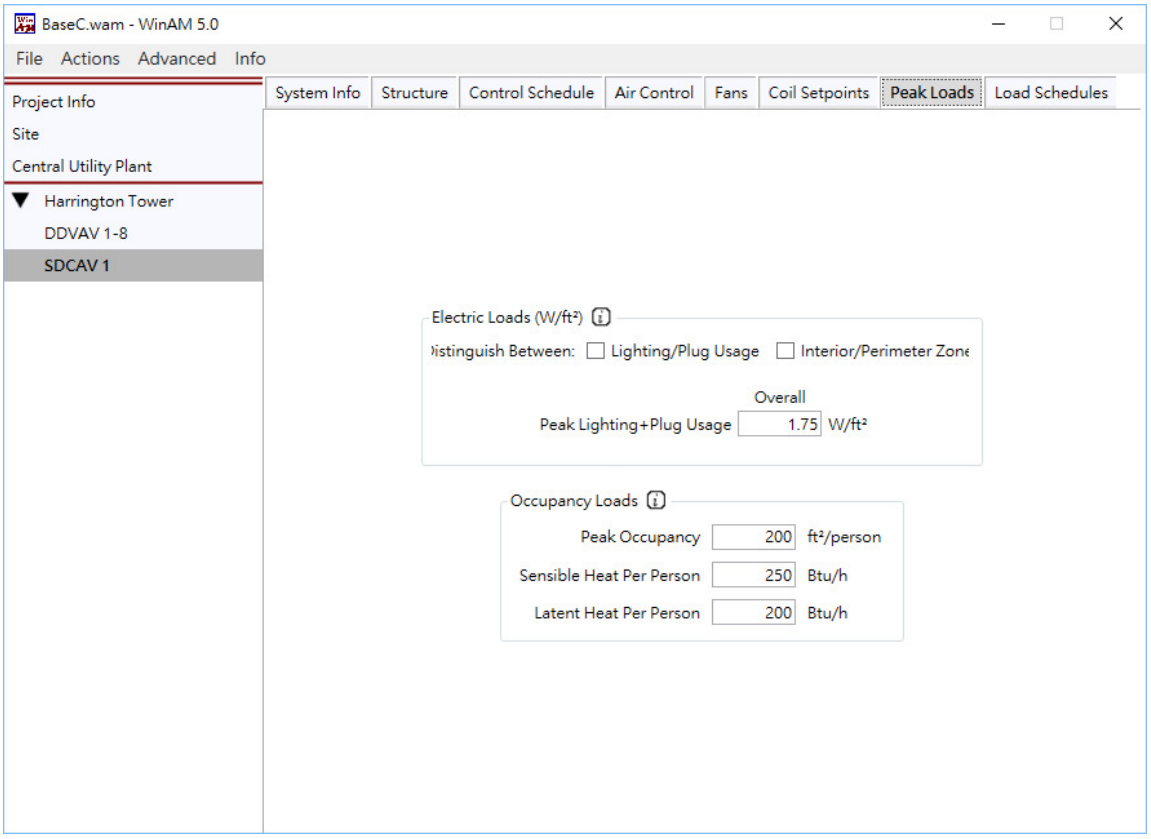
BaseC.wam - WinAM 5.0
File
Actions
Advanced
Info
Project Info
Site
Central Utility Plant
Harrington Tower
DDVAV 1-8
SDCAV 1
System Info
Structure
Control Schedule
Air Control
Fans
Coil Setpoints
Peak Loads
Load Schedules
Electric Loads (W/ft²)
istinguish Between:
Lighting/Plug Usage
Interior/Perimeter Zone
Overall
Peak Lighting+Plug Usage
1.75
W/ft²
Occupancy Loads
Peak Occupancy
200
ft²/person
Sensible Heat Per Person
250
Btu/h
Latent Heat Per Person
200
Btu/h

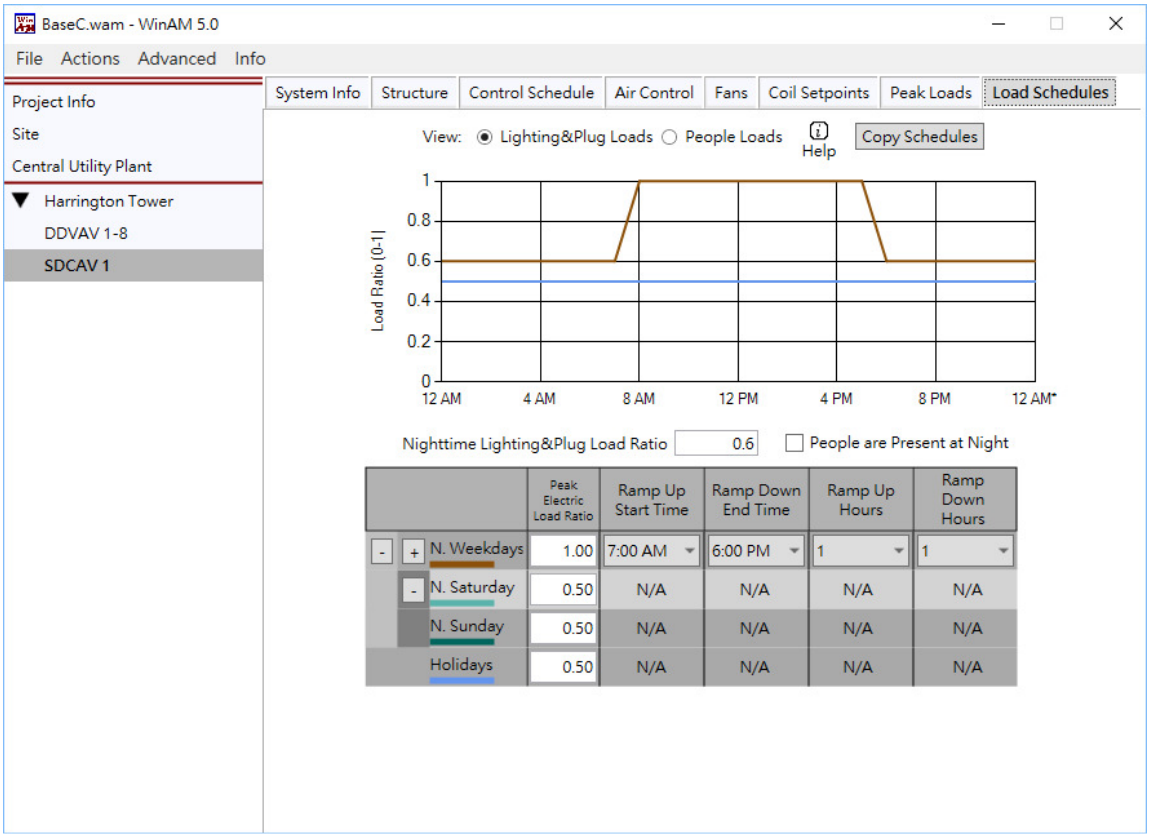
BaseC.wam - WinAM 5.0
File
Actions
Advanced
Info
Project Info
Site
Central Utility Plant
Harrington Tower
DDVAV 1-8
SDCAV 1
System Info
Structure
Control Schedule
Air Control
Fans
Coil Setpoints
Peak Loads
Load Schedules
View:
Lighting&Plug Loads
People Loads
Help
Copy Schedules
Load Ratio [0-1]
1
0.8
0.6
0.4
0.2
0
12 AM
4 AM
8 AM
12 PM
4 PM
8 PM
12 AM*
Nighttime Lighting&Plug Load Ratio
0.6
People are Present at Night
Peak Electric Load Ratio
Ramp Up Start Time
Ramp Down End Time
Ramp Up Hours
Ramp Down Hours
N. Weekdays
1.00
7:00 AM
6:00 PM
1
1
N. Saturday
0.50
N. Sunday
0.50
Holidays
0.50
N/A